



LUND UNIVERSITY

Climate Related Thermal Actions for Reliable Design of Concrete Structures

Larsson, Oskar

2012

[Link to publication](#)

Citation for published version (APA):

Larsson, O. (2012). *Climate Related Thermal Actions for Reliable Design of Concrete Structures*. [Doctoral Thesis (compilation), Division of Structural Engineering].

Total number of authors:

1

General rights

Unless other specific re-use rights are stated the following general rights apply:

Copyright and moral rights for the publications made accessible in the public portal are retained by the authors and/or other copyright owners and it is a condition of accessing publications that users recognise and abide by the legal requirements associated with these rights.

- Users may download and print one copy of any publication from the public portal for the purpose of private study or research.
- You may not further distribute the material or use it for any profit-making activity or commercial gain
- You may freely distribute the URL identifying the publication in the public portal

Read more about Creative commons licenses: <https://creativecommons.org/licenses/>

Take down policy

If you believe that this document breaches copyright please contact us providing details, and we will remove access to the work immediately and investigate your claim.

LUND UNIVERSITY

PO Box 117
221 00 Lund
+46 46-222 00 00

Report TVBK-1042
ISSN 0349-4969
ISRN LUTVDG/TVBK-1042/12-SE(158p)
ISBN 978-91-979543-2-7

Climate Related Thermal Actions for Reliable Design of Concrete Structures

Oskar Larsson

Doctoral Thesis

Lund University
Division of Structural Engineering
P.O. Box 118
SE-221 00 Lund, Sweden

Telephone: +46 46 222 9882
Internet: <http://www.kstr.lth.se>

Preface

The work presented in this thesis has been carried out at the Division of Structural Engineering at Lund University from 2007 to early 2012. The project has been financed by the Swedish Research Council FORMAS and the Swedish Road Administration. Their support and contributions are highly appreciated.

First of all I would like to thank my supervisor Prof. Sven Thelandersson for all his help and encouragement during my doctoral studies. His expertise and motivation skills are incredible and highly appreciated. In addition I thank my co-supervisor Fredrik Carlsson for his help during the first stages of my project, and Lilian Johansson for her help with the production of this thesis.

I would also like to thank my co-author Prof. Raid Karoumi from KTH for his help during an important stage of my project, and Johan Kölfors from Scanscot Technology for his assistance and guidance concerning numerical modelling.

Furthermore I would like to thank Per-Olof Rosenkvist, LTH, and Claes Kullberg, KTH, for their professional help with the practical aspects and experiments included in the research. I would also like to thank my other colleagues at the Division for their company and interesting discussions during these five years, especially my room companion Peter.

Finally I am very grateful for the support and patience of my beloved Annelie, my mother, father and sister, and my friends during this time. Thank you.

Oskar Larsson

Lund, March 2012

Sammanfattning

När temperaturen ändras i den omgivande miljön, kommer temperaturen också att ändras i en konstruktion. Komplexa interaktioner mellan klimatfaktorer bidrar till temperaturändringarna. När temperaturen varierar i ett material kommer det att expandera eller dra ihop sig och rörelser produceras. Om rörelserna är förhindrade, kan spänningar uppstå vilka kan bidra till sprickor i en betongkonstruktion. Omfattande sprickor har hittats i lådbroar i Sverige, med de flesta av sprickorna på den södra sidan. Detta tyder på en stor inverkan av solstrålning.

De temperaturlaster eller klimatsituationer som används vid beräkningar och analyser av temperaturer i betongkonstruktioner är ofta baserade på uppskattningar eller generaliseringar av klimatdata som är mer eller mindre noggranna jämfört med verkliga temperaturfält. Antaganden har gjorts om oberoende under vissa tidsperioder, i den europeiska normen har ett tredagars intervall antagits vara oberoende. De temperaturlaster som anges i normen bygger på klimatdata från Tyskland, där klimatet kan skilja sig från andra delar av Europa. Inte mycket information och riktlinjer ges avseende temperaturlaster på tvärsnittsnivå där stora spänningar kan uppkomma på grund av dessa effekter. Klimatsituationer som har använts vid analyser ger stora temperaturdifferenser, men nödvändigtvis inte det mest ogynnsamma spänningsfältet. Stora temperaturdifferenser antas ske antingen under en dag med en stor mängd inkommande solstrålning och en stor skillnad mellan lägsta och högsta lufttemperatur eller under en natt utan moln med en liknande men omvänd skillnad i lufttemperatur.

I denna avhandling presenteras detaljerade simuleringar som har använts för att kunna förutsäga temperaturen i en betongkonstruktion, där alla indata baseras på verkliga klimatdata med hög upplösning. Modellen har validerats mot temperaturmätningar utförda både i en enkel platta och i bågen på den Nya Svinesundsbron. Modellen är väl lämpad att använda för att förutsäga temperaturfördelningar i betong, eftersom den kan uppskatta temperaturvariationer med god noggrannhet. Långtidsdata från meteorologiska stationer användes i modellen för att uppskatta extremvärden för temperaturlaster baserade på årsmaxima. Resultaten visar att värdena i den europeiska normen kan vara en underskattning av svenska förhållanden.

Resultatande termiska spänningar från långtidssimuleringar har också beräknats och analyserats för lådtvärsnitt. Resultaten visade att rekommendationen i Eurokoden om temperaturskillnader på tvärsnittsnivå kan ge en överskattning av termiska spänningarna. En inkludering av den icke-linjära komponenten i temperaturfördelningen reducerar de beräknade dragpåkänningarna. Det som främst styr placering och storlek på de tvärgående termiska spänningarna är tjocklek på väggar och plattor. Störst dragspänning uppkommer i de tunnare elementen, oberoende av om de är horisontella eller vertikala. En simulering med en fullskalig 3D-modell av en verklig bro bekräftar tjocklekens betydelse, men visar också betydelsen av vilka randvillkor som används i analysen. De största termiska dragspänningarna uppkommer

på insidan på södra väggen, vilket bekräftar effekten av solstrålning på spänningsfältet i en konstruktion. En korttidssimulering med klimatdata från bara några dagar kan vara användbart för att uppskatta de termiska spänningarna. Det är dock viktigt att ha kunskap om vilken indata som använts, eftersom resultaten visar att en tre- eller fyradagars period inte alltid kan betraktas som en oberoende händelse.

Nyckelord: termisk spänning, solstrålning, FE-analys, klimatdata, lådbro

Abstract

When the temperature changes in the environment the temperature will also change in a structure. Complex interactions of climate factors affect the temperature changes. When the temperature is varied in a material it will expand or contract, and movements will be produced. If the movements are prevented, stresses may be induced which can contribute to cracks in the structure. Severe cracks have been found in box-girder bridges in Sweden, with the most cracks on the south side. This indicates a large impact of solar radiation.

Thermal actions or climate situations used in design and analysis of temperature loads in concrete structures are often based on approximations or generalisations of climate data which are more or less accurate compared to real temperature distributions. Assumptions concerning the independence of the actions during certain time periods have been made; in the European code three day intervals were assumed to be mutually independent. The thermal actions stated in the code are based on climate data from Germany, which may differ from the climate situation in other parts of Europe. Not much information and guidelines are given concerning thermal actions at cross-sectional level, where significant stresses may occur due to these effects. The climate situations used for analyses gives the largest thermal actions, but may or may not give the most unfavourable stress field. Large differentials are assumed to occur either during a day with a large amount of incident solar radiation and a large difference in daily minimum and maximum air temperature or during a night with no cloud-cover and a similar but reversed difference in air temperature.

In this thesis a detailed approach for simulating and predicting thermal actions is presented, where all the input factors are real climate data with a high resolution. The developed model has been validated against temperature measurements performed on both a simple slab and the concrete arch of the New Svinesund Bridge. The model is well suited to use for predicting temperature distributions in concrete, since it can capture temperature variations with high accuracy. Long-term climate data from meteorological stations were used with the model to identify extreme events of thermal actions based on annual maxima. The results show that the design values in the European code may be an underestimation of Swedish conditions.

The resulting thermal stresses from the long-term temperature simulations were also calculated and analysed for box cross-sections. The results showed that the recommendation in the Eurocode concerning temperature differentials at cross-sectional level may overestimate the thermal stresses in the transverse directions. An inclusion of the non-linear component of the temperature distribution reduces the calculated tensile stress level. The most important geometrical factor governing the transverse thermal stresses is the wall and slab thickness. The largest tensile stresses will appear in the thinner members, independent of the members being horizontal or vertical. A simulation using a full-scale 3D-model of a bridge confirms the influence of varying thickness, but shows the importance of the boundary conditions when using full-scale analysis. The largest thermal tensile stresses appear on the inside surface on the south web wall, which confirms the impact of solar radiation on the

stress field in a structure. A short-term simulation using climate data from just a few days can be useful for estimating the thermal stresses. It is important however to have knowledge of the input data, since the results show that a three or four days intervals cannot always be assumed to be mutually independent events.

Key words: thermal stress, solar radiation, FE-analysis, climate data, box-girder bridge

Contents

Preface	i
Sammanfattning	iii
Abstract	v
Contents.....	vii
Appended Papers	ix
Notations	xi
1 Introduction	1
1.1 Background.....	1
1.2 Objectives	2
1.3 Limitations	2
1.4 New Findings	2
1.5 Outline of Thesis	3
2 Temperature distribution in concrete	5
2.1 Background.....	5
2.2 Heat transfer.....	7
2.3 Thermal input factors	8
2.3.1 Solar radiation	8
2.3.2 Long-wave heat radiation	14
2.3.3 Convection	16
2.3.4 Enclosure temperature	18
2.4 Thermal material properties.....	18
2.4.1 Density	19
2.4.2 Specific heat.....	19
2.4.3 Thermal conductivity	20
2.4.4 Thermal properties of Asphalt	20
2.5 Temperature measurements.....	21
3 Thermal actions and stresses	23
3.1 Thermal behaviour in the longitudinal direction	24
3.2 Thermal behaviour at cross-sectional level.....	30
3.3 Mechanical material properties	32

3.3.1 Thermal expansion.....	32
3.3.2 Modulus of elasticity.....	33
3.3.3 Long-term effects.....	34
4 Thermal actions in design codes	43
4.1 Eurocode EN 1991-1-5.....	45
5 Extreme climate situations	53
5.1 Climate situations producing extreme values of thermal actions and stresses	54
5.2 Design climate situations.....	62
6 Other publications	65
7 Summary of appended papers	67
8 Conclusions	69
8.1 Further research needs.....	71
9 References	73

Appended Papers

- Paper I Larsson O. (2009), *Modelling of Temperature Profiles in a Concrete Slab under Climatic Exposure*, Structural Concrete, Vol. 10, No. 4, pp. 193-201
- Paper II Larsson O. and Thelandersson S. (2011), *Estimating Extreme Values of Thermal Gradients in Concrete Structures*, Materials and Structures, Vol. 44, No. 8, pp. 1491-1500
- Paper III Larsson O. and Karoumi R. (2011), *Modelling of Climatic Thermal Actions in Hollow Concrete Box Cross-Sections*, Structural Engineering International, Vol. 21, No. 1, pp. 74-79
- Paper IV Larsson O. and Thelandersson S. (2012), *Transverse Thermal Stresses in Concrete Box Cross-sections from Climatic Exposure*, Structural Concrete, submitted
- Paper V Larsson O. (2012), *Climatic Thermal Stresses in the Vätösund Box-girder Concrete Bridge*, Structural Engineering International, accepted

In Paper II and IV the simulations were performed by Oskar Larsson while the analysis of the results and the writing was mainly done by Oskar Larsson with valuable contributions from Sven Thelandersson

In Paper III the experimental planning and execution were done in collaboration with KTH and Raid Karoumi, with additional concrete temperature data obtained from Raid Karoumi. The writing and analysis was mainly done by Oskar Larsson, with contributions in some sections and comments by Raid Karoumi.

Notations

Some of the most used notations in the thesis are listed below

Notation		Unit
T	Temperature	[°C]
T_{avg}	Average temperature	[°C]
ΔT	Temperature differential	[°C]
T_{nl}	Non-linear temperature	[°C]
ρ	Density	[kg/m ³]
c	Specific heat capacity	[J/(kg·°C)]
k	Thermal conductivity	[W/(m·°C)]
q	Rate of heat	[W/m ²]
q_s	Heat flux from solar radiation	[W/m ²]
q_r	Long- wave radiation heat transfer	[W/m ²]
q_c	Convection heat transfer	[W/m ²]
a	Solar absorption coefficient	
G, I_t	Global solar radiation	[W/m ²]
I_h	Solar radiation on a horizontal surface	[W/m ²]
I_b	Direct solar radiation	[W/m ²]
$I_{b,n}$	Direct solar radiation on a surface perpendicular to the sun	[W/m ²]
I_d	Diffuse solar radiation	[W/m ²]
$I_{d,h}$	Diffuse solar radiation on a horizontal surface	[W/m ²]
I_g	Solar radiation reflected from ground	[W/m ²]
ρ_g	Reflection factor	[W/m ²]
β	Slope	[°]
γ	Surface azimuth angle	[°]
γ_s	Solar azimuth angle	[°]
θ	Incidence angle	[°]
θ_z	Zenith angle	[°]
α_s	Solar altitude angle	[°]
δ	Declination	[°]
λ	Latitude	[°]
ω	Hour angle	[°]
σ	Stefan-Boltzmann constant	[W/(m ² ·K ⁴)]
T_s	Absolute temperature of a surface	[K]
T_{sur}	Absolute temperature of the surroundings	[K]
T_{air}	Air temperature	[°C/K]
T_{sky}	Effective sky temperature	[K]
ε	Emissivity	
V	Wind speed	[m/s]
A	Area	[m ²]

b	Width of a section	[m]
h	Height of a section	[m]
ε_0	Axial strain	
ψ	Curvature	
E	Modulus of elasticity	[GPa]
I	Moment of Inertia	[m ⁴]
α	Thermal Expansion	[/°C]
ϕ	Creep coefficient	

1 Introduction

1.1 Background

All structures are affected by environmental loads during their life time. One environmental load is the effect of variations in temperature in both time and space in a structure. Annual and daily variations in air temperature, wind speed, solar radiation and cloud-cover will give spatial and time dependent temperature variations. The temperature variations will cause movements, which in turn may produce strains and stresses. For a concrete structure these stresses may contribute to cracks, which can be severe and cause structural and degradation problems. Especially large structures such as bridges, dams and silos are largely affected by temperature effects. In some cases the effects from temperature loads, or thermal actions, may even surpass the effects from other design loads.

One of the problems concerning the consideration of thermal actions in the design of bridges is the complexity of the heat transfer between the concrete surface and the surroundings. The temperature in the concrete is affected by the short-wave heat flux radiation from the sun, long-wave radiation heat transfer to or from the surrounding sky and environment and convection heat transfer due to differences in temperature between the air and the concrete which may be increased by increasing wind speeds. These factors have in many cases been treated by approximations and assumptions which may not give a correct description of the temperature variation in the concrete. The use of certain approximations could also fail to capture extreme events occurring due to rapid changes in the weather. A better model which treats the climatic input factors in more detail may give a better prediction of temperature variations in the concrete, and can capture rapid weather variations affecting the structure.

Today thermal actions are treated in codes by using representative values for various types of bridges. The vertical temperature gradient is included as a differential temperature across cross-sections. The representative values are based on calculations using climate data, where the results are analysed using statistical concepts. The climate data used are only for short periods of a time, usually three months, or general sets of data. The representative values of linear temperature differentials given in the Eurocode are from German conditions, and have previously been briefly checked by a general set of Swedish data as comparison. The methods in the Eurocode have the disadvantage of being based on short periods of time. If calculations using data with a higher resolution from entire years were performed, it would be possible to identify extreme occurrences of thermal actions with more accuracy. Stress analysis based on more realistic temperature distributions could also contribute to a better understanding of the effects of thermal actions. Furthermore, such results can be used to check whether thermal actions are treated satisfactory in structural design codes.

Climate situations for estimating thermal actions have been established from temperature data obtained by measurements and simulations using approximated methods. Assumptions of when severe thermal effects occur and which climate data is the cause of these effects have

been made which may not incorporate all possible extreme situations. Assumptions have also been made concerning how long time period of environmental changes affects the temperature in a concrete structure. Confirmations on the assumed climate situations are needed since it is important to understand when and how extreme climate situations occur.

1.2 Objectives

The overall aim of this thesis is to increase the knowledge of the causes for thermal actions in concrete structures and the behaviour of the structure due to these actions. The main objectives are:

- To develop a model suitable to use with extensive climate data for obtaining annual maxima of thermal actions due to environmental effects
- To identify climate scenarios which may give extreme occurrences of thermal actions
- To use the climatic scenarios for predicting thermal stresses

1.3 Limitations

The research in this thesis is focused on thermal actions from normal Swedish environmental conditions. No consideration has been taken to elevated temperatures from fire or for environmental conditions in other countries. The time frame of the long-term simulations is governed by the amount of available data for the required thermal factors. The research has been focused on the effects of non-uniform temperature distribution, and not the longitudinal expansion or contraction. No studies of the temperature effect on concrete structures from heat of hydration have been performed, only temperature effects from environmental variations.

All stress calculations have been performed with the assumption of uncracked concrete, a linear elastic material model was therefore used. This decision was made due to the time consuming long-term simulations, which would have been unrealistic if non-linear material models would have been used. It was also deemed easier to compare stress levels from the various simulations with each other for a linear elastic material.

1.4 New Findings

The main research findings and contributions in this thesis are:

- The more detailed approach in modelling climate factors when estimating temperature distributions in concrete structures gives a better tool for estimating thermal effects from the environment. The model can capture spatial and temporal temperature variations with accuracy based on climate input data which can easily be obtained for both simple and more complex cross-sections. (Paper I and III)

- The design values of positive linear temperature differentials in the Eurocode may be an underestimation of Swedish conditions. The inclusion of the material properties of asphalt show that the underestimation may be caused by the omission of this in the Eurocode. (Paper II)
- At cross-sectional level the transverse thermal stresses are overestimated if the recommended temperature difference in the Eurocode is used. An inclusion of the non-linear temperature component will reduce the thermal stresses. The thickness ratio between the members in a cross-section governs the magnitude and location of the thermal stresses. The largest tensile stresses will appear in the thinner member independent on the member being horizontal or vertical. (Paper IV)
- The climate scenarios identified as extreme events can be used to estimate thermal stresses with a great accuracy compared to using long-term data. This can be useful for estimating thermal stresses in large structures, where the boundary conditions in all directions have a large impact on the behaviour of the structure. (Paper V)

1.5 Outline of Thesis

The main part of this thesis consists of five appended academic research papers which deals with modelling of thermal actions from environment in one and two dimensions, extreme values of thermal actions based on long-term simulations, resulting climatic thermal stresses in box cross-sections and a full-scale investigation of a box-girder bridge using climatic scenarios.

In order to present background information and a more in depth description of the climatic scenarios, the thesis starts with a description of how the temperature distribution in a concrete structure is affected by the climate. Chapter 3 gives a description of how the behaviour of a concrete bridge in the longitudinal and transverse directions is affected due to thermal actions and how thermal stresses are influenced by creep of concrete. In chapter 4 the past and present considerations of thermal actions in building codes are described and in chapter 5 climatic scenarios and their occurrences are presented and analysed further. A summary of the appended papers is included followed by conclusions and future research needs.

2 Temperature distribution in concrete

2.1 Background

Thermal actions and stresses became an issue during the latest century due to reports of cracking in concrete bridges. In New Zealand severe cracking due to thermal effects was found in a prestressed concrete box-girder bridge in Auckland (Priestley 1978), while Leonhardt et al. (1965) reported of cracks in a box-girder bridge in Germany. Several box-girder bridges in Sweden have been found to have more cracks on the south side than the north. This indicates that the environment has a large impact on the structure, since the only significant factor that varies significantly between the south and north sides is the incident solar radiation. Durability concerns and more advanced calculation and analysis methods developed in the last century have led to the construction of bridges with fewer bearings and joints. This is of major importance for the occurrence of thermal stresses due to increased restraint since the bridges are less free to move. The appearance of thermal stresses has led to an interest in predicting the temperature distribution in concrete bridges and the associated thermal actions.

Over the last 40 years several studies have been presented concerning the temperature distribution in concrete structures and thermal effects in various parts of the world. Most previous studies have focused on simulations using numerical methods to obtain the temperature distributions, which were compared to experimental data from measurements. Emerson (1973) presented a method for calculating the temperature distribution in concrete based on climatic input factors using a finite difference calculation procedure. Hunt and Cooke (1975) and Priestley (1978) discussed the origin to and behaviour from vertical thermal gradients in concrete bridges based on conditions in New Zealand, this work was expanded further by Thurston et al. (1980) and Cooke et al. (1984). The use of finite element analysis was adopted in the 1980s by Elbadry and Ghali (1983a, 1983b) who used this method to calculate the temperature distribution over various bridge cross-sections. Mirambell et al. (1991) presented a comparison between experimental data and temperature calculations from two models using either a finite element or a finite difference procedure. The models were used to obtain design values for concrete bridges on the Iberian Peninsula. Branco and Mendes (1993) used a similar finite element approach to calculate the temperature distribution as the one used by Mirambell et al. Predictions and analyses of temperature distributions in concrete bridges have also been performed and presented for other parts of the world such as the United States (Shushkewich 1998), Australia (Hirst 1984), India (Dwivedi et al. 2006), China (Wang and Fang 2009), Italy (Saetta et al. 1995) and Germany (Zichner 1982, Fouad 1999). Hirst used a one-dimensional computer model to calculate the temperature distribution which was checked against the model developed by Emerson. Dwivedi et al. used FE-analysis for the heat transfer calculations with the climatic input factors adapted as described by Mirambell et al.

Analyses of environmental temperature distributions and thermal actions have also been performed on other types of structures such as concrete dams and silos. Agullo et al. (1996) presented an analytical model for simulating the thermal behaviour of dams based of the finite difference method, which was deemed suitable due to the geometry of the dam. Another study on thermal actions on concrete dams was presented by Sheibany and Ghaemian (2006), where the Karaj dam in Iran was analysed. Three-dimensional finite element analysis was used to simulate the annual variations in temperature, and the predicted temperatures were compared to temperature measurements from the dam. A thermal actions study on a concrete dam was also presented by Satta et al. (1995), where a two-dimensional FE-analysis was used. Priestley (1976) presented a study on the thermal stresses in concrete tanks from temperature gradients.

A few recent studies exist where the focus have been to measure the temperature gradient directly on concrete bridges without numerical simulation. Roberts-Wollman et al. (2002) measured the temperature through the depth of a segmental concrete box-girder bridge for 2.5 years. They coupled the measured data to ambient climate conditions recorded by the meteorological service in the United States and compared the thermal gradients to the US standard. Another study using monitoring of temperature variations was conducted by Barr et al. (2005), where temperature and strain measurements were performed on a prestressed girder bridge in the United States. In Japan temperature measurements on a concrete box-girder bridge were presented by Suzuki et al. (2007). The main focus in the study was cold nights when the roadway surface could freeze and cause accidents to happen.

The spatial temperature distribution in a structure can be divided into several parts as presented in Figure 2.1; one average temperature over the section, two linear temperature differentials, horizontal and vertical, and a non-linear temperature differential. In some parts of this thesis and in work by other authors the linear differentials are referred to as temperature or thermal differences/gradients.

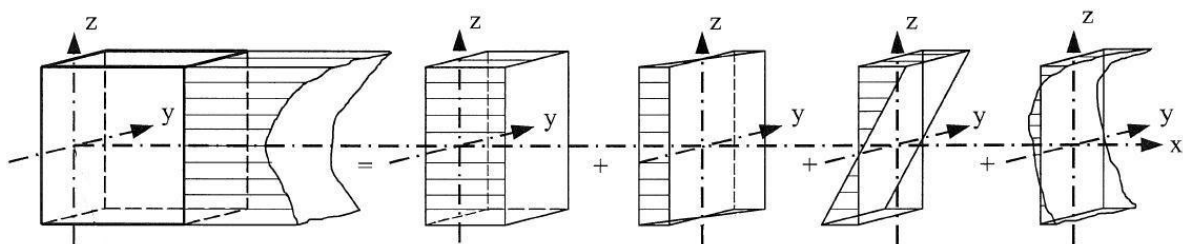


Figure 2.1 Temperature components in a concrete section (Figure reproduced from SS-EN 1991-1-5 with permission of SIS Förlag AB, www.sis.se)

Variations in the average temperature are mainly governed by annual variations in the surrounding climate such as annual variations in air temperature, while the linear and non-linear differentials mainly are governed by short-term variations in the surrounding climate.

Such short-term variations can be the effect of solar radiation, variations in cloud-cover or rapid changes in air temperature.

2.2 Heat transfer

The variation of the temperature field in a concrete structure can be described by a three-dimensional heat flow with Fourier's law as (Incropera et al. 2007)

$$\rho c \frac{\partial T}{\partial t} = k \left(\frac{\partial^2 T}{\partial x^2} + \frac{\partial^2 T}{\partial y^2} + \frac{\partial^2 T}{\partial z^2} \right) + q_v \quad (2.1)$$

where ρ is the density (kg/m^3), c is the specific heat capacity ($\text{J}/(\text{kg} \cdot ^\circ\text{C})$), $\partial T/\partial t$ is the change in temperature over time ($^\circ\text{C/s}$), k is the thermal conductivity ($\text{W}/(\text{m} \cdot ^\circ\text{C})$) of concrete, $\partial^2 T/\partial x^2$, $\partial^2 T/\partial y^2$, $\partial^2 T/\partial z^2$ are the second spatial derivatives (thermal conductions) of temperature in the x , y and z directions, respectively. The heat generated in the concrete due to hydration, q_v , can be considered negligible since the simulations are limited to already hardened concrete. For a one-dimensional heat flow, the thermal conduction is only active in one direction while for a two-dimensional heat flow in a section the thermal conduction is active in two directions. The boundary conditions for the three-dimensional heat transfer problem are described by

$$k \left(\frac{\partial T}{\partial x} n_x + \frac{\partial T}{\partial y} n_y + \frac{\partial T}{\partial z} n_z \right) - q = 0 \quad (2.2)$$

where q is the rate of heat transferred from the environment to the concrete surface per unit area (W/m^2), n_x , n_y , n_z are the direction cosines of the unit outward vector normal to the boundary surface, $\partial T/\partial x$, $\partial T/\partial y$, $\partial T/\partial z$ are the temperature change in the x , y and z directions. The rate of heat transferred from the surrounding environment to the concrete consists of three different parts

$$q = q_s + q_c + q_r \quad (2.3)$$

where q_s is the heat flux from incident solar radiation, q_c is the convection heat transfer and q_r is the long-wave radiation heat transfer. Convection is governed by air temperature and wind speed, while the long-wave heat radiation is governed by cloud-cover and the temperature of the surroundings. For a structure containing an enclosure, e.g. a box-girder bridge, the boundary condition for the inside surfaces are as Eq. 2.3 without the solar radiation part.

2.3 Thermal input factors

2.3.1 Solar radiation

Solar radiation consists of three different kinds of light with short wave-lengths; ultraviolet, visible and infra-red light (Duffie and Beckman 2006). The infrared part is sometimes referred to as near infra-red (NIR), to separate it from IR-light of greater wavelengths by heat radiation at the earth's surface. The average amount of solar radiation that strikes the earth every year is 1367 W/m^2 on a surface directed at the sun outside the atmosphere; this value is called the solar constant. During a year the variation in distance between the earth and the sun leads to a variation in radiation between 1320 and 1410 W/m^2 . During the passage of the light through the atmosphere some parts of the solar radiation is absorbed or scattered. How much of it that reaches the earth's surface depends on several factors such as how far the radiation has gone into the atmosphere, the air humidity, the amount of clouds and air particles (aerosols).

The solar radiation which reaches the earth's surface is called global or total radiation. The total amount of solar radiation absorbed by a surface close to the ground is calculated according to Duffie and Beckman (2006) as

$$q_s = a \cdot G \quad (2.4)$$

where a is the solar absorption coefficient and G is global radiation striking the surface. For heat radiation with longer wave lengths the absorptivity is equal to the emissivity of the material, a relation called Kirchhoff's law. If a surface is sunlit then Kirchhoff's law is no longer valid due to the sunlight's shorter wavelengths. The absorptivity is instead depending on the colour and texture of the surface. A light surface is absorbing less solar radiation than a dark surface. The solar absorptivity for concrete is varying over time due to colour changes when it gets older. Measurements of solar absorptivity for concrete have been performed by e.g. Reagan and Acklam (1979), Levinson and Akbari (2001), Marceau and VanGeem (2007). The studies have measured the solar reflectivity, which for an opaque material like concrete is equal to all solar radiation which is not absorbed. Various material combinations of different cement and aggregate types with different colours were tested. It was found in both studies that the colour had a large impact on the reflectivity, for concrete with standard Portland cement a span of $0.3 - 0.6$ was found depending on the material composition. Based on this a solar absorptivity of 0.6 or 0.5 was tested for the FE-simulations presented in Paper I, with 0.5 deemed to give the best agreement with the measured temperatures. This value was used in all appended papers.

A concrete bridge has in most cases a paving layer on top consisting of either asphalt or concrete, making the solar absorptivity of both materials an important factor. According to the measurements presented by Reagan and Acklam (1979) a value for the solar absorptivity of asphalt of 0.9 is reasonable to use, a value which was used in the calculations presented in the appended papers. In Table 2.1 the solar absorptivity for concrete and asphalt found in literature or in studies of thermal actions by other authors are listed. Most previous studies have used a solar absorptivity of 0.5 for concrete and 0.9 for asphalt. The listed solar

absorptivity listed varies more for concrete, which could be due to the variations in surface colour and texture. For asphalt this variation is smaller, and the absorption coefficient is therefore easier to predict.

Table 2.1 Solar absorptivity of concrete and asphalt used by other authors

Author	Solar absorptivity	
	Concrete	Asphalt
Emerson (1973)	0.5	0.9
Sheibany (2006)	0.5	
Branco and Mendes (1993)	0.7	0.9
Mirambell et al. (1991)	0.5	0.9
Elbadry and Ghali (1983b)	0.5	0.9
Dwivedi et al. (2006)	0.5	0.9
Fu et al. (1990)	0.65	
Roberts-Wollman et al. (2010)	0.7	0.9
Dickinson (1978)		0.85
Hirst (1984)		0.95
Threlkeld (1970)	0.64-0.78	0.86-0.91

The incident global solar radiation I_h on a horizontal surface can be defined as

$$G = I_h = I_b + I_d \quad (2.5)$$

where I_b is the direct, or beam, radiation, and I_d is the diffuse radiation. A tilted surface is also affected by reflected radiation from the ground or other buildings. The global radiation I_t on a tilted surface is then calculated as

$$G = I_t = I_b + I_d + I_g \quad (2.6)$$

where I_g is the reflected radiation. On a clear day in the summer the magnitude of the total global radiation is about 1000 W/m^2 and on a cloudy day about $300\text{-}400 \text{ W/m}^2$. Direct solar radiation is the radiation that strikes the earth's surface without having been scattered in the atmosphere. It's often referred to as beam radiation and can be expressed by

$$I_b = I_{b,n} \cos(\theta) \quad (2.7)$$

where $I_{b,n}$ is the direct radiation on a surface perpendicular to the sun and θ is the angle of incidence, which is the angle between the normal to the surface and the beam radiation on that surface as described in Figure 2.2.

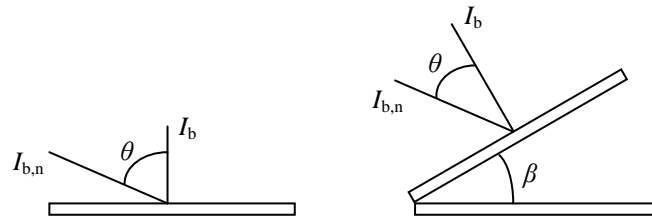


Figure 2.2 The incidence angle θ for a horizontal and a tilted surface with the slope β

To calculate the angle of incidence several other angles must be known. Figure 2.3 shows the definition of the slope, the surface azimuth angle, the zenith angle, the solar altitude angle and the solar azimuth angle.

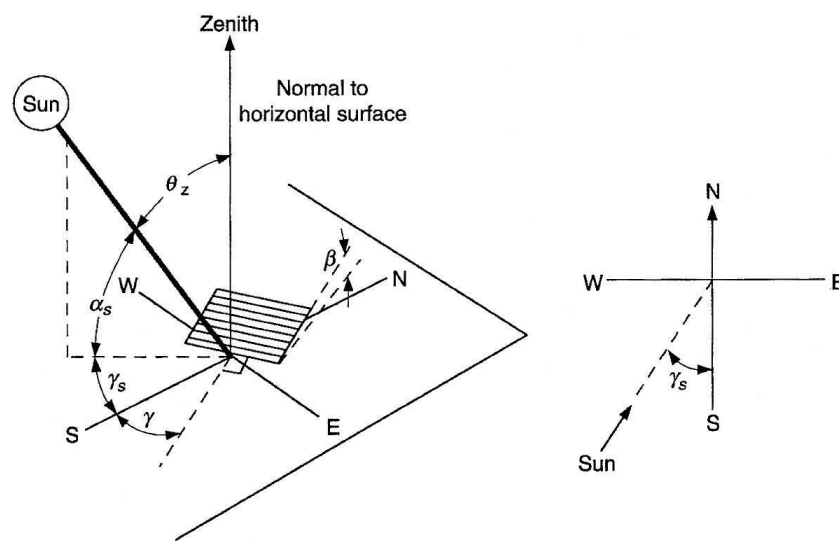


Figure 2.3 (Duffie and Beckman 2006)

- β Slope, the angle between the horizontal and the plane of the surface
- γ Surface azimuth angle, the rotation angle from south for the surface. West positive and east negative
- θ_z Zenith angle, the angle between the sun and the vertical. The angle of incidence for a horizontal surface
- α_s Solar altitude angle, the angle between the sun and the horizontal. The complement to the zenith angle
- γ_s Solar azimuth angle, the angular displacement from south of the projection of direct radiation on the horizontal plane

Figure 2.4 shows both the declination δ , which is the sun's angle related to the equator plane, and the latitude λ . One more angle needed is the hour angle ω which is the angular displacement of the sun from the local meridian due to the earth's rotation $15^\circ/\text{hour}$.

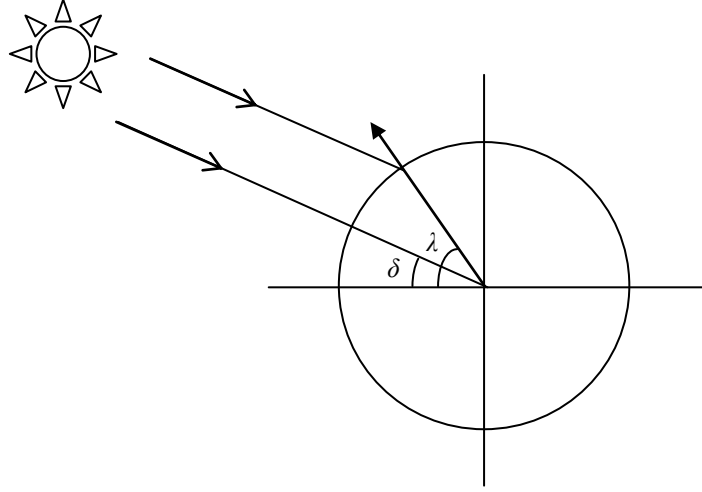


Figure 2.4 The declination δ for direct radiation and the latitude λ for a point at earth's surface.

The angle of incidence can be calculated with the following expression

$$\begin{aligned} \theta = & \sin(\delta)\sin(\lambda)\cos(\beta) - \sin(\delta)\cos(\lambda)\sin(\beta)\cos(\gamma) + \cos(\delta)\cos(\lambda)\cos(\beta)\cos(\omega) \\ & + \cos(\delta)\sin(\lambda)\sin(\beta)\cos(\gamma)\cos(\omega) + \cos(\delta)\sin(\beta)\sin(\gamma)\sin(\omega) \end{aligned} \quad (2.8)$$

For a horizontal surface the slope β is zero.

The diffuse component of the global solar radiation is all the radiation that is not direct; the radiation which is scattered in the atmosphere. The distribution of diffuse radiation is anisotropic, more uneven on clear days than on cloudy days. According to Duffie and Beckman (2006) the diffuse solar radiation can be roughly divided into three parts, which was suggested due to measurements from clear days. The three parts are presented in Figure 2.5. The first part is the circumsolar diffuse radiation, which is a result from forward scattering of radiation from angles near the sun. The second part is isotropic diffuse radiation, received uniformly from the sky dome. The third part is concentrated near the horizon and is called horizon brightening. The reason for horizon brightening is due to the angle of sight on the horizon, where more of the atmosphere is visible and more scattered light hits the surface.

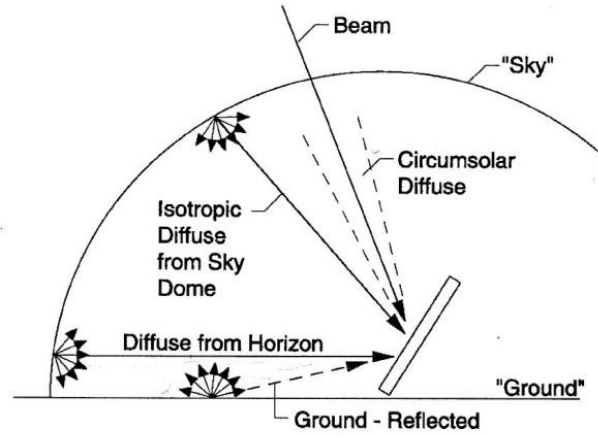


Figure 2.5 The different types of radiations on a tilted surface. (Duffie and Beckman 2006)

When it is necessary to know the diffuse component of solar radiation, for example to estimate the radiation on tilted or vertical surfaces, then sky models that describes the diffuse radiation mathematically can be used. An anisotropic model including all three parts was developed and described by Perez et al. (1987). Another simpler model is based on the assumption that the circumsolar and horizon diffuse parts are small, and all diffuse radiation I_d is then assumed isotropic. In such a model the diffuse component on a tilted surface is

$$I_d = I_{d,h} \left(\frac{1 + \cos(\beta)}{2} \right) \quad (2.9)$$

where $(1 + \cos(\beta))/2$ is the view factor to the sky for the surface and $I_{d,h}$ is the diffuse radiation on a horizontal surface. The isotropic model was used for the FE-calculations presented in Paper III to V. A tilted surface is also affected by radiation I_g reflected from the ground and its magnitude can be calculated from the total radiation against the ground by the expression

$$I_g = I_h \rho_g \left(\frac{1 - \cos(\beta)}{2} \right) \quad (2.10)$$

Where I_h is the global radiation on a horizontal surface, $(1 - \cos(\beta))/2$ is the view factor towards the ground and ρ_g is the reflection factor. For normal ground conditions the reflection factor can be set to 0.2 (Thevenard and Haddad 2005).

The solar radiation can be measured by using either pyranometers for global and diffuse radiation or a pyrliometer for the direct radiation. Solar radiation data from meteorological institutes are often obtained by such measuring equipment. Measurements of global and diffuse radiation can also be performed simultaneously in one device using a specially designed sunshine sensor. Such a device was used for the measurements presented in Papers I and III. If two of the global, diffuse and direct radiations are known, the third can be calculated based on Eq. 2.5, Eq. 2.7 and Eq. 2.9.

In several previous investigations by other authors no solar radiation data were available from a meteorological station. This has been handled in two ways; either by using a general set of climate data, which was done in Alavizadeh-Farhang (1999b) and Emerson (1973, 1977), or by approximating the incident solar radiation from the global extra-terrestrial solar radiation. When using general sets of data a common concept concerning the solar radiation used by several other authors, e.g. Hirst (1984), Soukhov (1994, 2000), Emerson (1973, 1977), Alavizadeh-Farhang (1999b), is the total solar radiation. It is defined as the sum of the solar radiation striking a surface during a whole day, often expressed in Wh/m^2 . When this concept is used the incident solar radiation during the day is approximated based on the following equation found in Emerson (1973, 1977)

$$I(t) = \frac{2S}{T_{\text{sd}}} \sin^2(\alpha) \quad (2.11)$$

where $I(t)$ is the intensity of the solar radiation at time t , S is the total solar radiation for the day and T_{sd} is the length of the solar day.

Elbadry and Ghali (1983b) used an approximation method based on the solar constant outside the earth atmosphere. The incident solar radiation was treated as

$$I = I_n \cos \theta \quad (2.12)$$

$$I_n = I_{\text{sc}} 0.9^{k_a t_u / \sin(\theta_a + 5^\circ)} \quad (2.13)$$

where I_n is the rate of solar energy incident on a surface normal to the sun, I_{sc} is the solar constant, k_a is the ratio of atmospheric pressure to pressure at sea level, t_u is a turbidity factor accounting for the effects of clouds and air pollution and θ_a is the solar altitude. The calculated solar radiation was only applicable between sunrise t_{sr} and sunset t_{ss} , which were calculated as

$$t_{\text{sr}} = 12 - \frac{1}{15} \cos^{-1}(-\tan(\delta) \tan(\lambda)) \quad (2.14)$$

$$t_{\text{ss}} = 12 + \frac{1}{15} \cos^{-1}(-\tan(\delta) \tan(\lambda)) \quad (2.15)$$

where δ and λ are the declination resp. latitude as presented in Figure 2.4. These approximations are useful when extreme values of thermal actions are needed for a certain bridge. However a disadvantage of using approximations for the solar radiation is that it is hard to capture the effects of clouds on the real structure. When calculating extreme values based on annual maxima of temperature differentials, it can therefore be more accurate to base the temperature calculations on real values.

2.3.2 Long-wave heat radiation

The heat transfer to a concrete surface by solar radiation consists of light with only short wave-lengths. All materials with a temperature above the absolute zero will emit thermal radiation with longer wave-lengths. Unlike thermal conduction or convection the transfer of energy by radiation does not require the presence of material medium. Radiation that is emitted by a surface originates from the thermal energy of matter bounded by the surface. The rate of energy released per unit area is called the emissive power E (Incropera et al. 2007). The upper limit of the emissive power, often called blackbody radiation, is given by the Stefan-Boltzmann law,

$$E_b = \sigma T_s^4 \quad (2.16)$$

where σ is the Stefan-Boltzmann constant of $5.67 \cdot 10^{-8} \text{ W}/(\text{m}^2 \cdot \text{K}^4)$ and T_s is the absolute temperature (K) of the surface. The heat flux emitted by a real surface, E_s , is the blackbody radiation reduced by the emissivity ε

$$E_s = \varepsilon \sigma T_s^4 \quad (2.17)$$

A surface can also receive long-wave heat radiation from its surroundings. In the case of a structure surrounded by the sky and ground, the irradiation from the surroundings may be approximated by emission from a black body with the temperature T_{sur} . If the surface is assumed to have the same absorptivity as emissivity for long-wave radiation, the net rate of radiation heat transfer at the surface is then the difference of the emitted heat radiation and the received heat radiation as

$$q_r = E_s - E_{\text{sur}} = \sigma \varepsilon (T_s^4 - T_{\text{sur}}^4) \quad (2.18)$$

where E_{sur} is the irradiation from the surroundings and ε is the emissivity of the surface. For a normal concrete surface the emissivity varies between 0.85 and 0.95 (Threlkeld 1970). The value used in the FE-calculations presented in the appended papers is 0.9. For a horizontal surface the temperature of the surroundings can be assumed to be the effective sky temperature T_{sky} , which is defined as the temperature the sky would have if it was a surface (Incropera et al. 2007). It can be obtained from measurements of the incident long-wave heat radiation from the sky by a pyrgeometer. From this the effective sky temperature T_{sky} (K) can be derived using the Stefan-Boltzmann law

$$T_{\text{sky}} = \sqrt[4]{\frac{q_{\text{sky}}}{\sigma \varepsilon_{\text{sky}}}} \quad (2.19)$$

where q_{sky} is the long-wave radiation from the sky. The emissivity of the sky ε_{sky} is assumed to be equal to the emissivity of concrete. A vertical surface such as a web wall is influenced

both by the sky and the ground concerning long-wave heat radiation. To calculate the radiation heat transfer q_r the effective sky temperature is replaced by an equivalent temperature, which is a fictitious temperature combining the sky temperature and the temperature of the ground. The ground can be assumed to have the same temperature as the air. The equivalent temperature for a vertical surface is calculated by using the following equation, with all temperatures in (K)

$$T_{eq} = \frac{T_{sky} + T_{air}}{2} \quad (2.20)$$

For the bottom surface on e.g. a box cross-section the air temperature is used instead of the equivalent sky temperature as T_{sur} in Eq. 2.18, since the long-wave radiative heat transfer to or from the bottom surface is only affected by the underlying ground, water and/or other parts of the structure.

In the studies found when general sets of data were used, Emerson (1973, 1977), Alavizadeh-Farhang (1999b), the long-wave heat radiation transfer was given a constant value for a certain climate condition. In investigations presented by e.g. Elbadry and Ghali (1983b), Sheibany and Ghaemian (2006), the long-wave radiation heat transfer was not treated by the use of incoming long-wave radiation. An approximation based on the ambient air temperature was instead used, in which the Stefan-Boltzmann law was rewritten in quasi-linear form to

$$q_r = h_r (T_s - T_{air}) \quad (2.21)$$

where h_r is a radiation heat transfer coefficient defined as

$$h_r = \epsilon ((T_s + T^*)^2 + (T_{air} + T^*)^2)(T_s + T_{air} + 2T^*) \quad (2.22)$$

where T^* is a constant to convert the temperature into Kelvin equal to 273.15 °C. These equations can also be found in Incropera et al. (2007). Mirambell et al. (1991) used a similar approximation for the long-wave radiation heat transfer as Elbadry and Ghali. The difference was the heat transfer coefficient which was expressed as

$$h_r = \epsilon(4.8 + 0.075(T_{air} - 5)) \quad (2.23)$$

The same approximation was used by Branco and Mendes (1993) and Dwivedi et al. (2006). The simplification to derive the radiation heat transfer coefficient from the temperature of the surroundings can be useful for various applications such as when the radiation heat transfer between a material and the surrounding walls in a furnace should be calculated (Incropera et al. 2007). One problem with using this simplification concerning concrete structures is that the surrounding surface can be considered to be the sky. When clouds are present the fictitious temperature of the sky is not very different from the air temperature. But during a clear night the temperature of the sky may be 10°C colder than the air, and thus giving a

larger rate of heat from the concrete surface than calculated by Eq. 2.21. Although the results in the other investigations show a fair agreement between measurements and calculations, all temperature variations may be difficult to capture using a simplification and some temperature differentials may be overestimated.

2.3.3 Convection

Convection heat transfer occurs between a bounding surface, the concrete, and a fluid in motion, the air, when the two are at different temperatures. The convective process can according to Incropera et al. (2007) be described as energy transfer occurring within the air due to the effects of random molecular motion, or diffusion, and bulk fluid motion. Close to the bounding surface the convection is dominated by diffusion, since the velocity of the fluid is low. Further out from the surface the velocity of the moving fluid may increase, which in turn increases the contribution of bulk fluid motion to the convection. Two classifications of convection are used to describe the flow. Forced convection occurs when the flow of air is caused by external sources such as wind, while for natural or free convection the flow is caused by buoyancy forces due to temperature variations in the air. Convection can be either pure forced or pure natural, or a combination of the two. The convective heat flux is modelled regardless of the nature of the convection using Newton's law of cooling (Incropera et al. 2007)

$$q_c = h_c (T_s - T_{\text{air}}) \quad (2.24)$$

where T_s is the surface temperature, T_{air} is the temperature in the surrounding air and h_c is the convection heat transfer coefficient in $\text{W}/(\text{m}^2 \cdot ^\circ\text{C})$. This coefficient depends on conditions in the boundary layer close to the surface, which are influenced by the roughness of the surface and the nature of the fluid motion. According to CEB (1976) the heat transfer coefficient for walls and slabs can be approximated by

$$h_c = 5.6 + 4V \quad \text{if } V \leq 5 \text{ m/s} \quad (2.25a)$$

$$h_c = 7.15V^{0.78} \quad \text{if } V > 5 \text{ m/s} \quad (2.25b)$$

where V is the wind speed. A similar set of empirical equations for surfaces was found in Nevander and Elmarsson (2001)

$$h_c = 6 + 4V \quad \text{if } V \leq 5 \text{ m/s} \quad (2.26a)$$

$$h_c = 7.4V^{0.78} \quad \text{if } V > 5 \text{ m/s} \quad (2.26b)$$

The expressions states that the natural convection is affecting the concrete at lower wind velocities, but at higher velocities the convection is dominated by forced convection. Eqs. 2.26 were used in all the investigations presented in the thesis.

The main factor governing the rate of heat from convection between the concrete and the surrounding environment is the air temperature. The shade air temperature T_{air} can be measured and used in Eq. 2.24 to calculate the convective heat flux. To be able to capture temperature changes in the concrete due to air temperature variations, the temperature should be measured at regular intervals. The climate data measured by the author had an interval of 1 hour, while most of the air temperature data obtained from the meteorological stations had an interval of 3 hours. In most research reported by other authors, only a few values of air temperature were available for the heat transfer calculations. Emerson (1973) used instead a linear approximation for obtaining the air temperature variation during a day. The daily maximum was assumed to occur at 15.00 ± 1 hour and the daily minimum at 05.00 ± 1 hour. Between these occurrences the temperature variation was assumed to be a straight line. In other studies of thermal actions, e.g. Agullo et al. (1996), Elbadry and Ghali (1983b), Branco and Mendes (1993), the air temperature have been approximated using a bi-sinusoidal function. The approximation for the air temperature during a day was expressed as

$$T = A \sin\left(2\pi \frac{t - b_1}{2b_2}\right) + B \quad (2.27)$$

$$T = A \sin\left(2\pi \frac{t + 12 - b_1 - b_2}{2(24 - b_2)}\right) + B \quad (2.28)$$

where

$$A = \frac{T_{\text{max}} - T_{\text{min}}}{2} \quad (2.29)$$

$$B = \frac{T_{\text{max}} + T_{\text{min}}}{2} \quad (2.30)$$

$$b_1 = \frac{h_{\text{max}} + h_{\text{min}}}{2} \quad (2.31)$$

$$b_2 = h_{\text{max}} - h_{\text{min}} \quad (2.32)$$

where T_{max} is the maximum daily temperature, T_{min} is the minimum daily temperature, h_{max} is the time corresponding to the maximum temperature, and h_{min} is the time corresponding to the minimum temperature. Eq. 2.27 is used for the temperature rise during the day starting at minimum daily temperature and Eq. 2.28 is for the temperature drop during the night starting at maximum daily temperature. One drawback with using an approximation is that sudden temperature drops and rises can be hard to capture. Sometimes, as an example, the weather during cold nights in the winter can change abruptly, causing a temperature rise of 30°C to occur in only a few hours. If measured data are used, this temperature rise is captured, while

with the use of an approximation the temperature rise will be spread out during more hours which then may not give as accurate results for the calculations and underestimates the effects.

2.3.4 Enclosure temperature

The inside cavity in a box-girder bridge will also influence the temperature distribution in the concrete. A heat exchange will occur between the internal air and the inside surfaces due to convection heat transfer and between the inside surfaces of the walls and slabs due to radiation heat transfer. To simplify the complex interactions the internal air temperature is used as input for both the radiative and the convective parts:

$$q_{in} = q_{c,in} + q_{r,in} = h_c(T_s - T_{in}) + \sigma \varepsilon_c(T_s^4 - T_{in}^4) \quad (2.33)$$

where $q_{c,in}$ is the convective heat transfer, $q_{r,in}$ is the radiative heat transfer, T_{in} is the internal air temperature with the other parameters as prior definitions. The convection coefficient can be set to $2 \text{ W}/(\text{m}^2 \cdot ^\circ\text{C})$ for the internal interactions according to Emerson (1973). If the internal air temperature is unknown, which is normally the case when using climate data as input, the inside cavity heat transfer has to be treated by determining the inside air temperature or couple the calculations directly to the surface temperatures. Branco and Mendes (1993) dealt with the heat exchange in the internal surfaces by convection and radiation by setting the heat exchange equal to the increase or decrease of internal energy of the box-air volume. This energy change was coupled to the internal air temperature in the box.

According to Bohn and Anderson (1986) the average core temperature for a fluid in an enclosed space depends on the average temperature of the inside walls. The inside air temperature, T_{in} , can therefore be calculated from the temperatures of the inside walls. This can in turn be incorporated in a FE-calculation by the use of iteration. The start value for T_{in} can be set to the ambient air temperature; the simulation is then repeated with a new T_{in} calculated from the previous results. This procedure was used in the FE-simulations in Papers III-V.

2.4 Thermal material properties

The material parameters of the structure have a large impact on the thermal actions and resulting stresses. A material which has a high heat conduction capacity such as steel will be less affected by in-stationary temperature differentials in the structure, since it has a large ability of evening out the temperature. A material with lower heat conduction capacity such as concrete will on the other hand get a more non-uniform spatial temperature distribution due to changes in boundary conditions, since it can't conduct heat to the cooler parts rapidly enough. Two material properties affecting the temperature are the previously described surface properties solar absorptivity and emissivity. Internal material properties affecting the temperature in a material are density, specific heat and thermal conductivity. The resulting

strains and stresses are affected by the thermal expansion coefficient and the modulus of elasticity, which are described in chapter 3.

The material properties can be measured directly for each specific concrete. The measurements are however time consuming and may not give proper results due to variations in exposure for the test specimens and the real structure. A general set of data which can be used for an arbitrary concrete structure was deemed important to find at the start of the project, since for most existing structures or future structures no data concerning these properties are available. The material data used in the appended papers are therefore based on values given in literature and in scientific papers by other authors.

2.4.1 Density

The thermal diffusivity of a material specified in Eq. 2.1, is governed by density and specific heat. The density of concrete is governed by the densities of the main components in concrete; water, cement and aggregate (Neville 1995). Since the largest part is aggregate, and due to the varying densities of different aggregate types, this is the most important factor. For normal concrete the density varies between 2100 and 2500 kg/m³ (Ljungkrantz et al. 1994). The density of the concrete used for the slab in Paper I was about 2400 kg/m³, which is the value used in all the appended papers. In Table 2.2 the material properties of concrete used in studies by other authors are listed. As can be seen in the table the most common value used for the density of concrete is 2400 kg/m³.

Table 2.2 Material properties of concrete used by other authors

Author	Density, (kg/m ³)	Specific heat, J/(kg · °C)	Conductivity, W/(kg · °C)
Emerson (1973)	2400	960	1.4
Sheibany and Ghaemian (2006)	2450	912	2.62
Branco and Mendes (1993)	2400	1000	1.5
Mirambell et al. (1991)	2400	960	1.5
Elbadry and Ghali (1983b)	2400	960	1.5
Alavizadeh-Farhang (1999b)	2350	1000	1.7
Dwivedi et al. (2006)	2400	960	1.5
Fu et al. (1990)			1.9
Hirst (1984)	2500	960	1.4

2.4.2 Specific heat

The specific heat represents the heat capacity of the concrete. It is not as dependent on the aggregate type as the density, but is instead more affected by the moisture content (Marshall 1972). The water-cement ratio and temperature are also important factors concerning this property, but since the temperature range under normal environmental conditions is small the effect of temperature change on the specific heat capacity will also be small. The specific heat capacity of concrete normally varies according to Neville (1995) between 840 and 1170 J/ (kg

· °C) and according to Ljungkrantz et al. (1994) between 800 and 1000 J/ (kg · °C). Based on this information a value of 900 J/ (kg · °C) was chosen for the concrete in the structures in the appended papers. As can be seen in Table 2.2, other authors have used values between 900 and 1000 J/ (kg · °C).

2.4.3 Thermal conductivity

Thermal conductivity describes the heat conduction capacity of the material. It is dependent on the density and composition of the concrete, the conductivity of the included components, and the moisture content. Khan (2001) found that the conductivity can vary between 1.6 and 3.6 W/(kg · °C) depending on the aggregate type and moisture content. The temperature level also affects the conductivity, but for normal environmental temperature fluctuations this effect can be neglected. According to Neville (1995) the thermal conductivity for a saturated concrete is generally varying between 1.4 and 3.6 W/(kg · °C). Since it is difficult to know the actual moisture content of the structure in use, Loudon and Stacey (1966) suggested typical values to use based on the density. A concrete exposed to weather with a density of 2400 kg/m³ has a thermal conductivity of about 2.5 W/(kg · °C), which is the case for most bridges. In Papers I and III the thermal conductivity was chosen to 2.5 W/(kg · °C) based on the information given above. This value gives a good agreement between measured values and the FE-calculations. In most studies of thermal actions presented by other authors listed in Table 2.2 a conductivity around 1.5 W/(kg · °C) has been used, which could be seen as quite low for concrete in a bridge which is highly weather exposed. A low thermal conductivity will produce larger temperature differentials, and if it is underestimated the differentials may be exaggerated.

2.4.4 Thermal properties of Asphalt

For most bridges in Sweden and Europe a paving layer of asphalt is placed on top of the bridge deck; although in some cases a concrete paving layer may be used. In either case the paving layer may or may not be mechanically connected to the bridge structure. If unconnected it will not affect the stress field in the bridge by restraint. A paving layer will, however, always affect the temperature distribution in the bridge, since it will cover most of the top side of the bridge deck and may give an insulating effect. It is therefore important to consider the effect of the paving layer when investigating or using thermal actions.

In Soukhov (2000) and in the background document of the Eurocode ENV 1991-2-5 (CEN 1996) it is stated that the difference in material properties between concrete and asphalt may be neglected. However it is shown in Paper II that significant variances in the linear temperature differentials are found due to varying material properties between concrete and asphalt. It is therefore important to consider this when calculating thermal actions.

The material properties with the highest differences compared to concrete are the solar absorptivity and the thermal conductivity. As was discussed in section 2.3.1 the solar absorptivity used in the FE-model is 0.9 for asphalt compared to 0.5 for concrete, which will increase the amount of energy absorbed by the material. The emissivity can be said to be the

same as for concrete; 0.9. The other property that has a significant difference compared to concrete apart from the solar absorptivity is the thermal conductivity. The conductivity for pure asphalt is low; a value of 0.06 is given by Incropera et al. (2007). The total conductivity depends on the mix of aggregate and asphalt, a value between 0.5 and 1.5 has been found in other studies (Carlson et al. 2010). The material properties for asphalt chosen and used in the studies presented in Paper II and V are a density of 2200 kg/m^3 , a specific heat of $880 \text{ J/(kg} \cdot ^\circ\text{C)}$ and a thermal conductivity of $0.8 \text{ W/(kg} \cdot ^\circ\text{C)}$. In Table 2.3 the density, specific heat and thermal conductivity for asphalt used in studies by other authors are presented. The density is about $2100\text{-}2200 \text{ kg/m}^3$ while the specific heat is varying from $840\text{-}880 \text{ J/(kg} \cdot ^\circ\text{C)}$. The conductivity for asphalt used in previous studies is mostly around $0.8\text{-}0.9 \text{ W/(kg} \cdot ^\circ\text{C)}$, while the concrete can have a conductivity of $2.5 \text{ W/(kg} \cdot ^\circ\text{C)}$ if it is weather exposed.

Table 2.3 Material properties of asphalt used by other authors

Author	Density, (kg/m^3)	Specific heat, $\text{J/(kg} \cdot ^\circ\text{C)}$	Conductivity, $\text{W/(kg} \cdot ^\circ\text{C)}$
Branco and Mendes (1993)	2200	900	0.8
Mirambell et al. (1991)	2200	880	0.83
Dwivedi et al. (2006)	2100	920	0.93
Elbadry and Ghali (1983b)	2100	920	0.93
Hirst (1984)	2100	840	0.7
Dickinson (1978)	2240	840	1.5 or 2.5

2.5 Temperature measurements

Measurements of temperature in a concrete structure can be performed in various ways. A common equipment to use is a thermo-couple, which consist of two isolated metal wires welded together in one end. This end can be cast into the concrete or placed into it after hardening. For the temperature measurements performed and presented in Paper I this type of sensor was used, since it is a robust and simple technique.

For the New Svinesund Bridge the temperature measurements were performed using PT100 temperature sensors cast into the concrete (Karoumi and Andersson 2007, Karoumi et al. 2009). It measures the resistance of a platinum element which changes with changing temperature. In the concrete arch of the bridge 28 such sensors were placed prior to casting at five sections, as seen in Figure 2.6. For more information about the bridge see Darholm et al. (2007). The results used for the study presented in Paper III were obtained from the section at the top of the arch, where it is more or less horizontal. At each section with temperature sensors strain gauges were also placed measuring the strain in the longitudinal direction of the arch. No measurements of transverse strains were available for the used section or from elsewhere in the concrete arch, which was unfortunate since the project has been focused on transverse stresses and strains. The results from the FE calculations of thermal stresses presented in Paper IV have therefore not been possible to verify against strain measurements.

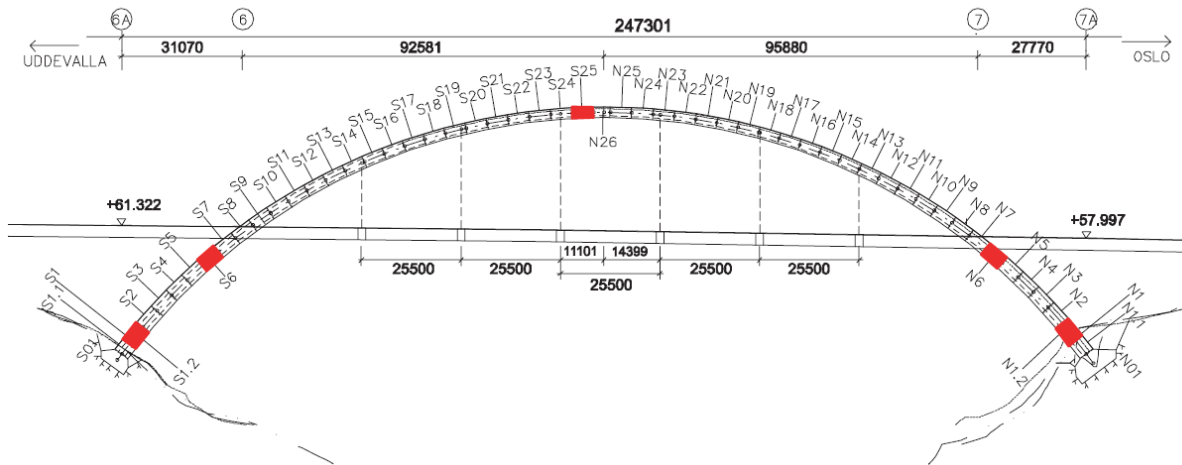


Figure 2.6 Positions of the measuring sensors (red) (Karoumi and Andersson 2007)

3 Thermal actions and stresses

As mentioned before spatial and time variations in temperature will produce various types of movements in a concrete structure. Due to the non-uniformity of the temperature distribution not only longitudinal but also transverse movements will occur. To handle these movements in design, it is convenient to divide the temperature profiles into its components as described in Figure 2.1. The average temperature T_{avg} and linear temperature differential ΔT components can be calculated for a one-dimensional distribution as

$$T_{\text{avg}} = \frac{1}{h} \sum T_i h_i \quad (3.1)$$

$$\Delta T = \frac{12}{h^2} \sum (T_i x_i h_i) \quad (3.2)$$

where T_i is the temperature in layer i , h_i is the height of the layer, h is the thickness of the section, x_i is the coordinate of the centre of layer i from the gravity point. The non-linear temperature component T_{nl} is then defined as the difference between the actual temperature and the average temperature and linear temperature differential for each point in the section as

$$T_{\text{nl}} = T - T_{\text{avg}} - \Delta T \quad (3.3)$$

The temperature components for a two-dimensional temperature distribution, which is the case for a box cross-section, can be calculated in a similar fashion. The average temperature T_{avg} is calculated as an integral over the entire cross section

$$T_{\text{avg}} = \frac{1}{A} \int_A T(x, y) dA \quad (3.4)$$

where $T(x, y)$ is the temperature in element dA , A is the cross-section area and dA is the element area. The linear temperature gradient ΔT over the cross-section is calculated vertically or horizontally as

$$\Delta T_x = \frac{12}{b^2} \int_A T(x, y) x dA \quad (3.5)$$

$$\Delta T_y = \frac{12}{h^2} \int_A T(x, y) y dA \quad (3.6)$$

where ΔT_x is the temperature gradient in the horizontal direction, ΔT_y is the temperature gradient in the vertical direction, b is the width of the cross section, h is the height, x and y are

horizontal and vertical coordinates respectively with origin in the centre of gravity. The average temperature and linear differential over each separate slab or wall can, simplified, be calculated as for a one-dimensional distribution. The non-linear component in a two-dimensional calculation is based on the same principle as for the one-dimensional case; it is the difference between the actual temperature and the combined average temperature and linear differential.

Due to the temperature variations in the concrete, the material will expand or contract depending on temperature rise or drop. Due to uneven temperature distribution, these movements are different in different parts of the structure. With the previously described division of the temperature field in mind the average temperature component can be said to mainly produce longitudinal movements along the bridge, while the linear temperature differential will give rise to curvature of the bridge in the transverse directions. The non-linear part of the temperature field will also contribute significantly to the movements in the structure. If the structure is free to move in all directions only self-equilibrating stresses will be induced. If the structure is restrained by the supports, continuity stresses will be induced which may contribute to cracking in the structure.

At cross-sectional level, a similar thinking concerning the movements can be applied. If the cross-section is solid and free to move, only self-equilibrating stresses will be produced. In a T-girder or a box-girder bridge, the various parts will be restrained by each other. A larger average temperature in a part of the section will cause the part to expand; the expansion will then be restrained by the adjacent parts and stresses will be produced. A temperature differential over, as an example, a wall in a box cross-section will produce a curvature in that wall, which will be more or less restrained by the adjacent parts producing restraint stresses in the wall.

3.1 Thermal behaviour in the longitudinal direction

In the longitudinal direction along a bridge the nature of the thermal behaviour depends highly on the support conditions. A simply supported structure will not be subjected to any imposed external restraint, but only internal restraint due to the geometry of the section. Figure 3.1 shows a simply supported beam which is subjected to a non-uniform temperature distribution over the cross-section with the top warmer than the bottom.

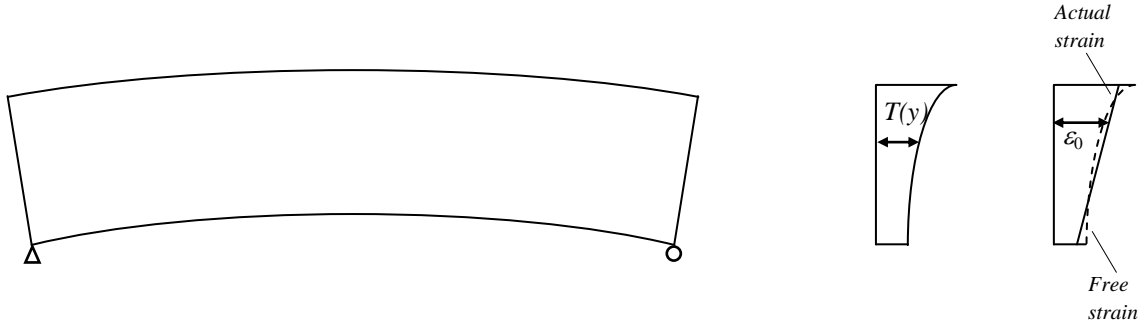


Figure 3.1 A simply supported beam subjected to a thermal load

According to Elbadry and Ghali (1986) the free strain in the longitudinal direction of such a beam at any location with coordinate y can be expressed as

$$\varepsilon_f = \alpha T(y) \quad (3.7)$$

where α is the thermal expansion coefficient and $T(y)$ is the temperature at coordinate y . To restrain this free strain an artificial stress is required which can be expressed as

$$\sigma_{\text{restraint}} = -E\alpha T(y) \quad (3.8)$$

where E is the modulus of elasticity of the concrete. The resultants on the section from this stress are

$$N = \int \sigma_{\text{restraint}} dA \quad (3.9)$$

$$M = \int \sigma_{\text{restraint}} y dA \quad (3.10)$$

The artificial restraint is then removed by introducing equal but opposite forces. With plane sections remaining plane the resulting strain at any location is given by

$$\varepsilon = \varepsilon_0 + \psi y \quad (3.11)$$

Where ε_0 is the axial strain at the centroid and ψ is the curvature which is given by

$$\varepsilon_0 = -\frac{N}{EA} \quad (3.12)$$

$$\psi = -\frac{M}{EI} \quad (3.13)$$

If Eqs. 3.8 – 3.10 are substituted into Eq. 3.12 and Eq. 3.13; expressions for the axial strain and curvature at a section of a statically determinate member are obtained

$$\varepsilon_0 = \frac{\alpha}{A} \int T(y) b dy \quad (3.14)$$

$$\psi = \frac{\alpha}{I} \int T(y) b y dy \quad (3.15)$$

where A is the cross-sectional area and I is the moment of inertia for the section. The difference between the free strain and the actual strain induces a stress distribution in the concrete expressed by

$$\sigma = E(\varepsilon_0 + \psi y - \alpha T(y)) \quad (3.16)$$

These stresses are self-equilibrating since their resultants must be zero. When the different temperature components are calculated or obtained from design codes, the equations for the axial strain and curvature can be simplified into

$$\varepsilon_0 = \frac{\alpha}{A} (T_{\text{avg}} - T_0) \quad (3.17)$$

$$\psi = \frac{\alpha}{I} \Delta T \quad (3.18)$$

where T_0 is the initial temperature of the structure, T_{avg} is the average temperature and ΔT is the linear temperature differential.

When the support conditions are different, e.g. when the bridge have more than one span or is no longer simply supported, the structure will be restrained and statically indeterminate reactions and continuity moments will appear. If the temperature distribution is non-uniform resulting continuity stresses are produced, which have to be added to the self-equilibrating stresses to obtain the total stress. Statically indeterminate reactions and bending moments can be calculated using the general displacement or force methods. The resulting continuity reactions and moments are proportional to free curvature of each span and the stiffness EI . According to Elbadry and Ghali (1986) the reaction and moment multipliers in continuous beams are as in Figure 3.2.

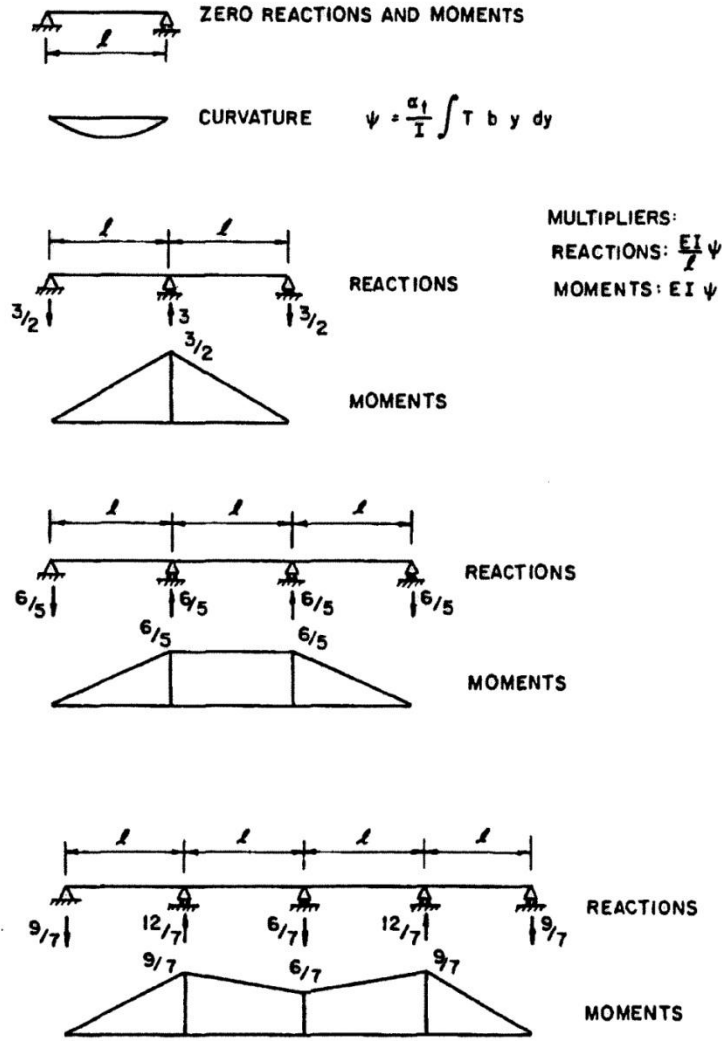


Figure 3.2 Reactions and bending moments in continuous beams due to temperature rise (Elbadry and Ghali 1986)

The continuity reactions and moments can then be expressed with

$$R = \frac{m\alpha E}{l} \int T(y) b y dy \quad (3.19)$$

$$M = m\alpha E \int T(y) b y dy \quad (3.20)$$

where m is the multiplier constant according to Figure 3.2 and l is the span length. For a structure with a cross-section where the temperature distribution in both the vertical and horizontal directions are of importance, such as a box-girder bridge, the axial strain and curvatures in both directions are given by

$$\varepsilon_0 = \frac{\alpha}{A} \iint T(x, y) dx dy \quad (3.21)$$

$$\psi_x = \frac{\alpha}{I_x} \iint T(x, y) y dx dy \quad (3.22)$$

$$\psi_y = \frac{\alpha}{I_y} \iint T(x, y) x dx dy \quad (3.23)$$

where ψ_x is the curvature in the horizontal direction, ψ_y is the curvature in the vertical direction, I_x is the moment of inertia around the y-axis and I_y is the moment of inertia around the x-axis. The self-equilibrating stresses induced in the cross-section is then

$$\sigma_{x,y} = E(\varepsilon_0 + \psi_x y + \psi_y x - \alpha T(x, y)) \quad (3.24)$$

Resulting thermal stresses in the longitudinal direction have been investigated and discussed by several authors. Prakash Rao (1986) presented a study on the resulting stresses caused by non-uniform temperature distribution in concrete bridges based on environmental data for Christchurch, New Zealand, Melbourne, Australia, and New Delhi, India. The critical temperature distributions which gave the largest longitudinal stresses in a concrete box-girder section for each location were obtained from finite difference calculations using climate input data. The critical distributions varied between the different locations, which in turn gave a variation for the resulting critical thermal stresses although the maximum values of the tensile stress were close to each other. The results showed that critical tensile stresses appeared near the bottom of the web due to differences in temperature between the top and bottom slabs. It could also be concluded that the longitudinal stresses were not directly dependent on the ambient air temperature; higher ambient temperatures did not always give larger stresses. The study stressed the importance of using both negative and positive gradients, although the bending moments caused by curvature and support restraint were larger in the afternoons due to positive gradient.

Stresses in a structure are typically caused by either external load, such as loads from traffic, or by restrained forces in the structure (Jokela 1983). Intentional or unintentional restraint forces due to restraint deformations of a structure, referred to as external restraint, are produced in statically indeterminate structures. Intentional restraint forces are caused by prestressing of a structure, while unintentional restraint forces can be caused by differences in shrinkage and temperature or by settlements of the supports. Stresses due to restrained strains in the cross-section, internal restraint, are produced by non-stationary temperature distribution or non-uniform shrinkage. Such stresses can appear both in statically determinate or indeterminate structures, but they do not develop longitudinal sectional forces in the structure, since the sum of the stresses in each cross-section of the structure is zero.

The restraint in the structure, and thus the resulting section forces, is significantly reduced if cracks are present in the structure. The cracks reduce the moment of inertia in the structure which in turn reduces the stiffness. When the concrete is assumed to be linear-elastic, the thermal stresses may be overestimated due to the neglect of cracks. Often, when load-bearing structures are designed for serviceability, the actual external loads on the structure do not contribute to cracking. If unexpected cracks do occur it is often due to secondary stresses in the structure which have not been considered in the design.

A method for calculating thermal stresses in cracked concrete beams (Cooke et al. 1984) and bridges (Thurston et al. 1984) was developed in New Zealand and based on the work performed by Priestley (1978) and Hunt and Cooke (1975). This development was done to be able to adopt partially prestressed concrete bridges, so that controlled cracking could take place under thermal loading. The results showed that cracking at critical sections reduced the thermal moments with 46 % for a box-girder model and 27 % for a T-beam model. In this study the cracking was extensive due to very large thermal gradients of about 40 °C which occurred in conjunction with high stress levels from dead load and live load. One conclusion from the investigation was that for more realistic conditions with lower thermal gradients it is unlikely that such extensive cracking would occur, and the thermal moments would thus not be reduced in such a magnitude. This led in turn to the conclusion that such an investigation with consideration of cracked sections as was performed here is only merited for the largest prestressed bridges.

The effects of cracking on restraint forces and stresses due to temperature were also investigated by Elbadry and Ghali (1995). They presented an analytical model for determining the effect of a progressive reduction in the stiffness on the stresses in indeterminate structures. Cracking had a beneficial effect on the restraint forces and stresses, but if such cracks are allowed they have to be controlled by an adequate amount of reinforcement. Further studies of this were presented by Ariyawardena et al. (1997) where reinforced concrete beams were subjected to thermal gradient with the rotations of the beam ends prevented. The bending moment due to the thermal gradient was much higher in a fully prestressed member compared to a partially prestressed cracked member. A similar nonlinear analysis of concrete dams subject to thermal loads was presented by Majorana et al. (1990).

Studies of the effect of temperature gradients in beams, walls and slabs with cracked concrete were presented by Elgaaly (1988) and Vecchio et al. (1993). Elgaaly proposed allowable thermal gradients for such structures as a function of design parameters such as concrete compressive strength and reinforcement area. The study was focused on the ultimate limit state, when cracking already had occurred. Vecchio et al. tested reinforced concrete slabs under combined thermal and mechanical load and found that cracks and thermal creep effects reduced the stiffness of the concrete rapidly, which reduced the restraint forces. At ultimate load conditions the effect of temperature was minimal. This indicates that thermal actions are more important at serviceability limit state.

3.2 Thermal behaviour at cross-sectional level

At cross-sectional level a non-uniform temperature distribution will produce various movements. Depending on the geometry, e.g. solid or box section, T-girder or slab, the movements will in turn produce stresses. For a hollow box cross-section, the walls and slabs will cause internal restraint in the cross-section. If a temperature differential over a wall is present the wall wants to curve, the adjacent slabs will restrain the movements in the wall and stresses will be induced.

In the Eurocode for thermal actions (SS-EN 1991-1-5 2003) it is stated that for large bridges with concrete box cross-sections care should be taken during the design due to temperature differentials over the walls. A value for a linear temperature differential of 15 °C is given as a recommendation. No information concerning transverse effects is given in the background document of the Eurocode (CEN 1996). Few studies of thermal actions in the transverse direction at cross-sectional level of a bridge structure by other authors exists, most studies have been focused on longitudinal stresses and behaviour. Elbadry and Ghali (1983a, 1986) calculated stresses in the transverse direction by considering a plane frame made up of a segment between two cross-sections in the box. A non-linear temperature variation was applied and the resulting stresses were calculated using the displacement method. They found that the bending moments arising in the calculations were high enough to produce stresses of 4.14 MPa at the bottom surface of the top slab, which would contribute to cracking in the structure as in Figure 3.3.

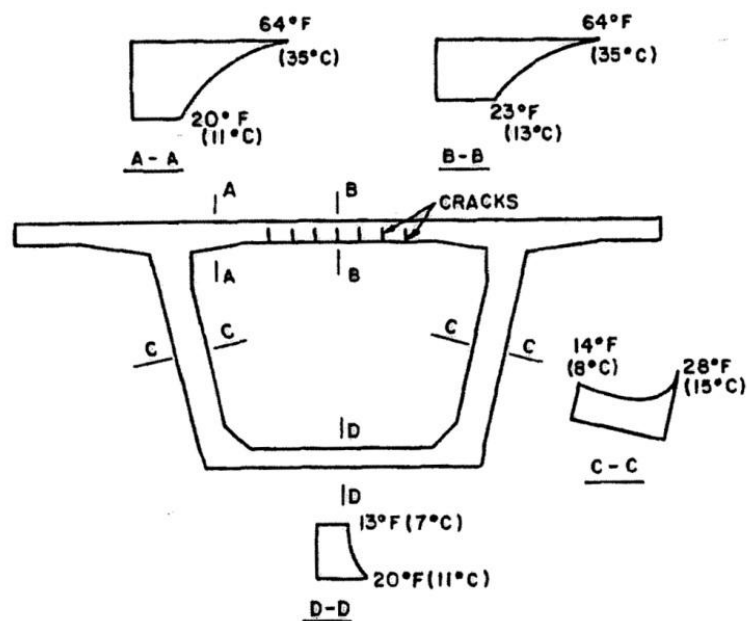


Figure 3.3 Temperature distributions over different parts of a bridge cross-section with resulting cracks (Elbadry and Ghali 1986)

Mirambell and Aguado (1990) investigated the effect of various geometrical parameters at cross-sectional level on the thermal response of concrete bridges. They found that the thickness ratio between the upper and bottom slabs and the superstructure depth were the

parameters with the largest influence on the thermal response and stress distributions. It was also found in the results that the ratio between the web and upper slab thicknesses did not have a large effect on the longitudinal stress distribution in the cross-section. The stress distribution along the web axis was shown to be almost unaffected by the thickness difference. Unfortunately only the longitudinal stress distribution along the web axis was shown, and not the transverse stress distributions over the webs and slabs individually. In the results presented in Paper IV, where cross-sections with varying geometry were investigated, the difference in thickness between the webs and the slabs was found to be the most significant geometrical factor. This discrepancy shows the difficulties in modelling thermal actions, and the variations that may be found between different cross-sections and climate zones.

Prakash Rao (1986) stated that the transverse moments in a box-girder are more affected by the temperature difference between the top and bottom surfaces of the top slab than the differences in average temperature between the top and bottom slabs. This agrees with the results presented in this thesis, where the average temperature difference is deemed to have a small, if any, impact on the transverse thermal stresses. In his investigation only one cross-section was investigated however, with a larger thickness for the webs than the slabs. A general conclusion concerning the location of the largest transverse moments and stresses can therefore not be drawn from the study.

A bridge cross-section can at some level be seen as a reinforced concrete frame structure. The effect of thermal gradients on concrete frame structure has been studied not only for bridges but for general frames by e.g. Vecchio (1987) and Vecchio and Sato (1990). An iterative analytical procedure was developed which could incorporate the effect of temperature and mechanical loads on a concrete section using effective stiffness factors.

The most extensive study found on transverse effects was presented by Sveinson (2004). He analysed two cross-sections in a concrete box-girder bridge in the transverse direction. The temperature distribution of the bridge was calculated with the same program as used by Elbadry and Ghali (1983a, 1986), with approximations for the thermal factors as described in section 2.3. The convection heat transfer was altered to incorporate variations in wind speed around the bridge girder. The results showed that the temperature differential through the walls and slabs can lead to significant transverse stresses and bending moments when the frame action of the cross-section is considered. The temperature gradient over each wall and slab gave a larger effect on the transverse bending moments than the temperature gradients in the horizontal and vertical directions of the entire cross-section. The stresses from temperature effects in this case, when added to the stresses due to self-weight and traffic loads, increased the total bending stress by 50 % for a 14 m deep cross-section and 24 % for a 4.5 m deep cross-section. The results indicate the importance of considering transverse bending moments and stresses due to temperature differentials in the walls and slabs of a box cross-section.

Pei-Heng et al. (2010) used a 3D solid FE-model to calculate stresses induced by temperature distribution in a concrete bridge. This was done following the discovery of longitudinal cracks

in several box-girder bridges in China. The thermal stresses were calculated based on temperature distributions specified in the Chinese code JTG D60-2004, where two situations are specified; either a positive gradient of 14°C and a negative gradient of -7 °C, or a positive gradient of 20 °C and a negative gradient of -10 °C. The first loading case is similar to the characteristic values in the Eurocode. A maximum lateral, or transverse, tensile stress of 2.58 MPa was obtained when the web wall had a thickness of 2.4 times the thickness of the top slab for loading case 2. For loading case 1 the maximum lateral tensile stress was 1.88 MPa. In both cases the maximum stress appeared in the thinner top slab. This can be compared to the results presented in Paper V where the maximum thermal tensile stress was about 1.4 MPa when the bridge was prevented from movement in the longitudinal direction and 1.9 MPa when there was no mid span casting. Here the maximum tensile stress appeared in the thinner south web wall. The occurrence of the maximum stress in the thinner parts in these studies confirms the results presented in Paper IV, where the thickness ratio between the slabs and walls was deemed the most important geometrical factor. The largest tensile stresses appear in the thinner member independent of whether the member is horizontal or vertical.

A general lack in the design recommendations concerning transverse effects due to temperature differentials over the individual walls and slabs exists within the present codes (AASHTO 1989, SS-EN 1991-1-5 2003). A description of the stated recommendations is given in chapter 4 of the thesis, where it can be seen that the cross-section should be designed with consideration to the thermal effects. This lack of information was a motivation for the additional investigation presented in Paper IV, where various geometries were tested.

3.3 Mechanical material properties

3.3.1 Thermal expansion

The expansion coefficient for concrete depends on the thermal expansion of the cement paste and aggregate, and the moisture content. Since concrete consists of about 70 % aggregate, the expansion coefficient of the aggregate is the most important factor (Ljungkrantz et al. 1994). In Table 3.1 the coefficient of thermal expansion for concretes with various aggregate types are presented.

Table 3.1 Measured thermal expansion coefficient of concretes with different aggregate types, $\times 10^{-6}$ ($^{\circ}\text{C}$) (Ljungkrantz et al. 1994)

Aggregate	Condition	Cement content (kg/m^3)				
		200	300	400	500	600
Quartz, crushed	Wet	11.6	11.6	11.6	11.6	11.6
	Dry	12.7	13.0	13.4	13.8	14.2
Quartz, sand, gravel	Wet	11.1	11.1	11.2	11.2	11.3
	Dry	12.2	12.6	13.0	13.4	13.9
Granite	Wet	7.9	8.1	8.3	8.5	8.8
	Dry	9.1	9.7	10.2	10.9	11.8
Limestone	Wet	5.4	5.7	6.0	6.3	6.8
	Dry	6.6	7.2	7.9	8.7	9.8
Basalt	Wet	7.2	7.4	7.6	7.8	8.0
	Dry	8.5	9.1	9.6	10.4	11.1

The stresses due to thermal effects in concrete are directly dependent on the magnitude of the thermal expansion coefficient. To reduce such stresses one way could be to reduce the expansion coefficient, by e.g. changing aggregate type etc. In the Eurocode SS-EN 1991-1-5 (2003), the recommended value for the expansion coefficient is $10 \cdot 10^{-6}$ ($^{\circ}\text{C}$), which is also the value used in the FE-calculations presented in Paper IV and V. The thermal expansion coefficients of concrete and asphalt found in work presented by other authors are presented in Table 3.2 where it can be seen that the coefficient for concrete varied between $8 \cdot 10^{-6}$ to $12 \cdot 10^{-6}$ ($^{\circ}\text{C}$). For asphalt a larger thermal expansion coefficient of $15 \cdot 10^{-6}$ to $20 \cdot 10^{-6}$ ($^{\circ}\text{C}$) was used. However if the asphalt paving is not mechanically connected to the bridge deck the expansion of this paving will not affect the stresses in the concrete. The thermal expansion coefficient for asphalt in Paper V is therefore set to the same as for concrete, with a much lower stiffness to eliminate the mechanical influence of the paving layer.

Table 3.2 Thermal expansion coefficients for concrete and asphalt used by other authors

Author	Concrete ($\times 10^{-6}$) ($^{\circ}\text{C}$)	Asphalt ($\times 10^{-6}$) ($^{\circ}\text{C}$)
Elbadry and Ghali (1983b)	8	20
Dwivedi et al. (2006)	10	20
Hirst (1984)	12	15
Sheibany and Ghaemian (2006)	8.05	

3.3.2 Modulus of elasticity

Another important factor governing the stresses in a structure is the modulus of elasticity, E . At low stress levels the concrete can be considered as linear; it can therefore be seen to a certain degree an elastic material (Neville 1995). An increase in modulus of elasticity will then give a corresponding increase in the stress level with increasing strain. The modulus of

elasticity is somewhat correlated with the strength of the concrete; a larger strength will give a larger modulus of elasticity (Ljungkrantz et al. 1994).

The strength and modulus of elasticity depends highly on the material composition; for concrete mainly the aggregate type, cement and water content. The elastic modulus can vary between 10 and 100 GPa for different aggregate types (Ljungkrantz et al. 1994), this will affect the concrete. For regular concrete the elastic modulus for cement paste is lower; it depends on the water-cement ratio and the amount of air in the cement paste. An increase in aggregate content will therefore give an increase in modulus of elasticity. It is also affected by the moisture content and the temperature. An increase in moisture content gives a slight increase in modulus of elasticity. In the interval 0 to 100 °C the effect of temperature can be neglected. If the temperature is below zero a slight increase of the modulus of elasticity is achieved due to frozen water in the concrete pores.

Most data concerning the modulus of elasticity of concrete are collected for concrete in compression (Neville 1995). For concrete in tension the best assumption is that the modulus of elasticity is equal to the modulus in compression. For the research performed and presented in Paper IV and V the modulus of elasticity was set to 30 GPa, with this one value chosen to be able to compare the various results. The focus in the present research is less on absolute values of stress and more on relative effects, which is the reason for choosing an arbitrary value. In the next sections the long-term concrete behaviour is described, and how this will be affected by spatial and temporal temperature variations.

3.3.3 Long-term effects

When subjected to a sustained load the strain in a concrete structure will increase and the concrete exhibits creep. Creep has a significant effect on concrete structures, since the increase in strain can be several times as large due to creep as from initial loading which will give larger deformations. For indeterminate structures creep may have a beneficiary effect since it may relieve stress concentrations and restraint from shrinkage or temperature due to the reduction of stiffness from creep effects.

The ambient conditions around a structure have a large impact on the creep. One important factor is the relative humidity of the surrounding air; generally it can be said that lower relative humidity give larger creep. In reality it is not the relative humidity that directly influences the creep, but the drying in the concrete which occurs due to the lower RH (Neville 1995). If the load is applied while the concrete is drying the creep is enhanced compared to if the concrete has reached hygral equilibrium with the surroundings before the load is applied. Figure 3.4 shows creep of concrete specimens cured in the same conditions but stored in different RH while loaded. It can be seen that the specimen in 50 % RH exhibits a much larger creep than the specimen in 100 % RH. The other environmental factor affecting creep is the temperature in the surrounding environment, which will be described further in the next section.

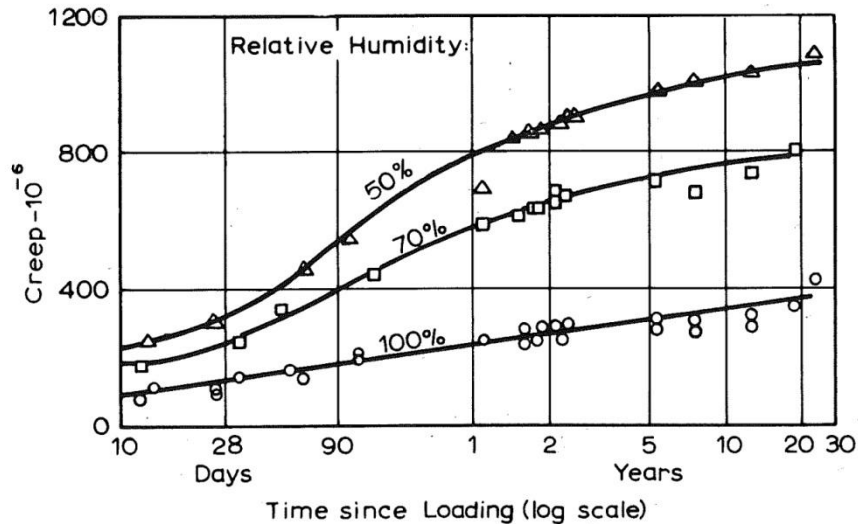


Figure 3.4 Creep of concrete cured in fog for 28 days, then loaded and stored at different relative humidities (Neville 1995)

Creep is also affected by the proportions of the concrete mix (Neville 1995). In concrete it is only the hydrated cement paste which undergoes creep and not the aggregate itself. The magnitude of creep therefore depends on the volumetric content of the aggregate and cement paste. An increase in aggregate content from 65 to 75 volume per cent may decrease creep by 10 per cent. The properties of the cement and aggregate used in the concrete will as a consequence also affect the creep magnitude, since they affect the strength of the concrete.

Creep also depends on the time of application of the load. This effect is most pronounced in the curing phase when the concrete hardening is still significant. The research considered here is primarily concerned with concrete at higher ages, which means that the effect of aging on creep can be neglected. In that case creep is proportional to the stress for moderate stress-strength ratios.

3.3.3.1 Effect of temperature on creep

For a structure at normal temperatures such as a bridge, the temperature effect on creep is usually considered as less than the effect of relative humidity (Neville 1970). The descriptions of effects on creep from temperature is limited in this thesis to concrete under service and not concrete during the curing phase, since this is outside the scope of this research. Creep in concrete increases with increasing temperature, and decreases with decreasing temperature. According to measurements presented by Nasser and Neville (1966) the creep for a concrete with stress/strength ratio of 0.7 increased with about 3.5 times when the temperature was 71 °C (160 °F) compared to 21 °C (70 °F), see Figure 3.5. The effect of creep decreased when the temperature was increased to 96 °C (205 °F). Almost no effect on the rate of creep was observed if the temperature was 46 °C (115 °F), this indicates that the largest temperature effects on creep occurs when the temperature is in the span 50 °C to 90 °C.

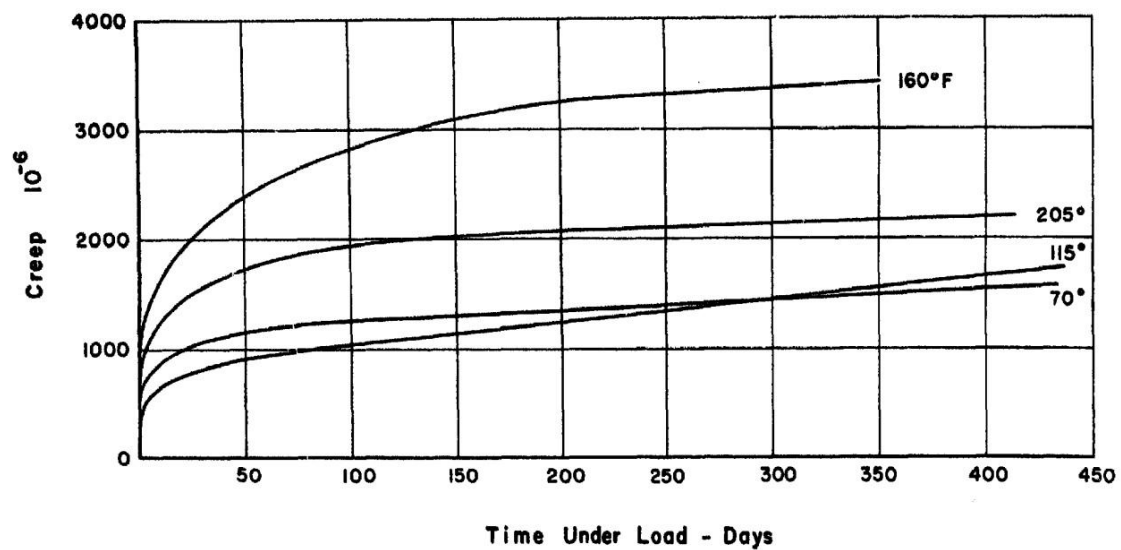


Figure 3.5 Relation between creep and time under load for a stress-strength ratio of 0.7 and different temperatures (Nasser and Neville 1966)

When considering the influence of sustained temperature on creep it can, according to England and Ross (1962) and England (1977, 1980), be convenient to separate the effects of uniform temperature from the effects of temperature gradients and variations in time. In a statically determinate structure under loading an increase in uniform temperature increases the rate of the time-dependent deformations of the structure. A temperature gradient increases or decreases this deformation rate further depending on the direction of the gradient. Although deformations occur only self-equilibrating stress will develop in statically determinate structures if subjected to a linearly varying temperature as stated earlier. In an indeterminate structure the presence of a thermal gradient leads to major stress redistributions which may cause a loss of serviceability (England 1980).

Alavizadeh – Farhang (2000) presented tests on beams subjected to flexural bending at various temperatures and tensile stress-strength ratios. Three sustained temperature levels (20 °C, 35 °C and 50 °C) and four stress-strength ratios (20 %, 40 %, 60 % and 80 %) were used for the test program. The results were compared to a reference beam at 20 °C; all the other beams were loaded for 24 hours. The results for the beams at 20 °C gave no indication of any creep, while the results for the beams at 50 °C gave a creep factor between 0.5 and 0.8. For the beams at 35 °C the creep factor determined from deflection measurements was around 0.2 after 24 hours, while the creep factor from strain measurements was between 0.25 and 0.35.

3.3.3.2 Creep at cyclic temperature

All the investigations listed above show that sustained elevated temperature will give an increase of the creep in a concrete structure. However for a structure subjected to temperature variations in the surrounding environment the temperature is not elevated for long periods of time, especially not in Swedish conditions where the maximum temperature in the material

rarely is above 40 °C and if so only for a few hours. Few investigations exist when the temperature is varied in cycles, and even fewer when the temperature is at normal operating conditions for a bridge.

Hansen and Eriksson (1966) performed loading tests on cement paste and cement mortar beams under varying temperatures. The cement mortar beams consisted of 50 % cement paste with a largest aggregate size of 4 mm. The beams were cured in water for 20 days; the water was then heated in cycles at a rate of either of 2 °C per min or of 2 °C per hour. For most beams the load was applied after the first heating cycle, while a few beams were loaded prior to the heating. The tests showed that the deflections increased significantly when the beams were heated after loading. A second temperature cycle produced smaller deflections than the first; the deflections only occurred during heating. If the beams were subjected to a temperature cycle before the load was applied, the deflections were significantly reduced. The deflections were also affected by the rate of the temperature change; if a large rate of heating of 2 °C per min was used the deflections were larger than if a heating of 2 °C per hour was used. For bridges subjected to temperature changes due to variations in the environment, it is not likely with a temperature change of 2 °C per min. The temperature change is closer to 2 °C per hour in such a structure.

Fahmi et al (1972) compared creep measurements performed on concrete specimens subjected to either a sustained elevated temperature of 60 °C or thermal cycles between 23°C and 60 °C. The specimens were either placed in 50 % RH or 100 % RH, to test the effect of relative humidity on the creep. The load was first applied during 37 days in 23 °C for the two RH-levels; the temperature was then increased to 60 °C for about 100 days for the sustained temperature tests. A rapid increase in creep was observed for both cases during the heating of the specimens. The results presented in Figure 3.6 showed that after 37 days the creep was almost two times as large for the specimens in 50 % RH compared to the specimens stored in 100 % RH. The elevated temperature affected the specimens stored in 100 % RH more than the lower RH specimens, where the creep stabilized after 2-3 weeks. For the specimens stored in 50 % RH a combination of the elevated temperature and a change in moisture conditions in the concrete due to the elevated temperature contributed to the rapid increase of creep strain. The final ratio for the total creep strain to the elastic strain at loading was about 4 for 50 % RH and 3.7 for 100 % RH.

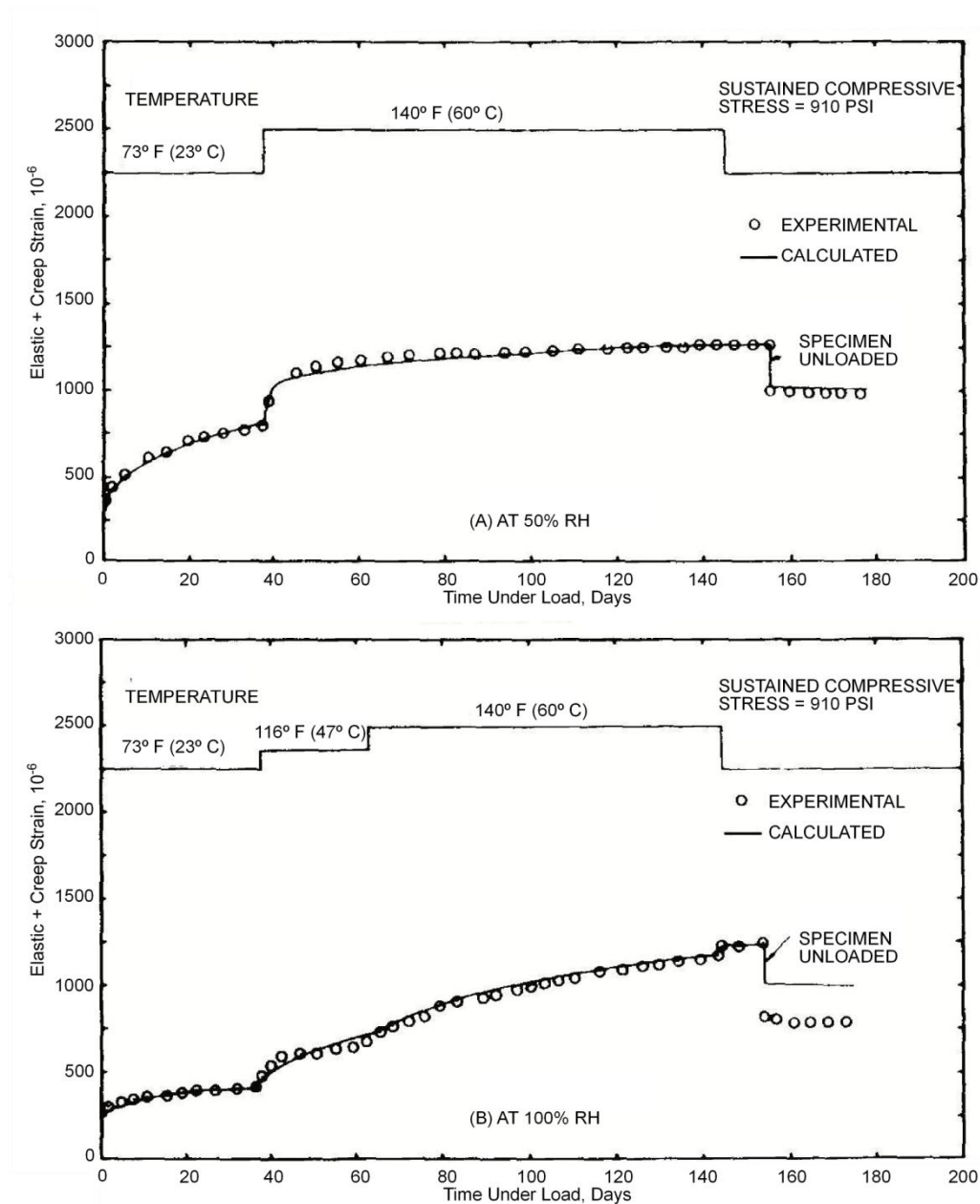


Figure 3.6 Comparison of experimental and calculated creep of concrete at sustained temperatures (Fahmi et al. 1972)

For the specimens with cyclic temperatures the same procedure was used until 37 days; one specimen in 50 % RH and one in 100 % RH. The first thermal cycle was applied after 37 days; the heating took about 3 hours each time. The elevated temperature of 60 °C was applied in about one week for each cycle, with the time between cycles also being one week. The largest increase in creep strain was caused by the first thermal cycle for both specimens, see Figure 3.7. For the specimen stored in 50 % RH almost no effect on the creep was observed from the additional thermal cycles compared to the sustained case. This small effect may according to the authors be attributed to irreversible changes in the cement gel occurring during the first heating cycle. For the other specimen stored at 100 % RH however, each additional cycle caused an increase in creep strain. The total creep strain ratio to the elastic

creep was 3.7 for 50 % RH and 4.5 for 100 % RH. The investigation showed that the creep at sustained or cyclic elevated temperatures is highly dependent on the relative humidity.

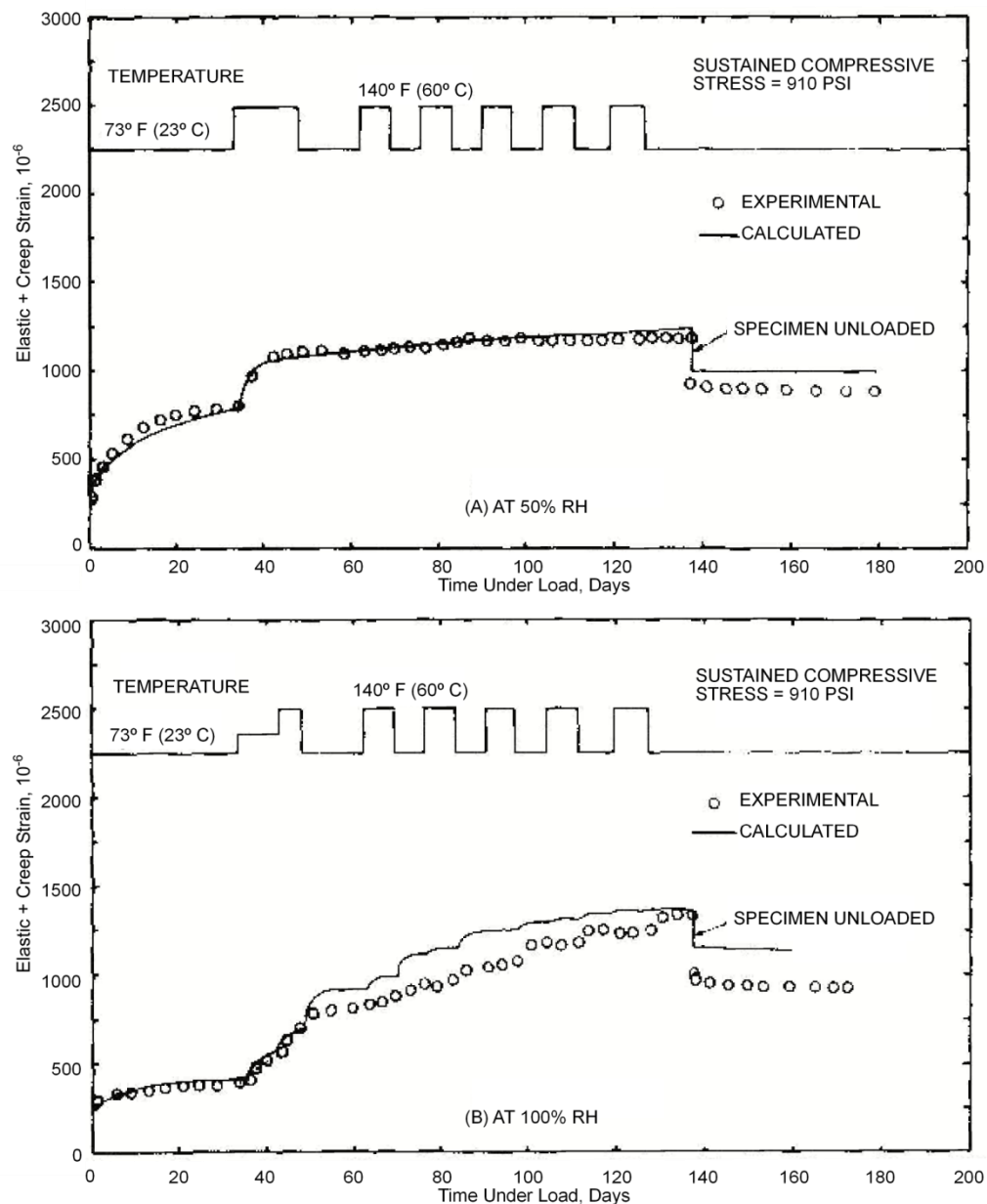


Figure 3.7 Comparison of experimental and calculated creep of concrete at cyclic temperature (Fahmi et al. 1972)

An example where the temperature variations of the environment may have influenced the structural behaviour was given by England (1980) and can be seen in Figure 3.8. A vertical bridge pier was drifting south, which may be caused by creep due to effects from solar radiation. According to England the upper end had a cyclic displacement pattern caused by curvature changes in the pier due to thermal variations. The creep effects in this situation caused a ratcheting behaviour which generated a long-term displacement in one direction even though the motion appears to be repetitive. The author states, however, that shrinkage also may have a part in these deformations. Clark and Church (1989) performed tests on

concrete beams subjected to combined effects of thermal and mechanical loading. Tests were conducted under both short-term and long-term cyclic loading. The results were significantly affected by creep; the uncertainties were however large since it is difficult to establish whether the creep is affected by temperature or other factors. The neglect of transitional thermal creep in design should not have serious consequences.

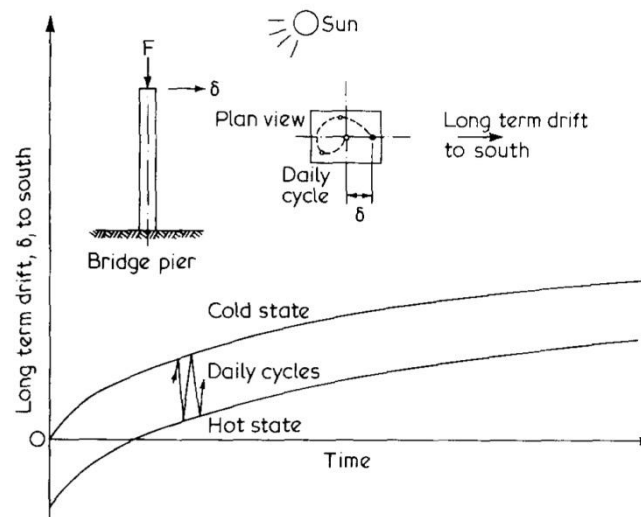


Figure 3.8 Solar heating effects on deflection behaviour of bridge pier (England 1980)

Vandevaille (2000) conducted an experimental study on the creep and shrinkage of concrete at variable and constant ambient conditions. This study was conducted due to the fact that most experimental data in literature were obtained from test with constant temperature and relative humidity. Concrete cylinders were cast at four times during a year, to account for all seasons. It was concluded that creep was influenced by the season of the casting, and that the relative humidity had a large influence on the shrinkage. From the test results no general valid conclusions could be drawn concerning the temperature variation effects. It was difficult to separate the effects of temperature from the effects of relative humidity on the creep behaviour.

Numerical simulations of thermal creep due to cyclic temperatures were performed and presented by Xu and Burgoyne (2005). The temperature distribution in the vertical direction for a two-span continuous beam was varied between a uniform distribution and a linear differential distribution where the top was warmer than the bottom. The temperature distributions were cycled in 10 day periods. This situation is not realistic for a structure exposed to temperature variations due to variations in the environment, which was also mentioned by the authors. The temperature levels were 15 °C for the sustained temperature and a linear variation from 15 to 30 °C for the temperature differential. The results showed that the creep effects on the middle support reaction and bending moment due to cyclic temperature are large during the first cycles, but is reduced with time. This reduction of temperature influenced creep with time was also found by Shkoukani and Walraven (1993) although they used higher temperatures cycles of about 60 °C as maximum value.

With all the described studies of creep due to cyclic temperature variation in mind, it can be deduced that it is difficult to distinguish the effects on creep by temperature from the effects of cyclic relative humidity. These factors are linked which in turn increases the difficulties of establishing the effects on creep. The creep is as shown often more dependent on the relative humidity than the actual temperature for cyclic conditions.

The creep deformations for concrete can be calculated as

$$\varepsilon_{cr} = \frac{\sigma}{E_c} \varphi \quad (3.25)$$

where σ is the compressive stress, E_c is the modulus of elasticity of concrete, and φ is the creep coefficient. According to the previous Swedish national code Bro 2004 (2004), the creep coefficient should be set to 0.3 when temperature changes were considered. This number originated from reverse calculations from an older standard. In the national code from 1976 various modulus of elasticity were given for concrete subjected to different loads. The creep coefficient in Bro 2004 was calculated from the ratio of these E-modulus values. It is also possible to calculate an effective modulus of elasticity E_{eff} according to

$$E_{eff} = \frac{E_c}{1 + \varphi} \quad (3.26)$$

The implementation of the Eurocodes in Sweden in 2009 altered the approach concerning the creep coefficient. Now each designer can calculate the creep coefficient based on the type and duration of the load in question according to SS-EN 1992-1-1 (2005). No standard value is given for the creep coefficient for thermal loads. The effective modulus of elasticity is still calculated as in Eq. 3.26.

In all results in this research project the temperature variations that cause large temperature differentials can be seen to be fast processes. The temperature differentials vary in a daily cycle, with outer or top sides warmer during daytime and inner or bottom sides warmer during night-time. Based on the information given in literature and in studies of creep in cyclic conditions by other authors, it can be deduced that during this short time periods it is unlikely that a creep effect will change the stiffness of the concrete in a significant way. Temperature differentials with a time dependence of at most 8-12 hours are therefore recommended to be considered without any creep coefficient in calculations. The study indicates that there is no additional creep due to these effects, but there can still be a creep effect due to annual variations in the average temperature of the structure. This approach can be said to be conservative and on the safe side, since creep does not increase thermal stresses in a concrete structure. As stated before the focus in the present research is less on absolute values of stress and more on relative effects. Moreover, if creep effects are included the absolute stress values can be modified accordingly. Therefore no effects of creep are included in the research presented in the appended papers.

4 Thermal actions in design codes

Until the 1960s temperature variations in concrete bridges were considered in design by the use of expected average temperature changes (Priestley 1978). The longitudinal movements occurring due to thermal expansion or contraction were accounted for by the use of sliding joints and bearings. Increasing problems such as cracking due to non-uniform temperature distributions led to the development of various national codes concerning thermal actions. The codes were based on measurements of temperature distributions and early numerical simulations. The first national codes established that in order to be able to assess the effects of thermal actions, the average bridge temperature, often referred to as the effective bridge temperature, and a non-uniform spatial temperature differential over cross-sections were needed. In the procedure of developing the new codes for Europe during the 1990s the experience gained from the various countries and studies was used as a basis. A brief description of a few old national codes from European countries is included in this chapter.

In the United Kingdom the rules for thermal actions originated from several theoretical and experimental studies performed in the UK from 1962 and onward (CEN 1996). The work included both theoretical studies and experiments. Emerson performed several studies in the 1970's on temperature in bridges, concerning both the effective bridge temperature and the temperature differential (Emerson 1973, 1977). A method for predicting the maximum and minimum effective bridge temperature based on a geographical distribution of the maximum and minimum shade air temperature was developed. The procedure to predict effective bridge temperature developed in the UK was used further on as a basis for the effective bridge temperature in other parts of Europe.

Before 1973 a linear design temperature differential was assumed with a magnitude of $8.3\text{ }^{\circ}\text{C}$ in the UK. This was however identified by Emerson as inadequate and a non-linear distribution was specified in subsequent codes. The proposed maximum temperature differential had a multiple straight line form, with allowances made for the effect of surfacing thickness. The recommended non-linear temperature distributions in the BS 5400 are adopted in method 2 of the Eurocode, which is presented further on in this chapter. In the background document of the Eurocode (CEN 1996) a comment on the recommended temperature variation concerning the complexity of the environmental input factors is included. This states that since large temperature differentials can occur from a range of different environmental conditions, it is difficult to assign return periods based on design climate situations.

In Germany the development of rules concerning thermal actions started in the 60's as well (CEN 1996). The first requirements were only a rough estimation of thermal actions, due to a lack of suitable measuring equipment for obtaining the temperature in the cross-section of a bridge. More extensive research was carried out during the 70's and 80's which led to the development of the new version of the DIN 1072 which was published in 1985. Here it was established that the surfacing has a large impact on the temperature in bridges, calculations were therefore performed on bridge cross-section both with and without surfacing to establish

the thermal effects. In the DIN 1072 the constant average temperature and the vertical linear temperature differential were considered as thermal design loads. The non-linear part was not considered since the effects from this part were deemed to be strongly dependent on the cross-section geometry and should instead be included in the detailing of the cross-section. This simplified method was used in most national codes in Europe (e.g. Sweden, Germany, and France) and is included as method 1 in SS-EN 1995-1-1 (2003), which is presented in the next section.

For southern Europe the national codes were based on more individual design considerations for each new bridge (CEN 1996). For important bridges or bridges located in special environments in Italy, a uniform temperature change and a temperature gradient between the top and bottom surfaces of at least 10 °C should be considered. For a box cross-section a temperature difference of ± 10 °C should be considered between the outer and inner surfaces. For Portugal it was specified that each bridge should be designed for uniform and differential temperature variations. The values for the temperature differential should be calculated according to the local conditions and material properties of the structure. Spain had a similar level of detail for the design codes of thermal actions as United Kingdom. The uniform temperature was calculated based on 9 temperature zones including every region of Spain. The positive vertical temperature differential should be calculated from a number of calibration coefficients given as a function of geometrical variables of the cross-section multiplied with a reference gradient depending on the bridge location. The negative differential was deemed small and a value of -2 °C was given. Here a temperature difference between the outside and inside surface of a box section was given; +14 °C (outside warmer) or -6 °C (inside warmer).

For Sweden the first bridge codes used a linear approach as in Germany. A positive linear temperature differential of 10 °C and a negative linear differential of -5 °C were specified as design values for concrete bridges. For structures where separate parts can have differing temperature, a temporary temperature difference of 10 °C should be assumed between the parts. There was also an addition in the Swedish code Bro 94 concerning the difference between the inner and outer surfaces of a box cross-section. A difference of 15 °C should be assumed. The previous national code Bro 2004 (2004) was in use until 2009 when it was replaced with Eurocodes.

In the American code AASHTO Guide Specifications: Thermal Effects in Concrete Bridge Superstructures (1989) the effective bridge temperature is treated in the same manner as for the Eurocode, using an effective bridge temperature correlated to the regional maximum and minimum shade air temperature. The positive and negative temperature differentials are treated by the use of a multiple straight line similar to method 2 in the Eurocode which is based on the old British Standard. Different values for the differentials depending on the location of the bridge are specified.

4.1 Eurocode EN 1991-1-5

The European codes were assimilated into the development of the Eurocode, in the background document of ENV 1991-2-5: Thermal actions (CEN 1996) the procedure of this development was presented. The system of the Eurocodes specifies that the characteristic value of an action is its main representative value. For climatic loads such as temperature, wind and snow loads, the characteristic value is defined as the value with a return period of 50 years which corresponds to an annual probability of exceedance of 0.02 (SS-EN 1990, 2002). Reduction factors are used to reduce the characteristic values to three other representative load values, combination, frequent and quasi-permanent, for use in load combinations and in the serviceability limit state.

In the Background document it is stated the temperature distribution through the depth of a bridge deck can be divided into an effective bridge temperature T_N , a linear temperature differential ΔT_M and a non-linear temperature differential ΔT_E . The effective bridge temperature is used to determine the magnitude of longitudinal movement due to expansion and contraction that a bridge has to manage. Due to restraint at the bearing positions, axial strains may be induced due to these movements. The uniform temperature component causing the longitudinal movements is defined as the difference between the effective bridge temperature and the start temperature of the bridge when it was restrained. The temperature differentials are defined as in Figure 2.1.

The main factor governing the effective bridge temperature is the shade air temperature, while it was stated that the main factor concerning the positive linear temperature differential is the total solar radiation (labelled TSR). Based on this it was deemed possible to consider the extreme values of effective bridge temperature as a function of extreme values of shade air temperature and average values of TSR and extreme values of the positive linear temperature differential as a function of extreme values of TSR and average ranges of shade air temperature. It was assumed that large positive differentials, top warmer than bottom, only occurs during the months of June, July or August.

To calculate the temperature distributions, and thus the thermal actions, a one-dimensional heat flow model based on the finite difference method was used. The one-dimensional heat flow was chosen due to the large thermal inertia and relatively low diffusivity of concrete. The following data were used as input:

- Solar radiation according to Eq. 2.11 using the daily TSR, the time of sunrise and the duration of the solar day
- Temperature: daily maximum and minimum shade air temperature and the corresponding time of occurrence, the effective bridge temperature at starting time (08:00)
- Geometry of the bridge cross-section
- Material properties: solar absorptivity, emissivity, heat transfer coefficient, thermal conductivity, density and specific heat.

The heat transfer coefficient was assumed to be constant, with a value of 19-23 W/m² for the top surface and 9 W/m² for the bottom surface. When compared to Eqs. 2.26 based on wind speed, the heat transfer coefficients correspond to a constant wind speed of 3.25-4.25 m/s for the top and 0.75 m/s for the bottom. Nothing was stated in the description about the consideration of long-wave radiation heat transfer.

For the calculations it was also assumed that no significant benefit would be acquired by using different material parameters for asphalt or concrete paving layers. The surfacing was modelled as an additional layer of concrete in all cases. The standard thickness was set to 50 mm, with other thicknesses also investigated. As mentioned in section 2.4, the thermal material properties of asphalt and concrete are similar for density, emissivity and specific heat. However the difference in solar absorptivity coefficient and thermal conductivity makes the assumption that no significant changes in temperature distribution depend on the paving layer material less valid. This can be seen in the results presented in Paper II where the temperature differential in a concrete slab is larger when using an asphalt paving layer than if a concrete layer is used.

The representative values were obtained by a statistical analysis of the temperature components which were calculated using the heat flow model with climate data from a meteorological station in Giessen, Germany as input data. The analysis was based on the work by Soukhov (1994), where two methods were presented for calculating linear temperature differentials. The first method was an “exact” method, where the values of the temperature differentials are calculated for a longer period and used in a stochastic process model. In the second method a statistical analysis was performed for the environmental factors, and the representative values of the linear temperature differential were obtained from simulations using representative values of the environmental factors.

For the first method the temperature distribution is calculated for simulations from 1st of June to 31st of August during 1981-1990. It was assumed that the extreme values could be obtained from random events which occurred during a 3-day period, since 3-day values were assumed to be independent. The temperature profiles obtained were divided into the three parts as described earlier, and the 3-day maxima of the thermal actions were determined. For one summer this gave 30 values and hence 300 sets of data from 10 years were available for the statistical analysis. The ten year period was only used for calculations of 3-day maxima for one type of cross-section; the box section of the Lucka Bridge in Germany. The bridge has a box cross-section with a total depth of 1.95 m. For other cross-sections than Lucka Bridge the year 1982 was chosen as representative, since the mean values of uniform temperature and linear temperature differential for this year were close to the mean values for the entire period. 30 sets of data were thus available for the analyses of other cross-sections. All results were calculated using a 50 mm concrete surface on the top of the cross-sections.

The three day maxima of ΔT_M were fitted to an Extreme type III distribution according to Eq. 4.1, which was motivated by the fact that the solar radiation has an upper cut off limit.

$$F_X(x) = \exp \{ -[(x_0 - x)/(x_0 - u)]c \} \quad (4.1)$$

with the inverse probability distribution function when the distribution parameters x_0 , u and c are known as

$$x_p = F_X^{-1}(p) = x_0 - (x_0 - u)[- \ln(p)]^{1/c} \quad (4.2)$$

where x_0 is an upper cut-off limit of ΔT based on the upper limit of the total solar radiation, which is the sum of the solar radiation during one day, p is the probability that the given value x is not exceeded; u and c are the distribution parameters with the following relationship to the mean and standard deviation

$$m_x = x_0 - (x_0 - u)\Gamma(1 + 1/c) \quad (4.3)$$

$$\sigma_x^2 = (x_0 - u)^2 [\Gamma(1 + 2/c) - \Gamma^2(1 + 1/c)] \quad (4.4)$$

where Γ is the Gamma function. Considering their return periods, the representative values of the linear temperature differentials were calculated. For the characteristic value the return period is as mentioned 50 years. The corresponding safe probability p_K for 30 three-day intervals used by Soukhov was then

$$p_K = 1 - \frac{1}{30 \cdot 50} = 0.999333 \quad (4.5)$$

For the other representative values other return periods were assigned; 1 year for the combination, 2 weeks for the frequent and 6 days for the quasi-permanent since this is 50 per cent of the three-day maxima. This gave corresponding safe probabilities of

$$p_i = 1 - \frac{1}{30} = 0.966667$$

$$p_1 = 1 - \frac{1}{4.67} = 0.785867$$

$$p_2 = 0.5$$

The representative values were obtained using Eq. 4.2 with the results for the positive linear differential as presented in Table 4.1.

Table 4.1 Representative values of positive linear differentials

Depth (m)	Characteristic, ΔT_{MK} (°C)	Combination, ΔT_{MI} (°C)	Frequent, ΔT_{MI} (°C)	Quasi-permanent, ΔT_{M2} (°C)
Box girder				
1.95 (Lucka)	11.8	9.4	7.3	5.8
2.0	11.7	9.4	7.5	6.1
3.3	10.6	8.3	6.5	5.2
4.7	9.8	7.6	5.9	4.7
T-girder				
1.2	19.1	14.8	11.5	9.4
1.8	16.2	12.3	9.4	7.6
2.4	14.4	10.8	8.1	6.4
Slab				
0.6	18.4	15.3	12.5	10.5
0.9	14.1	11.7	9.5	7.9
1.2	11.2	9.1	7.3	6.0

Only the positive linear temperature differential was considered in the explanation given in the background document, therefore no description of the statistical analysis concerning the proposed negative linear differential is given here. The characteristic values proposed from the statistical analyses and incorporated in SS-EN 1991-1-5 (2003) were as follows:

Box-girder: $\Delta T_{MK,pos} = 10$ °C $\Delta T_{MK,neg} = -5$ °C

T-girder: $\Delta T_{MK,pos} = 15$ °C $\Delta T_{MK,neg} = -8$ °C

Slab: $\Delta T_{MK,pos} = 15$ °C $\Delta T_{MK,neg} = -8$ °C

The motivation for choosing these values was that the real deck depth of modern bridges is quite large. It should however be noted that in the described statistical analysis from the background document the characteristic values have a large variation depending on the depth of the studied cross-section which is neglected in SS-EN 1991-1-5. The size effect was much smaller in the investigation presented in Paper II, which can be seen in Table 2 in that paper.

To check the validity of the calculations the results were compared to linear temperature differentials obtained by measurements performed at the concrete box-section bridge in Lucka, Germany. The measurements were performed 1984-1988, but the investigation of the results was limited to 1984-1985 due to more measured results during these years. For the positive linear differential the time period 1st of April to 30th of September was taken into account and for the negative differential the 1st of November to the 31st of March. Hourly values of linear temperature differentials were obtained from the results of the measuring points in the bridge. Using the 3-day maxima concept as established earlier, the mean and standard deviation for the maximum positive and negative linear temperature differentials

were obtained and fitted to a type III extreme value distribution, giving the following characteristic values

$$\Delta T_{MK,pos} = 14.5\text{ }^{\circ}\text{C}$$

$$\Delta T_{MK,neg} = -9.5^{\circ}\text{C}$$

The upper limit from the fitted type III extreme value distribution of $\Delta T_{M,pos}$ was calculated to be 18 °C and the lower limit of $\Delta T_{M,neg}$ was calculated to -11°C. It is unclear in the description in the background document (CEN 1996) why a different time period was chosen for the positive differentials. For the numerical calculations three months compared to six months for the measurements.

In Soukhov (2000) the alternative model which could be used for the calculations of the characteristic values and the other representative values (combination, frequent, quasi-permanent) was presented. This method was developed from the need to find a procedure for calculating the thermal actions in a less time consuming manner. Since the important thermal factors when calculating the positive linear differentials had been identified, total solar radiation and shade air temperature range, a statistical analysis could be made directly for the thermal factors. The maximum for each three day period was extracted for the total solar radiation and only associated values for the shade air temperature was used. The associated values were described as the maximum and minimum shade air temperature of the same day as when the maximum total solar radiation occurs. The probability distribution function for the 3-day maxima of total solar radiation was fitted to a type III extreme value distribution. The representative values from this investigation showed a good agreement with the values from the more direct method. The characteristic values were 0.5-2.5 % smaller, but the other representative values were almost identical.

In the above described procedures the 3-day maxima were fitted to type III extreme value distribution (Weibull). It is also possible to fit extreme values of thermal actions to a type I extreme value distribution (Gumbel). This is shown both in Paper II and in Silveira et al. (2000) to be a valid assumption; however Marková (2010) presented results which showed that a Weibull distribution could be a better representation.

The characteristic values listed in the background document of the Eurocode are based on bridges in Germany. For other climate situations in Europe more studies were needed. Investigations for Swedish conditions were performed concerning both the effective bridge temperature (Alavizadeh-Farang 1999a) and the linear temperature differentials (Alavizadeh-Farang 1999b). National checks and adaptations of the representative values have also been performed in other European countries such as Czech Republic (Markova) and Italy (Barsotti and Froli 2000). For the Swedish investigation a similar extensive investigation as for the Eurocode was deemed impossible to perform within the time and frame of the project. The investigation focused instead on checking if chosen extreme cases of climate conditions gave similar values as the representative values in the Eurocode. The temperature in the established

cross-section types in the Eurocode was calculated using a finite element program for two certain sets of daily climate data. No extensive climate data were available for the investigation, and the statistical approach used for the Eurocode values was therefore not deemed possible to make.

In the investigation the general environmental conditions, used for calculation of the positive linear temperature differential, were chosen based on information given in Emerson (1977). For concrete decks a summer day with a large amount of total solar radiation, a shade air temperature range of 15 °C and a low wind speed may be used. For the negative linear temperature differential a clear winter night with outgoing long-wave radiation, a shade air temperature range of 15 °C and a low wind speed may be used. The climate situations are described further in chapter 5. The shade air temperatures in the two data sets were obtained from the weather station in Målilla in Sweden, while the daily total solar radiations and outgoing long-wave heat radiation during the night, referred to as re-radiation, were calculated based on values taken from radiation tables containing typical solar radiation data for Sweden. One data set containing values for two consecutive days was used for the positive linear differential, and one data set containing values for three consecutive days for the negative one. The values of the data sets are presented in Table 4.2. These short-term periods were deemed to be sufficient to obtain maximum values for the differentials. This can be said to be quite unsecure, as can be seen in the results presented in chapter 5 of this thesis.

Table 4.2 Climate conditions used for calculations in Alavizadeh-Farang (1999b)

Climate condition 1	Minimum shade air temperature (°C)	Maximum shade air temperature (°C)	Total solar radiation (Wh/m²)	Wind speed (m/s)
Day 1	0.6	20	3024	1
Day 2	3.3	26	7402	1
Climate condition 2			Re-radiation (W/m²)	
Day 1	-14	-0.5	-180	1
Day 2	-12	-8	-150	1
Day 3	-39	-10	-150	1

The calculations of temperature profiles were performed using a finite element program; all cross-sections used had a surfacing of 50 mm concrete on top. The results from the investigation are presented in Table 4.3, where the characteristic values from the Eurocode also are included.

Table 4.3 Eurocode characteristic and calculated characteristic values by Alavizadeh-Farhang (1999b)

Group of superstructure	SS-EN 1991-1-5		Calculated values	
	Positive differential (°C)	Negative differential (°C)	Positive differential (°C)	Negative differential (°C)
Group 3: Concrete deck on				
-concrete box girder	10	-5	8.9	-3.7
-concrete T-girder	15	-8	11.6	-11
-concrete slab	15	-8	11.4	-6.6

The main conclusion in Alavizadeh-Farhang (1999b) was that the Eurocode values for concrete bridges could be adopted for concrete bridges, since the linear temperature differentials show a good agreement with values given in Table 6.1 in SS-EN 1995-1-1. The lack of climate data in the investigation does however signal the importance of a more thorough investigation.

The procedure for the thermal actions in the Eurocode and the comparison with Swedish conditions can be compared to the procedure used for the research presented in Paper II where the annual maxima of the linear temperature gradient were obtained. The temperature profiles were determined from calculations using data from entire years instead of using only three months in the summer or general sets of data. Unfortunately only a limited amount of data exists for Swedish conditions due to lack of measured long-wave radiation. The time periods in the investigations were 16, 15, 15 or 8 years for Stockholm, Lund, Luleå and Borlänge respectively. Based on the annual maxima representative values with a return period of 5 years were estimated, which may be compared to the characteristic values in the Eurocode. The values for a 600 mm slab with no surfacing or a 50 mm surfacing of either asphalt or concrete are presented in Table 1 in Paper II. Here it can be seen that for no surfacing and 50 mm asphalt layer the 5 year values of the positive linear differential are close to or above the characteristic values in the code. This indicates that the representative values in the code are underestimated, which may be a result of the assumption of independent 3-day periods. If a concrete layer is used the values are reduced, which is interesting since the representative values in the Eurocode are calculated with a concrete paving layer. The values in the Eurocode may be underestimated due to the assumption that there is no significant difference between asphalt and concrete.

In SS-EN 1991-1-5 (2003) an alternative method for considering the effect of non-uniform temperature distribution is also presented. The Swedish National Annex in SS-EN 1991-1-5 (2003) states that both method 1 and method 2 is allowed to use for design. Method 2 specifies a differential temperature model which incorporates the linear and non-linear temperature differential parts of the temperature distribution with a small part of the effective bridge temperature. The differential temperature is then described by a multiple straight line with values for the different gradients based on the depth of the cross-section according to Figure 4.1. A similar approach is used in the American standard AASHTO (1989).

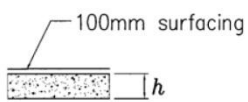
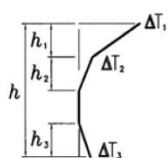
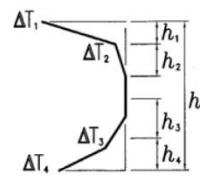
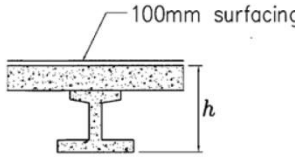
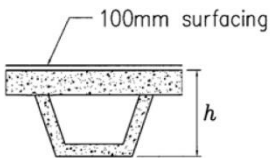
Type of Construction	Temperature Difference (ΔT)																																																																	
	(a) Heating	(b) Cooling																																																																
 3a. Concrete slab	 $h_1 = 0.3h$ but $\leq 0.15m$ $h_2 = 0.3h$ but $\geq 0.10m$ but $\leq 0.25m$ $h_3 = 0.3h$ but $\leq (0.10m + \text{surfacing depth in metres})$ (for thin slabs, h_3 is limited by $h - h_1 - h_2$)	 $h_1 = h_4 = 0.20h$ but $\leq 0.25m$ $h_2 = h_3 = 0.25h$ but $\leq 0.20m$																																																																
 3b. Concrete beams	<table><tr><th>h</th><th>ΔT_1</th><th>ΔT_2</th><th>ΔT_3</th></tr><tr><td>m</td><td></td><td>°C</td><td></td></tr><tr><td>≤ 0.2</td><td>8.5</td><td>3.5</td><td>0.5</td></tr><tr><td>0.4</td><td>12.0</td><td>3.0</td><td>1.5</td></tr><tr><td>0.6</td><td>13.0</td><td>3.0</td><td>2.0</td></tr><tr><td>≥ 0.8</td><td>13.0</td><td>3.0</td><td>2.5</td></tr></table>	h	ΔT_1	ΔT_2	ΔT_3	m		°C		≤ 0.2	8.5	3.5	0.5	0.4	12.0	3.0	1.5	0.6	13.0	3.0	2.0	≥ 0.8	13.0	3.0	2.5	<table><tr><th>h</th><th>ΔT_1</th><th>ΔT_2</th><th>ΔT_3</th><th>ΔT_4</th></tr><tr><td>m</td><td></td><td>°C</td><td></td><td></td></tr><tr><td>≤ 0.2</td><td>-2.0</td><td>-0.5</td><td>-0.5</td><td>-1.5</td></tr><tr><td>0.4</td><td>-4.5</td><td>-1.4</td><td>-1.0</td><td>-3.5</td></tr><tr><td>0.6</td><td>-6.5</td><td>-1.8</td><td>-1.5</td><td>-5.0</td></tr><tr><td>0.8</td><td>-7.6</td><td>-1.7</td><td>-1.5</td><td>-6.0</td></tr><tr><td>1.0</td><td>-8.0</td><td>-1.5</td><td>-1.5</td><td>-6.3</td></tr><tr><td>≥ 1.5</td><td>-8.4</td><td>-0.5</td><td>-1.0</td><td>-6.5</td></tr></table>	h	ΔT_1	ΔT_2	ΔT_3	ΔT_4	m		°C			≤ 0.2	-2.0	-0.5	-0.5	-1.5	0.4	-4.5	-1.4	-1.0	-3.5	0.6	-6.5	-1.8	-1.5	-5.0	0.8	-7.6	-1.7	-1.5	-6.0	1.0	-8.0	-1.5	-1.5	-6.3	≥ 1.5	-8.4	-0.5	-1.0	-6.5
h	ΔT_1	ΔT_2	ΔT_3																																																															
m		°C																																																																
≤ 0.2	8.5	3.5	0.5																																																															
0.4	12.0	3.0	1.5																																																															
0.6	13.0	3.0	2.0																																																															
≥ 0.8	13.0	3.0	2.5																																																															
h	ΔT_1	ΔT_2	ΔT_3	ΔT_4																																																														
m		°C																																																																
≤ 0.2	-2.0	-0.5	-0.5	-1.5																																																														
0.4	-4.5	-1.4	-1.0	-3.5																																																														
0.6	-6.5	-1.8	-1.5	-5.0																																																														
0.8	-7.6	-1.7	-1.5	-6.0																																																														
1.0	-8.0	-1.5	-1.5	-6.3																																																														
≥ 1.5	-8.4	-0.5	-1.0	-6.5																																																														
 3c. Concrete box girder																																																																		

Figure 4.1 Temperature differentials for bridge decks – type 3 concrete decks (Figure reproduced from SS-EN 1991-1-5 with permission of SIS Förlag AB, www.sis.se)

Both the first method of using a linear differential and the second method with a multiple straight line approach are useful for designers. A linear differential is simpler to use in design since it produces a straightforward curvature as explained in chapter 3. The second method is more appropriate to use for more complex structures, where the benefits of the non-linear component with an often reduced stress level are needed. For both methods it is however important to consider thermal actions for the details of the structure, where a temperature difference between various parts may give unfavourable effects.

It is also important to consider the difference in temperature between inside and outside surfaces in box sections. The Eurocode SS-EN 1991-1-5 (2003) section 6.1.4 states that “care should be taken when designing large bridges, since large temperature differences can appear between the inside and outside of the web walls”, and a recommended value of 15 °C is given. This is a very brief statement, and was the basis of the study presented in Paper IV where the transverse effects in box cross-section were analysed. Nothing regarding these effects are stated in AASTHO (1989), here an inside cavity only affects the values for the temperature differential over the entire cross-section.

5 Extreme climate situations

As described in the previous chapter it was assumed that for the calculations of the thermal actions in the Eurocode, extreme events of positive linear temperature differentials would occur during the summer months of June, July and August. This assumption was made on the basis that a large positive differential occur when the structure is subjected to a large influx of solar radiation and a large range of shade air temperature. According to Emerson (1977) the largest positive differential occurs between May and August and the largest negative differential at night time during any night of the year. To calculate the temperature differentials certain environmental conditions were given by Emerson. The environmental conditions were not extreme events; the reason for this was that if the extreme occurrences of all thermal factors would have been used it gave a magnitude of the temperature differentials not seen in measurements of temperature distributions in bridges in the United Kingdom. The alternative method for calculating representative values as in the Eurocode (Soukhov 1994, Soukhov 2000) also use calculated general climate situations as a base for the statistical analysis.

For concrete decks an extreme day with a daily total solar radiation on a horizontal surface of 7500 Wh/m^2 was proposed by Emerson (1977) along with a daily range of shade air temperature of $15 \text{ }^\circ\text{C}$ and a wind speed of approximately 2 m/s . Temperature range was defined as the difference between the maximum and minimum temperatures during a certain time period. The conditions were deemed to give the maximum possible positive temperature differential for concrete decks. The maximum reversed or negative differential was deemed to occur during a winter night with a re-radiation of -110 W/m^2 , a daily shade air temperature range of $15 \text{ }^\circ\text{C}$ and a wind speed of approximately 2 m/s . The absolute values of shade air temperature did not have any effect on the results. These climate conditions were also used as a base for the chosen climate conditions used by Alavizadeh-Farhang (1999b), which were presented in Table 4.2 and 4.3.

Roberts-Wollman et al. (2002) used a similar approach with selected climate conditions for calculating positive temperature differentials in bridges. Approximate standardised empirical equations based on ambient climatic conditions were used to calculate the temperature. For a bridge with 50 mm asphalt paving layer on top the equation was

$$\Delta T = 18.5 \left(\frac{Sa}{29.809} - 0.9 \right) + 0.163(TV - 11.1) + (27.5 - 4.9v + 0.844v^2 - 0.0986v^3 + 0.00515v^4) \quad (5.1)$$

where ΔT is the positive temperature differential, S is the daily total solar radiation, a is the solar absorptivity, TV is the ambient temperature variation and v is the wind speed. The ambient temperature variation and average wind speed were obtained from a meteorological station, while the solar radiation was obtained using theoretical solar radiation from approximation equations found in Duffie and Beckman (2006). The results in their

investigation showed that the empirical equation approximation overestimated the positive temperature differential compared to measurements with as much as 2.8 times. This shows that such empirical equations as used by Roberts-Wollman et al. can be useful for certain cases, but may give unreliable results for other situations. Another conclusion was that the positive temperature differential was mainly affected by the amount of solar radiation, which confirms the previous studies in this field.

The described investigations have been using selected climate conditions to estimate the thermal actions governing the behaviour of the whole structure. At cross-sectional level for box-girder bridges, a lack of information and guidelines exists to whether the same climate conditions and approaches are applicable. The temperature difference between the outside and inside of the walls and slabs are affected in a similar way as described in the previous studies, but a deeper investigation is needed to confirm this statements.

The basis for the thermal actions in the Eurocode as described in section 4.1 was measurements and simulations performed in Germany between 1981-1990 for concrete box cross-sections or for the year 1982 for slab- or T-sections. The thermal actions were extracted directly from the thermal simulations. For the extreme climate situations used, e.g. by Emerson (1977), the climate data was directly adapted to a worst case climate scenario which then have been used for design. None of the extreme values of thermal actions or climate situations have been extracted from cases where the resulting thermal stresses have been analysed. It is therefore interesting to study the actual climate data which produce the largest tensile stresses, especially for box-sections, and use this as a foundation for comparing climate situations.

5.1 Climate situations producing extreme values of thermal actions and stresses

When general sets of data or approximations of the thermal factors are used for estimating thermal actions the maximum values of differential temperature will occur at certain times of the day. This is in several cases the results from the use of approximations of solar radiation and air temperature, described in chapter 2, where occurrence times for the maximum and minimum values are needed for the various factors. In the long-term simulations presented in Paper II and IV the temperature distributions have been calculated using climate data for 15 full years from Stockholm and Luleå. The results presented in those papers have been focused on the extreme values of thermal actions and thermal stresses which may occur in concrete structures. In this section an additional investigation of the occurrence of the extreme values and the corresponding input data producing these values is presented.

In Paper IV the resulting thermal stresses in the transverse direction for the top section of the arch with a box cross-section of the New Svinesund Bridge were presented. The location and magnitude of the largest tensile stresses were also identified. The annual maximum linear temperature differential over the top slab coincided with the annual maximum tensile stress for most years, which also was presented in the paper. This indicates that there is a connection

between large thermal tensile stresses and linear temperature differentials at cross-sectional level. However, as is also concluded in Paper IV, when only the linear temperature differential over each wall is used the thermal tensile stress may be overestimated compared to when the non-linear component is included.

From the results of the investigation using long-term simulations of concrete slabs with different sizes and paving layers (Paper II) the time of occurrence of the annual maximum positive linear temperature differential is extracted. The date and time for every year for the cases with 600 mm thick slab with either no paving or an asphalt layer are presented in Table 5.1.

Table 5.1 Date and time for the occurrence of maximum positive linear temperature differential in a 600 mm thick concrete slab

Year	Stockholm				Luleå			
	Asphalt		No paving		Asphalt		No paving	
	Date	Time	Date	Time	Date	Time	Date	Time
1983	24 May	16	24 May	15	8 Jul	14	8 Jul	13
1984	30 Jul	17	30 Jul	16	1 Apr	15	26 Jul	16
1985	23 Jun	18	23 Jun	17	11 Jul	17	18 Jun	17
1986	26 Jun	19	26 Jun	18	9 Aug	19	26 Jun	18
1987	3 Jul	19	3 Jul	18	19 Jul	20	22 Jun	18
1988	27 Apr	16	27 Apr	15	28 Jun	17	12 May	14
1989	23 May	16	23 May	15	25 May	16	23 Jul	14
1990	29 May	18	29 May	18	7 Jun	18	6 Jun	18
1991	3 Jul	19	3 Jul	17	18 Jul	19	8 Jun	17
1992	26 May	20	26 Jun	19	9 Jun	20	25 Jun	19
1993	14 Jun	15	14 Jun	14	12 Jun	17	26 Jun	14
1994	6 Jul	17	22 Jul	16	21 Jun	17	6 Jul	16
1995	9 Jul	18	29 May	17	14 Jun	17	2 Jun	17
1996	22 May	20	22 Apr	19	31 May	18	24 May	18
1997	31 May	20	31 May	19	20 Apr	19	20 Apr	18

From the results in the table it can be deduced that the annual maximum positive linear temperature differential occurs in the afternoon between 13 and 20 hours sometime from late April to July. When a paving layer is used in the simulations the occurrence time was about one hour later than for no paving. This was expected, since the paving layer serves as insulation and the effects of solar radiation on the concrete is therefore delayed. For Stockholm the day of the occurrence is the same for both cases for most years, while for Luleå the date is almost always different between the two cases. This phenomenon is difficult to explain due to the complexity of the interactions between the thermal input factors, but the insulation effect of the paving layer clearly changes the occurrence of the linear differentials.

To analyse the appearance of thermal stresses, the time of occurrence of the yearly maxima of the thermal tensile stress at various parts of the cross-section from the New Svinesund Bridge have been extracted and presented in Table 5.2. The maximum tensile stress in the cross-section appears on the inside surface of the top slab for both Stockholm and Luleå. Only the dates and times from the cases with the bridge located in an east to west direction are presented, since this case gave the largest thermal stresses.

Table 5.2 Date and time for the occurrence of maximum thermal tensile stress in the top section of the New Svinesund Bridge

Year	Stockholm		Luleå	
	Date	Time	Date	Time
1983	8 Jul	15	2 Dec	13
1984	29 Apr	17	11 Jan	12
1985	26 May	16	18 Jun	17
1986	26 Jun	16	24 Jan	5
1987	23 May	17	30 May	16
1988	27 Apr	15	12 May	15
1989	23 May	16	19 Dec	16
1990	29 May	16	6 Jun	17
1991	19 May	16	4 Apr	16
1992	19 May	17	25 Jun	16
1993	9 Jun	16	30 Dec	10
1994	3 Jul	16	14 Feb	16
1995	26 May	16	2 Jun	17
1996	22 May	16	1 Jan	19
1997	1 Jun	17	31 Mar	16

For the bridge located in Stockholm it can be observed in the table that the maximum tensile stress every year occurs sometime from late April to the beginning of July, with May as the most frequent month of occurrence. One more observation is that the maximum tensile stress in this cross-section occurs during the afternoon between 15 and 17. The time frame is similar to the occurrence of the maximum linear differentials presented in Table 5.1, but confined to a shorter period of time in the afternoon. When the time of occurrence for the annual maximum tensile stress in the cross-section for the input data from Luleå is analysed it can be seen that the annual maximum occurs during various seasons. For Luleå the annual maximum tensile stress occurs either between December and February or between the end of April to the beginning of July. In winter the maximum can occur both during the night and the day, while in spring it is the same as for Stockholm; between 15 and 17. This indicates that a large positive temperature differential may not only be caused by a large influx of solar radiation, but also by another combination of thermal factors.

To analyse which types of thermal factor combinations that gives the extreme events, the climate input data when the annual maxima occurred have been extracted. Data from the case with the bridge placed in Stockholm from three days prior to the maximum stress occurrence were extracted and presented in Table 5.3. Here it can be seen that the maximum incident solar radiation during the three days are similar for all years, with a mean value of 787 W/m^2 . The ambient air temperature had a large range for all climate events; the total range over the three days varied from 11 to $23 \text{ }^\circ\text{C}$, while the largest range over 24 hours was between $11 \text{ }^\circ\text{C}$ and $20 \text{ }^\circ\text{C}$. The wind speed in the last 24 hours prior to the occurrence of the maximum tensile stress was low; $0\text{-}7 \text{ m/s}$. The total range over the three days of the effective sky temperature, see section 2.3.2 for the definition, was also large for all years, between $21 \text{ }^\circ\text{C}$ and $28 \text{ }^\circ\text{C}$. In most cases the sky temperature was about $10 \text{ }^\circ\text{C}$ lower than the air temperature at night, which indicates that the weather was clear since a cloud-cover would have raised the sky temperature. The only differing factor for some of the years is the air temperature level. For most years the maximum air temperature is between $20 \text{ }^\circ\text{C}$ and $30 \text{ }^\circ\text{C}$, while for a few years the extreme event occurs when the maximum air temperature is 10 to $15 \text{ }^\circ\text{C}$.

For the climate input data from Luleå two different climate situations which give the yearly maxima was found, as opposed to Stockholm where there was only one. The climate data from three days prior to the occurrence of the annual maximum tensile stress have been analysed and the important findings are presented in Table 5.4. Here it can be seen that the incident solar radiation is either low, during the winter case, or high, during the spring case. The range for the ambient air temperature is large just as for Stockholm. There is however a difference between the two cases; for the winter occurrence the total range is about $30 \text{ }^\circ\text{C}$, while for the spring the range is about $15\text{-}20 \text{ }^\circ\text{C}$. The wind speeds are a bit larger for the winter case than for the spring. The spring case for Luleå has about the same wind speeds as the Stockholm situations. The range in sky temperature is also a major difference between the two cases. For the winter case the total range is between 27°C and up to $42.5 \text{ }^\circ\text{C}$ over the three days, while for the spring case the total range is $15\text{-}20 \text{ }^\circ\text{C}$. Based on the climate data analysis the cause of the large positive differentials occurring during winter is a rapid large increase in air temperature combined with an incoming cloud-cover which raises the sky temperature. Due to the slow heat transport in the concrete, the inside cavity will still hold a very low temperature and large temperature differentials occur.

Table 5.3 Climate situations from three days prior to the occurrence of the annual maximum thermal tensile stress for the top section of the New Svinesund Bridge with Stockholm climate data

	1983	1984	1985	1986	1987	1988	1989	1990	1991	1992	1993	1994	1995	1996	1997
Max Solar radiation (W/m²)	759	699	800	792	789	719	800	801	815	746	824	870	769	802	822
Air temperature (°C)															
<i>max</i>	28.2	20	21.1	28.8	23.7	8.5	24.2	16.1	15.1	26	23.8	27.6	21.7	17.2	20
<i>min</i>	12.9	-1.8	0.8	7.8	2.1	-2.7	1.3	0.9	0.2	5.8	5.8	8.4	4.2	1.7	1.4
<i>Total range</i>	15.3	21.8	20.3	21	21.6	11.2	22.9	15.2	14.9	20.2	18	19.2	17.5	15.5	18.6
<i>24-hour range</i>	15.3	18.4	14.2	16.4	19.7	11.2	18.4	15.2	14.9	17.2	18	15.8	14.7	15.5	15.4
Wind speed (m/s)															
<i>max</i>	5	4	6	4	5	6	5	4	3	5	5	4	5	7	4
<i>min</i>	0	0	2	0	0	1	0	0	0	0	1	1	0	1	1
Sky temperature (°C)															
<i>max</i>	37.1	33.6	30.9	23.1	15.4	18.3	16.5	14.4	14.4	19.4	21.8	22.9	20.2	8.7	13.6
<i>min</i>	16.1	6	5.3	0.7	-7	-14.6	-10.2	-10.5	-11.3	-8.1	-4.2	1.7	-5	-12.4	-13.5
<i>Total range</i>	21	27.6	25.6	22.4	22.4	32.9	26.7	24.9	25.7	27.5	26	21.2	25.2	21.1	27.1
<i>24-hour range</i>	17.7	20.2	19.8	17	20.2	26.1	21.5	22.7	24.3	24.2	26	20.6	23.6	19.7	27.1

Table 5.4 Climate situations from three days prior to the occurrence of the annual maximum thermal tensile stress for the top section of the New Svinesund Bridge with Stockholm climate data

	1983	1984	1985	1986	1987	1988	1989	1990	1991	1992	1993	1994	1995	1996	1997
Max Solar radiation (W/m²)	39	28	749	33.2	737	702	10	740	517	729	18	218	650	11	462
Air temperature (°C)															
<i>max</i>	-1.7	-1.1	22.8	-0.8	18.8	17.6	-0.6	15.5	9.6	22.1	0.1	1.6	21.1	-1.1	5.3
<i>min</i>	-25.9	-25.7	9.2	-32.5	3.6	-2.7	-30.9	5.3	-13.2	7.2	-27.6	-27.2	8.1	-30.9	-15.6
Total range	24.2	24.6	13.6	31.7	15.2	20.3	30.3	10.2	22.8	14.9	27.7	28.8	13	29.8	20.9
24-hour range	16.7	24.6	13.6	31.7	12.2	17.4	17	7.7	10.8	13.2	12.5	16.9	11	21.7	16.4
Wind speed (m/s)															
<i>max</i>	6	10	5	12	4	4	7	5	4	4	6	5	3	7	8
<i>min</i>	0	3	0	0	1	0	4	2	2	0	0	0	1	2	2
Sky temperature (°C)															
<i>max</i>	1.7	0.2	18.1	2.1	4.7	1.4	6.9	21	6.7	13.4	3.3	-5.7	16.2	-8.1	0.9
<i>min</i>	-36.5	-35.4	-2.5	-34.7	-11.8	-19.9	-34	-5.2	-35.8	-8.1	-28.8	-32.9	1.9	-30.1	-30.8
Total range	38.2	35.6	20.6	36.8	16.5	21.3	40.9	26.2	42.5	21.5	32.1	27.2	14.3	22	31.7
24-hour range	28.5	27.9	15.3	27.2	16.5	13.7	28.4	22	35.3	21.5	18.7	23.7	11.7	17.7	29.3

On the inside surfaces of the vertical walls the stress level was much lower due to the greater thickness which increased the non-linearity of the stress distribution as described in Paper IV. When the occurrences of the maximum tensile stress are analysed, the time is about the same as for the top slab cases, see Table 5.5 for the results. The annual maxima of the thermal tensile stress on the inside surface of the south wall, for the case with the bridge going east to west, all occur around 16 to 18 hours for the bridge placed in Stockholm. If the bridge is placed in Luleå the same time interval for the occurrence of the maximum tensile stresses is present for the spring case. For the climate case which gives large stresses during winter, the time of occurrence can be at any time during the day or night.

Table 5.5 Date and time for the occurrence of maximum thermal tensile stress on the vertical south wall in the top section of the New Svinesund Bridge

Year	Stockholm		Luleå	
	Date	Time	Date	Time
1983	8 Jul	16	3 Dec	11
1984	29 Apr	18	11 Jan	13
1985	26 May	18	18 Jun	17
1986	26 Jun	17	24 Jan	10
1987	5 Jun	17	30 May	18
1988	27 Apr	16	12 May	17
1989	23 May	18	19 Dec	16
1990	30 Apr	19	6 Jun	18
1991	19 May	17	8 Jun	18
1992	15 May	17	25 Jun	18
1993	9 Jun	17	19 Dec	22
1994	3 Jul	18	14 Feb	19
1995	26 May	17	2 Jun	18
1996	22 May	18	1 Jan	21
1997	30 Jun	18	31 Mar	18

When the bridge runs north to south the east wall receives large incident solar radiation before noon and the west wall receives it after noon. For a wall facing east this would indicate that the largest thermal differential occurs during the morning, and thus large thermal stresses. For the cross-section used here however, the annual maximum tensile stress occurs in the afternoon around 14 or 15 hours, see Table 5.6. This can be compared to the occurrence of the maximum positive linear temperature differential in the east wall around 10 to 12 hours. This effect could be caused by the increased non-linearity of the stress distribution in the vertical walls, which is explained more in Paper IV. The maximum stress will therefore occur closer to the occurrence of the maximum tensile stress on the inside of the top slab, since this is much larger. A conclusion regarding this phenomena can unfortunately only be drawn if other cross-sections are investigated, which has only been made for the case with the bridge running east to west. For one year the maximum positive linear temperature differential in the

east wall occurs at 19 hours, which may be explained by the same phenomena as for the winter case in Luleå with a rapid change in air temperature and cloud-cover. For the west wall the largest tensile stress on the inside wall occurs around 18 to 20 hours in the evening, which coincides with the occurrence time of the largest linear temperature differential.

Table 5.6 Date and time for the occurrence of maximum thermal tensile stress and maximum linear differential in the vertical east and west walls in the top section of the New Svinesund Bridge with Stockholm data

Year	East				West			
	Maximum tensile stress		Maximum positive linear differential		Maximum tensile stress		Maximum positive linear differential	
	Date	Time	Date	Time	Date	Time	Date	Time
1983	8 Jul	14	8 Jul	11	8 Jul	16	7 Jul	19
1984	17 Jun	14	17 Jun	10	29 Apr	18	29 Apr	19
1985	5 Jul	15	5 Jul	10	26 May	19	26 May	19
1986	26 Jun	15	26 Jun	11	26 Jun	18	26 Jun	19
1987	5 Jun	14	31 Jan	19	23 May	19	23 May	19
1988	27 Apr	14	28 Apr	11	28 Apr	16	9 Jun	19
1989	23 May	15	23 May	11	23 May	19	3 Jul	20
1990	29 May	15	29 May	12	30 May	20	30 Apr	20
1991	3 Jul	14	3 Jul	11	19 May	18	19 May	18
1992	26 Jun	15	15 May	12	19 May	19	19 May	19
1993	10 Jun	15	10 Jun	12	9 Jun	18	9 Jun	19
1994	3 Jul	15	7 Oct	11	27 Jul	18	6 May	19
1995	26 May	15	26 Jun	11	23 Apr	17	3 May	18
1996	13 May	17	7 Jan	8	13 May	18	12 May	19
1997	1 Jul	15	12 May	10	1 Jun	19	1 Jun	18

For climate situations used by other researchers, e.g. Emerson (1977), Alavizadeh-Farhang (1999b), Soukhov (2000) it was assumed that a large positive temperature differential only occur during days with large incident solar radiation. For the situation in United Kingdom this may be true, due to the location being on similar or lower latitude than Stockholm. For countries further north close to the Arctic Circle the results in this investigation show that an assumption of using climate data or climate situations from the summer or spring months is not always valid. The time of the occurrence of the maximum tensile stresses is also different from the time span assumed in the Eurocode of June to August. For Swedish conditions large thermal actions and stresses caused by high solar radiation influx and a large range in air temperature can occur from April to July. The geometry of the structure has a large impact on this time period, since the winter case only was found for the box cross-section and not for the slab due to the presence of an inside cavity in the box case.

5.2 Design climate situations

According to the background document for Eurocode on thermal actions (CEN 1996) three days can be considered as independent of three other days, and the 3-day maxima of thermal actions were defined. One of the objectives in this thesis was to find climate situations which can be used in design of concrete bridges. The stated three-day independent period was therefore used as a basis for short-term climate simulations using data from only a few days. The short-term data were used to calculate the temperature distribution for the Svinesund Bridge cross-section, and thus the resulting thermal stresses.

The climate data was chosen based on the results from the study presented in Paper IV of extreme events of thermal stresses and the analysis of the thermal input data in section 5.1. As mentioned in previous chapters and in Paper IV the maximum tensile stress appears on the inside surface of the top slab. Four climate situations were chosen for the comparisons, two from Stockholm and two from Luleå. In all cases the input data from four days was chosen, the day of the occurrence of the annual maximum tensile stress of the chosen year and the three days prior to this day. For Stockholm the years 1986 and 1991 and for Luleå the years 1987 and 1989 were chosen. This corresponds to the cases for Stockholm when the maximum air temperature was either hot, 29 °C in 1986, or a bit colder, 15 °C in 1991. For Luleå one climate situation with large incident solar radiation and a large range of air temperature was chosen (1987), along with a winter situation (1989) with almost no incident solar radiation but a 30 °C range in air temperature and a 40 °C range in effective sky temperature. In all simulations the start temperature of the cross-section was set to the starting air temperature.

The maximum tensile stresses on the inside surface of the top slab obtained from the short-term simulations are presented in Table 5.7 along with the corresponding annual maximum tensile stress from the long-term simulations. The results show that for three of the four cases the tensile stress levels are close with a difference of only 0.1 MPa. For the fourth case however, the short-term result is only two thirds of the long-term result. This was for the case with a large influx of solar radiation but with a lower air temperature. It shows that a climate situation which gives large stresses is not always dependent on only a few days before, but more days could be required to obtain accurate values. The assumption made for the calculations in the Eurocode could therefore be a bit too generalized, since three days are clearly not independent for all climate combinations.

Table 5.7 Tensile stress on the inside surface of the top slab (MPa)

	Short-term	Long-term
Stockholm		
1986	2.75	2.65
1991	1.58	2.26
Luleå		
1987	2.10	2.05
1989	2.16	2.18

The three simulations which give more accurate results show however, that it is possible to use short-term simulations of climate situations to obtain an extreme event. The key is to have a climate situation which is either with a large influx of solar radiation and clear skies, or a situation with a very large range in shade air temperature. When the input data is analysed in more detail it was found that for Stockholm 1991 it was a warm period, followed by a short cold period which in turn became a warm period again which caused the large stresses. The short-term simulation started during the cold period, and the start temperature of the cross-section was therefore underestimated. As a consequence of this a lower stress level was obtained in the simulation. When using a shorter period it is important to have a reasonable start temperature, especially when only a few days are considered.

In Paper V a FE-simulation using climate data from one week was presented. The week chosen was the warm week in June 1986 for Stockholm, since this was the time when the maximum tensile stress in the cross-section occurred in the long-term simulations as explained earlier. Stockholm data was chosen since this was the closest meteorological station to the bridge. The results presented in this section in Table 5.7 show that this week is reasonable to use, since the short-term result was close to the long-term. It can be deduced that the chosen time-period can be seen as an extreme event, and may therefore give unfavourable stresses.

6 Other publications

In addition to the five appended papers, a number of conference papers have been written and presented orally at international conferences.

Larsson O. (2008), *Thermal Actions on Concrete Structures due to Climatic Exposure*, The XXth Symposium on Nordic Concrete Research & Development, Bålsta, Sweden (Poster)

Larsson O. (2010), *Estimating Extreme Thermal Actions in Concrete Structures*, The Third fib International Congress and Exhibition, Washington D.C., USA

Larsson O. (2010), *Estimation of Extreme Climatic Thermal Actions in Concrete Structures*, 34th IABSE International Symposium on Bridge and Structural Engineering, Large Structures and Infrastructures for Environmentally Constrained and Urbanised Areas, Venice, Italy

Larsson O. (2011), *Extreme Values of Climatic Thermal Stresses in Concrete Box Cross-section*, XXI Nordic Concrete Research Symposium, Hämeenlinna, Finland

Larsson O. (2011), *Transversal Climatic Thermal Stresses in Concrete Box Cross-sections*, IABSE-IASS Symposium: Taller, Longer, Lighter, London, United Kingdom

7 Summary of appended papers

Paper I

This paper describes the development and validation of a finite element model capable of predicting the temperature in a concrete structure due to climatic exposure. This FE-model is a thoroughly described transient heat transfer model using climate factors as input data. A validation of the model was performed using measurements from a simply supported concrete slab placed outdoors. Additional measurements of the climate input factors were also performed in the vicinity of the slab. The results show that the model can predict the temperature distribution in one dimension in the concrete slab in a satisfying manner using the climatic input factors and a general set of material properties. The model is well suited for use in further research.

Paper II

The FE-model presented in Paper I was here used with extensive climate data obtained from measurements performed by the Swedish Meteorological and Hydrological Institute (SMHI). The previous validation of the model was extended to include calculations using values obtained from the nearest meteorological station. This showed a difference in the temperature levels when station values were used due to differences in air temperature, but the model could still capture the temperature variations in the concrete. The results from the long-term simulations showed that the values specified for the positive linear temperature differential for concrete slabs in the Eurocode could be underestimated. When a paving layer of 50 mm is used, the material of the layer has a large impact. An asphalt layer gives a larger positive linear differential than a concrete layer due to the varying material properties in particular surface absorptivity. For the negative linear differential the Eurocode values seems reasonable.

Paper III

The research presented in this paper is an extension of the development and validation of the FE-model presented in Paper I. Measurements of temperature and strains in various sections of the New Svinesund Bridge have been performed by Professor Raid Karoumi at KTH. Additional measuring equipment were placed at the bridge site to obtain climatic input data. The model was used with the input data to simulate the temperature in the top section of the concrete arch in the bridge; the temperatures were compared to the measured values inside the concrete. An iterative method of estimating the air temperature inside the box section was developed, since the model should be able to be used for situations where no measured inside air temperature exists. The results show that the model is able to predict the temperature in a two-dimensional box cross-section using climatic input data. It is well suited to be used for further research of the New Svinesund Bridge and other structures.

Paper IV

The resulting transverse stresses in a box cross-section from non-uniform temperature distributions are analysed and presented in this paper. The model of the top section of the arch

in the New Svinesund Bridge was used together with extensive climate data from Stockholm and Luleå to calculate the temperature distributions over a time period of 15 years. The temperature distributions were used as basis for the stress calculations, where varying thermal expansion due to differential temperature caused stresses to develop in the section. Separate stress calculations were performed with the non-linear temperature component removed as a comparison to the approach described in Eurocode. The results show that the maximum tensile stress occurring in the section was close to the tensile strength of the used concrete. If the non-linear component is removed, the tensile stress level on the inside surfaces is overestimated. Other geometries were also tested for a one-year set of data, with results showing that the thickness of the slabs and walls of a box-section is the most important geometrical factor. If the thickness differs between the members in a box-section, the largest transverse thermal tensile stresses will appear in the thinner member independent of whether the member is horizontal or vertical.

Paper V

In the research presented in this paper a full-scale three-dimensional FE-model was used with climatic input data to estimate the resulting thermal stresses. The same approach for the climate data in the model is used as in the other papers. The Vätösund Bridge located north of Stockholm was used for the geometry of the model; the bridge was chosen due to the discovery of extensive cracking on the inside surface of the south wall. The results show that the largest tensile stresses appear on the inside of the south wall, which is in agreement with the location of the cracks. The tensile stress in the north wall is lower. The boundary conditions at mid span have a large impact on the location and magnitude of the tensile stresses. If a mid-span connection exists, as is the case for the Vätösund Bridge, large tensile stresses appear in the entire wall, while if there is no connection the largest tensile stresses appear at the top of the wall.

8 Conclusions

The conclusions based on the presented investigations and the results from the appended papers are summarized below.

When hourly values of thermal factors are used as input data, it is possible to simulate the spatial and temporal variation of temperature in a concrete structure with reasonable accuracy. When compared to measurements performed on a concrete slab, the developed FE-model is able to capture both the temperature level and the temperature variation across the section. Large positive temperature differentials in a slab occur during warm days with large amount of incident solar radiation, which is the main factor governing this gradient. The ambient air temperature is the governing factor for the spatial average temperature in the slab. The negative temperature differential is mainly governed by outgoing long-wave heat radiation which occurs during clear nights. The FE-model was found to be well suited to use for further studies of temperature distributions and thermal actions in concrete structures.

When the temperature in the slab was simulated using input data from the closest meteorological station, it was found that the average temperature was underestimated. This difference was due to a lower air temperature at the site of the station than at the test site. The simulated linear differentials were however still close to the measured differentials, which makes the model suitable to use for estimating linear differentials using data obtained from meteorological stations. The long-term simulations showed that the positive linear temperature differentials in the Eurocode may be underestimations of Swedish conditions for concrete slabs. If no paving or a paving layer of 50 mm asphalt is present, values with a return period of 5-years are close to or above the characteristic values given in the code with a return period of 50 years. A concrete paving layer will reduce the positive differential compared to an asphalt paving; this difference between asphalt and concrete paving is neglected in the Eurocode. All values of negative linear differentials seem reasonable compared to the design values in the code. The thickness of the concrete slab has a small impact on both positive and negative linear differentials.

The FE-model is also well suited to capture the temperature variations in a box-cross-section caused by climatic variations in the surrounding environment. Variations in both vertical and horizontal directions and through the depth of each slab and wall were predicted with good accuracy. A slight difference was found between modelled temperature and measured data in the top slab. This indicates that the model may have overestimated the influence of solar radiation slightly, since the difference was smaller in the other measurement points. The iterative approach for considering the effect of the inside air temperature gave results close to the results from the simulations using measured air temperature inside the cavity. The model was therefore deemed to be suitable to use for cases where no inside air temperature is available, which is the case when climate data from meteorological stations is used.

For a box cross-section such as the top section of the arch of the New Svinesund Bridge the largest thermally induced tensile stresses produced by environmental exposure appear on the inside surface of the top slab. If the non-linear temperature component is removed and new simulations performed using only the linear temperature differential over the walls and slabs, the tensile stresses are overestimated. A marginal reduction of this overestimation is achieved if the variation in average temperature between the different parts is included, but the difference is still significant. On the inside surfaces of the vertical walls the maximum tensile stress is much lower than for the top slab, about three times as low. The stress distributions in the vertical walls are much more non-linear than the distribution in the top slab, which is the major reason for the lower stresses. Due to this non-linearity the tensile stress overestimation when removing the non-linear component is larger than for the top. When the cross-section is rotated, the top and bottom slab used as vertical walls and vice versa, the largest tensile stress is produced on the inside surface of the wall facing south. The stress distribution is now more non-linear in the top, which shows the importance of the geometry of the cross-section and that the orientation has a limited influence. The investigations of other sizes of cross-sections show that a difference in thickness between the parts of a section is the most important geometrical factor compared to total height and width. The largest transverse thermal stresses will appear in the thinner member, independent on the member being horizontal or vertical.

The annual maxima of tensile stresses in the section occur when a large temperature differential is present in the slab or wall where the maximum stress appears. For the Svinesund section analysed with climate data from Stockholm the largest tensile stresses occur during the afternoon sometime from late April to mid-July. The climate situation when the large stresses occur is, as expected, a large influx of solar radiation and a large short term variation of ambient air temperature. For the climate conditions in Luleå another climate situation producing large thermal tensile stresses was identified. Here large stresses may also occur when an extreme increase in air temperature occurs during winter, an increase of about 30 °C in just a few hours. This is a situation not previously considered for design purposes. When compared to the occurrences of large positive differentials for the concrete slab studies, it can be seen that the winter case is only valid for box cross-sections. For a slab the largest positive differential occur during the afternoon sometime during spring or summer.

If a short sequence of climate data of four days is used, a similar value for the maximum tensile stress can be achieved as if data from a full year is used. It is not always certain that four days are independent however, and the climate data used for the short-term simulations have to be checked beforehand. The climate situation which gave the largest tensile stress for the Svinesund section, a week in June in Stockholm 1986, was deemed suitable for simulating an extreme event, since the short-term tests gave a good agreement with the long-term results. When this week was used as input in a three-dimensional full scale model of the Vätösund bridge, the results show that the largest tensile stresses were produced at the inside surface of the south wall. The stresses are almost perpendicular to the bottom surface of the bridge, which agrees with crack inspections, where severe cracks have been found on the same surface. The study also shows the importance of the mid-span boundary conditions for the design and analysis of a cantilever concrete bridge. An extensive study using a full scale FE-

model with climatic input data from a short period is possible to use, it is however important to use a thoroughly investigated set of data and the appropriate boundary conditions.

8.1 Further research needs

The possibility to use extensive climate data to predict extreme values of thermal actions and identify the climate situations producing these actions was a main focus of this thesis. Based on the findings future research needs have been discovered which can be of importance concerning the design and assessment of concrete structures subjected to environmental thermal actions. Some interesting points are

- The results in the thesis show the importance of the geometry of a cross-section concerning transverse effects from thermal actions. To find a general design recommendation however, more extensive studies of cross-sectional properties should be performed. Better recommendations can be useful for avoiding unexpected stress fields.
- The cyclic nature of the environmental thermal actions may contribute to fatigue problems in bridges. This may be more important for steel bridges, but may also have an impact on reinforced concrete bridges.
- The climate in the world is changing for various reasons. Investigations of how other climate loads will be affected by this have been performed, but for thermal loads this is still an uncharted field. The thermal actions will change due to climate change; investigations are needed to find in what way.

Better understanding of thermal actions now and in the future will be important since large structures are built, which will probably increase in both number and size. Concrete will be used as construction material due to its flexibility and strength. Due to safety and durability concerns, it is important to know how the loads affect the structure and what is suitable to use for design purposes. This understanding can reduce the cost and increase the lifetime of the structures, and give a designer better possibility to predict the behaviour of a structure.

9 References

- AASTHO (1989), *Guide Specifications – Thermal Effects in Concrete Bridge Superstructures*, American Association of State Highway and Transportation Officials, Washington D.C, United States
- Agullo L., Mirambell E. and Aguado A. (1996), *A Model for the Analysis of Concrete Dams due to Environmental Thermal Effects*, International Journal of Numerical Methods for Heat and Fluid Flow, Vol. 6, No. 4, pp. 25-36
- Alavizadeh-Farhang A. (1999a), *Applicability of the Effective Bridge Temperatures Derived from ENV 1991-2-5:1997 for Bridge Design Purposes in Sweden*, Structural Design and Bridges, KTH, Stockholm, Sweden
- Alavizadeh-Farhang A. (1999b), *Applicability of the Positive and Negative Linear Temperature Differences from ENV 1991-2-5:1997 for Bridge Design Purposes in Sweden*, Structural Design and Bridges, KTH, Stockholm, Sweden
- Alavizadeh-Farhang A. (2000), *Concrete Structures Subjected to Combined Mechanical and Thermal Loading*, Doctoral Thesis, KTH, Stockholm, Sweden
- Ariyawardena N., Ghali A. and Elbadry M. (1997), *Experimental Study on Thermal Cracking in Reinforced Concrete Members*, ACI Structural Journal, Title No. 94-S40, pp. 432-441
- Barr P.J., Stanton J.F. and Eberhard M.O. (2005), *Effects of Temperature Variations on Precast, Prestressed Concrete Bridge Girders*, Journal of Bridge Engineering, Vol. 10, No. 2, pp. 186-194
- Barsotti R. and Froli M. (2000), *Statistical Analysis of Thermal Actions on Concrete Segmental Box-girder Bridge*, Structural Engineering International, Vol. 10, No. 2, pp. 111-116
- Bohn M.S. and Anderson R. (1986), *Temperature and Heat Flux Distribution in a Natural Convection Enclosure Flow*, Journal of Heat Transfer, Vol. 108, pp. 471-475
- Branco F.A. and Mendes P.A. (1993), *Thermal Actions for Concrete Bridge Design*, Journal of Structural Engineering, Vol. 119, No. 8, pp. 2313-2331
- Bro 2004 (2004), VV Publ. 2004:56, Swedish Road Administration, Svensk Byggtjänst, Stockholm, Sweden

Carlson J. D., Bhardwaj R., Phelan P. E., Kaloush K. E. and Golden J. S. (2010), *Determining Thermal Conductivity of Paving Materials Using Cylindrical Sample Geometry*, Journal of Materials in Civil Engineering, Vol. 22, No. 2, pp. 186-195

CEB (1985), *Bulletin 167 Thermal Effects in the Design of Concrete Structures*, CEB, Lausanne, 1985

CEN (1996), *Background document of ENV 1991-2-5 Thermal Actions*, European Committee for Standardization, Brussels, Belgium

Clark L.A. and Church J.G. (1989), *Effects of Creep on Cracked Reinforced Concrete Beams under Combined Force and Thermal Loads*, Proceedings - Institution of Civil Engineers, Vol. 87, 415-428

Cooke N., Priestley M.J.N. and Thurston S.J. (1984), *Analysis and Design of Partially Prestressed Concrete Bridges under Thermal Loading*, PCI Journal, Vol. 29, No. 3, pp. 94–114

Darholm T., Lundh L., Ronnebrant R., Karoumi R. and Blaschko M. (2007), *Technical book about the Svinesund Bridge*, Swedish Road Administration, Uddevalla, Sweden

Dickinson E.J. (1978), *A Method for Calculating the Temperature Gradients in Asphaltic Concrete Pavement Structures Based on Climate Data*, Australian Road Research, Vol. 8, No. 4, pp. 16-34

Duffie J.A. and Beckman W.A (2006), *Solar Engineering of Thermal Processes (3rd edition)*, Wiley, Hoboken, United States

Dwivedi A.K., Bhargava P. and Bhandari N.M. (2009), *Temperature Effects in the Design of Concrete Bridges*, Advances in Bridge Engineering, London, pp. 555-568

Elbadry M.M. and Ghali A. (1983a), *Nonlinear Temperature Distribution and its Effects on Bridges*, IABSE Proceedings, No. 3, pp. 169-191

Elbadry M.M. and Ghali A. (1983b), *Temperature Variations in Concrete Bridges*, Journal of Structural Engineering, Vol. 109, No 10, pp. 2355-2374

Elbadry M.M. and Ghali A. (1986), *Thermal Stresses and Cracking of Concrete Bridges*, ACI Journal, Title No. 83-90, pp. 1001-1009

Elbadry M.M. and Ghali A. (1995), *Control of Thermal Cracking of Concrete Bridges*, ACI Structural Journal, Title No. 92-S42, pp. 435-449

Elgaaly M. (1988) *Thermal Gradient in Beams, Walls and Slabs*, ACI Structural Journal, Title no. 85-S9, pp. 76-81

Emerson M. (1973), *The Calculation of the Distribution of Temperature in Bridges*, TRRL Report LR 561, Crowthorne, United Kingdom

Emerson M. (1977), *Temperature Differences in Bridges: Basis of Design Requirements*, TRRL Report LR 765, Crowthorne, United Kingdom

England G.L. and Ross A.D. (1962), *Reinforced Concrete under Thermal Gradients*, Magazine of Concrete Research, Vol. 14, No. 40, pp. 5-12

England G.L. (1977), *Steady-state Stresses in Concrete Structures Subjected to Sustained and Cyclically Varying Temperatures*, Nuclear Engineering and Design, Vol. 44, pp. 97-107

England G.L. (1980), *Creep and Temperature Effects in Concrete Structures: Reality and Prediction*, Applied Mathematical Modelling, Vol. 4, pp. 261-267

SS-EN 1990 (2002), *Eurocode – Basis of structural design*, European Committee for Standardization, Swedish Standards Institute, Stockholm, Sweden

SS-EN 1991-1-5 (2003), *Eurocode 1: Actions on structures - Part 1-5: General actions - Thermal actions*, European Committee for Standardization, Swedish Standards Institute, Stockholm, Sweden

SS-EN 1992-1-1 (2005), *Eurocode 2: Design of concrete structures - Part 1-1: General rules and rules for buildings*, European Committee for Standardization, Swedish Standards Institute, Stockholm, Sweden

Fahmi H.M., Polivka M. and Bresler B. (1972), *Effect of Sustained and Cyclic Elevated Temperature on Creep of Concrete*, Cement and Concrete Research, Vol. 2, pp. 591-606

Fouad N.A. (1999), *Temperature Loading of Concrete Bridges due to Environmental Thermal Actions*, fib Symposium, 12th - 15th Oct., Prague, Czech Republic

Fu H.C., Ng S.F. and Cheung M.S. (1990), *Thermal Behaviour of Composite Bridges*, Journal of Structural Engineering, Vol. 116, No. 12, pp. 3302-3323

Hansen T. C. and Eriksson L., (1966), *Temperature Change Effect on Behavior of Cement Paste, Mortar, and Concrete under Load*, Journal of the American Concrete Institute, Title No. 63-23, pp. 489-502

Hirst M.J.S. (1984), *Thermal Loading of Concrete Bridges*, Canadian Journal of Civil Engineering, Vol. 11, pp. 423-429

Hunt B. and Cooke N. (1975), *Thermal Calculations for Bridge Design*, Journal of the structural division, Vol. 101, No. ST9, pp. 1763-1781

Incropera F. P., Dewitt D.P., Bergman T.L. and Lavine A.S. (2007), *Fundamentals of Heat and Mass Transfer* (6th edition), Wiley, Hoboken, United States

Jokela J. (1983), *Behaviour and Design of Concrete Structures under Thermal Gradients*, Nordic Concrete Research, No. 3, pp. 100-128

Khan M.I. (2001), *Factors Affecting the Thermal Properties of Concrete and Applicability of its Prediction Models*, Building and Environment, Vol. 37, pp. 607-614

Karoumi R. and Andersson A. (2007), *Load Testing of the New Svinesund Bridge: Presentation of results and theoretical verification of bridge behaviour*, TRITA-BKN. Rapport 96, Royal Institute of Technology (KTH), Stockholm

Karoumi R., Ronnebrant R., Harryson P. and Darholm T. (2009) *Understanding the Real Behaviour of The New Svinesund Bridge by Monitoring*, The Fifth Symposium on Strait Crossings, Trondheim, Norway

Leonhardt F., Kolbe G. and Peter J. (1965), *Temperaturunterschiede gefährden Spannbetonbrücke*, Beton- und Stahlbetonbau, No. 7, pp. 157-163

Levinson R. and Akbari H. (2001), *Effects of Composition and Exposure on the Solar Reflectance of Portland Cement Concrete*, LBNL-48334, Lawrence Berkeley National Laboratory, United States

Ljungkrantz C., Möller G. and Petersons N. (1994), *Betonghandbok, Material*, Svensk Byggtjänst, Stockholm, Sweden

Loudon A.G. and Stacey E.F. (1966), *The Thermal and Acoustic Properties of Lightweight Concretes*, Structural Concrete, Vol. 3, No. 2, pp. 58-95

Majorana C.E., Zavarise G., Borsetto M. and Guiseppetti M. (1990), *Nonlinear Analysis of Thermal Stresses in Mass Concrete Castings*, Cement and Concrete Research, Vol. 20, pp. 559-578

Marková J. (2010), *Models of Thermal Actions for Bridges*, Reliability, Risk and Safety, Three Volume Set, Theory and Applications, Taylor & Francis Group, London, United Kingdom

Marceau M.L. and VanGeem M.G. (2007), *Solar Reflectance of Concretes for LEED Sustainable Sites Credit: Heat Island Effect*, SN2982, Portland Cement Association, Skokie, Illinois, United States

- Marshall A.L. (1972), *The Thermal Properties of Concrete*, Building Science, Vol. 7, pp. 167-174
- Mirambell E., Aguado A., Mendes P. and Branco F. (1991), *Design Temperature Differences for Concrete Bridges*, Structural Engineering International, Vol. 1, No. 3, pp. 36-40
- Mirambell E. and Aguado A. (1990), *Temperature and Stress Distributions in Concrete Box Girder Bridges*, Journal of Structural Engineering, Vol. 116, No. 9, pp. 2388-2409
- Nasser K.W. and Neville A.M. (1966), *Creep of Concrete at Temperatures above Normal*, Nuclear Engineering and Design, Vol. 4, pp. 90-96
- Nevander L.E. and Elmarsson B. (2001), *Fukthandbok*, Svensk Byggtjänst, Stockholm, Sweden
- Neville A.M. (1970), *Creep of Concrete: Plain, Reinforced and Prestressed*, North-Holland, Amsterdam, Netherlands
- Neville A.M. (1995), *Properties of Concrete (4th edition)*, Longman, Harlow, United Kingdom
- Pei-Heng L., Mao-Hua Z. and Wei-Zhen C. (2010), *Analysis of Temperature Stress for Concrete Box Girders Cracking*, 2010 International Conference on Mechanical Automation and Control Engineering, Wuhan, China, pp. 1590 – 1594
- Perez R., Seals R., Ineichen P., Stewart R. and Menicucci D. (1987), *A New Simplified Version of the Perez Diffuse Irradiance Model for Tilted Surfaces*, Solar Energy, Vol. 39, No. 3, pp. 221-231
- Prakash Rao D.S. (1986), *Temperature Distributions and Stresses in Concrete Bridges*. ACI Journal, Title No. 83-52, pp. 588-596
- Priestley M.J.N. (1976) *Ambient Thermal Stresses in Circular Prestressed Concrete Tanks*, ACI Journal, Title No. 73-45, pp. 553-560
- Priestley M.J.N (1978), *Design of Concrete Bridges for Temperature Gradients*, ACI Journal, Title No. 75-23, pp. 209-217
- Reagan J.A. and Acklam D.M. (1979), *Solar Reflectivity of Common Building Materials and its Influence on the Roof Heat Gain of Typical Southwestern U.S.A. Residences*, Energy and Buildings, Vol. 2, pp. 237-248

Roberts-Wollman C.L., Breen J.E. and Cawrse J. (2002), *Measurements of Thermal Gradients and their Effects on Segmental Concrete Bridge*, Journal of Bridge Engineering, Vol. 7, No. 3, pp. 166-174

Saetta A., Scotta R. and Vitaliani R. (1995), *Stress Analysis of Concrete Structures Subjected to Variable Thermal Loads*, Journal of Structural Engineering, Vol. 121, No. 3, pp. 446-457

Sheibany F. and Ghaemian M. (2006), *Effects of Environmental Action on Thermal Stress Analysis of Karaj Concrete Arch Dam*, Journal of Engineering Mechanics, Vol. 132, No. 5, pp. 532-544

Shkoukani H. and Walraven J.C. (1993), *Creep and Relaxation of Concrete Subjected to Imposed Thermal Deformations*, Creep and Shrinkage – Proceedings of the fifth international RILEM symposium, pp. 45-50

Shushkewich K.W (1998), *Design of Segmental Bridges for Thermal Gradient*, PCI Journal, Vol. 43, No. 4, pp. 120-128

Silviera A.P., Branco F.A. and Castanheta M. (2000), *Statistical Analysis of Thermal Actions for Concrete Bridge Design*, Structural Engineering International, Vol. 10, No. 1, pp. 33-38

Soukhov D. (1994), *Two Methods for Determination of Linear Temperature Differences in Concrete Bridges with the help of Statistical Analysis*, Darmstadt Concrete, Vol. 9, pp. 193-210

Soukhov D. (2000), *Representative Values of Thermal Actions for Concrete Bridges*, Progress in Structural Engineering and Material, Vol. 2, No. 4, pp. 495-501

Suzuki J., Ohba Y., Uchikawa Y., Hoshikawa K. and Kimura K. (2007), *Monitoring Temperatures on a Real Box-Girder Bridge and Energy Budget Analysis for Basic Information on Bridge Cooling and Surface Freezing*, Journal of Bridge Engineering, Vol. 12, No. 1, pp. 45-52

Sveinson T.N. (2004), *Temperature Effects in Concrete Box-girder Bridges*, Ph.D. Thesis, Department of Civil Engineering, University of Calgary, Canada

Thevenard D. and Haddad K. (2005), *Ground Reflectivity in the Context of Building Energy Simulation*, Energy and Buildings, Vol. 38, pp. 972-980

Threlkeld J.L. (1970), *Thermal Environmental Engineering*, (2nd edition), Prentice Hall, Inc., Englewood Cliffs, United States

Thurston S.J., Priestley M.J.N and Cooke N. (1980), *Thermal Analysis of Thick Concrete Sections*, ACI Journal, Title No. 77-38, pp. 347-357

- Thurston S.J., Priestley M.J.N and Cooke N. (1984), *Influence of Cracking on Thermal Response of Reinforced Concrete Bridges*, Concrete International, Vol. 6, No. 8, pp. 36-43
- Vandewalle L. (2000), *Concrete Creep and Shrinkage at Cyclic Ambient Conditions*, Cement and Concrete Composites, Vol. 22, pp. 201-208
- Vecchio F.J. (1987), *Nonlinear Analysis of Reinforced Concrete Frames Subjected to Thermal and Mechanical Loads*, ACI Structural Journal, Title no. 84-S51, pp. 492-501
- Vecchio F.J. and Sato J.A. (1990), *Thermal Gradient Effects in Reinforced Concrete Frame Structures*, ACI Structural Journal, Title no. 87-S27, pp. 262-275
- Vecchio F.J., Agostino N. and Angelakos B. (1993), *Reinforced Concrete Slabs Subjected to Thermal Loads*, Canadian Journal of Civil Engineering, Vol. 20, pp. 741-753
- Wang J. and Fang Z. (2009), *Temperature Variation of Concrete Box-girder Bridge*, Frontiers Of Architecture And Civil Engineering In China, Vol. 3, No. 4, pp. 407-413
- Xu Q. and Burgoyne C. (2005), *Thermal-creep Analysis of Concrete Bridges*, Bridge Engineering, Vol. 158, No. 3, pp. 107-115
- Zichner T. (1982), *Thermal Effects on Concrete Bridges*, CEB Bulletin d' information No 154, pp. 291- 313

I

Modelling of temperature profiles in a concrete slab under climatic exposure

O. Larsson

Effects of surrounding climate impose temperature variations in both time and space for concrete structures. The associated thermal strains may give rise to stresses and cracking due to external or internal restraint. This will affect the performance of the structure. It is therefore important to analyse the temperature variations and the extreme situations that can occur. To predict the dynamic thermal conditions in concrete structures a finite-element model has been developed. The ability of the model to describe correctly the various boundary conditions such as solar radiation, outgoing long-wave radiation and convection is investigated in this paper. Field temperature measurements in a concrete slab placed outdoors are used for the validation. The necessary climatic input data for the model were obtained from measurements in the vicinity of the slab. The results show that the model can describe with good accuracy the effects of different climatic factors in extreme situations and is well suited to use in further studies.

[doi: 10.1680/stco.2009.10.4.193]



Oskar Larsson
Lund University,
Sweden

Introduction

Thermal actions due to environmental influences can be a significant problem in modern concrete bridges with large spans. These thermal actions lead to temperature variations in both time and space in the concrete. The movements associated with temperature changes will affect the performance and durability of a bridge. For a concrete section the temperature profile can be divided into four time-dependent components, as illustrated in Figure 1.

- An average temperature change producing longitudinal movements.
- A linear temperature variation over the cross-section in the vertical direction leading to curvature.
- A linear temperature variation over the cross-section in the horizontal direction leading to curvature.
- A non-linear temperature distribution producing eigenstresses due to differential thermal movements between sub-elements in the cross-section.

The linear parts of a temperature profile will be referred to as linear temperature gradients in this paper.

For a concrete cross-section the time-

dependent temperature field $T(y, z, t)$ will be affected by temporal variations in climatic factors such as air temperature, solar radiation, wind speed and long-wave radiation, see Figure 2. The temperature profile also depends on the material properties of the concrete: density, thermal conductivity, specific heat and surface colour.

Extreme values of average temperature change are mainly attributable to annual variation in air temperature, whereas the linear gradients as well as the non-linear temperature field are mainly attributable to solar radiation and daily climate changes.

If the movements associated with temperature changes are restrained, stresses are induced in the structure. These stresses may contribute to cracking, which is a significant problem in concrete structures. It is known from inspections of concrete bridges that cracks are more frequent on faces exposed to solar radiation. This is a clear indication that thermal actions have a significant influence on the performance. Thermal actions have more significant effects in serviceability limit states, but they can also affect the performance of the structure in ultimate limit states owing to fatigue- and brittle-type failure modes.

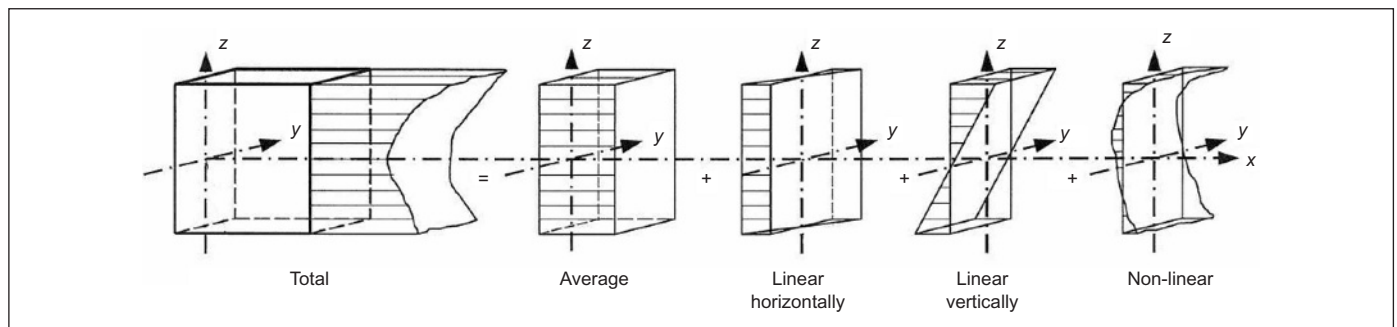
To prevent and limit cracks it is therefore important to develop methods to perform more detailed evaluation of thermal effects and the stresses these effects induce. The use of such methods is motivated for large bridges with special design conditions, for assessment of existing bridges where thermal actions can be expected to contribute significantly, and in connection with monitoring to distinguish

thermally induced response from other effects.

Background

In the 20th century many concrete bridges with larger spans were constructed. These bridges were designed with a reduced number of joints and bearings, because of durability concerns and more advanced analysis methods. This led to more problems with thermal effects and several accidents were reported.² In 1985 a Comité Euro-International du Béton (CEB) task group was formed to develop a guide concerning practical information and suggestions to engineers about thermal actions in concrete structures.³ Analysis of temperature variations in concrete bridge cross-sections have since then been made by several different authors for different climate areas in the world, for example Mirambell *et al.*,⁴ Dwivedi *et al.*⁵ and Soukhov.⁶ Earlier research used finite-difference analysis to execute the calculations,⁷ but most recent researchers have used the finite-element (FE) method to evaluate temperature variations.

In the background document of ENV 1991-2-5,⁸ the different approaches concerning thermal effects in concrete structures for different European countries are discussed. The background document led to the development of ENV 1991-1-5¹ where a method is presented for calculating the temperature variations with a statistical approach. This has been created for some areas in Europe.



△ Figure 1 Components of a temperature profile in a cross-section¹

Research has also been carried out regarding Swedish conditions, but using temperatures only from some areas and a general set of climate data.^{9,10} This research was used to develop the Swedish standard based on Eurocode.¹¹ No investigation has been made using large sets of climate data from several years.

To make calculations of temperature variations in concrete with large sets of data a FE model has been developed. The FE model will be used with extensive climate data to perform a statistical evaluation of temperature differences and variations in concrete bridges for Swedish conditions. The main problem when predicting temperature conditions in a structure is to describe the boundary conditions and the climatic exposure. Solar radiation, long-wave radiation and convection are

factors that must be captured in a correct manner in the analysis. It is therefore important to perform an extensive validation of the model and its ability to cope with climatic variations.

Measurements

To validate the model, field temperature measurements have been performed. A reinforced concrete slab was cast and placed on a steel scaffold outdoors; the slab was placed to get as little interference from surrounding buildings as possible. Ten thermocouples were placed in the centre of the slab at various heights, before casting (see Figure 3), with the top one on the upper surface. The size of the slab was designed to obtain a

one-dimensional heat flow in the centre. On an adjacent building various equipment was mounted to monitor the environmental factors required in the FE model. This equipment comprised a BF3 sunshine sensor to measure global and diffuse solar radiation (W/m^2), an Oregon scientific weather station to measure wind speed (m/s), rain (mm) and temperature ($^{\circ}\text{C}$), and an Eppley pyrgeometer to measure incoming long-wave radiation from the sky (W/m^2).

Finite element implementation

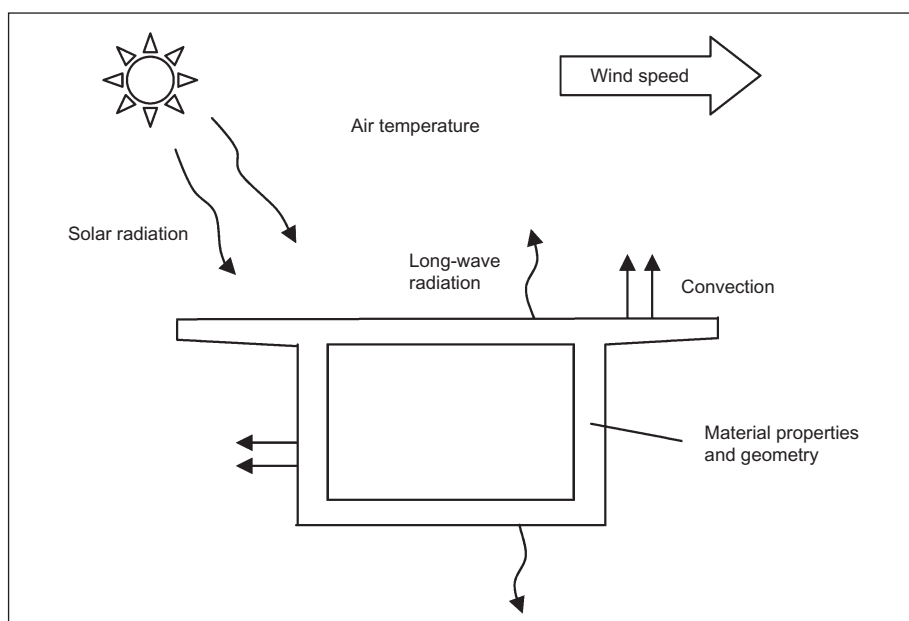
For a concrete slab with sufficient length and width in relation to the depth the heat transfer in the centre can be described as one-dimensional. The differential equation for a one-dimensional heat transfer problem can be written as^{2,12}

$$\rho c \frac{dT}{dt} = \frac{d}{dx} \left(k \frac{dT}{dx} \right) + q_v \quad (1)$$

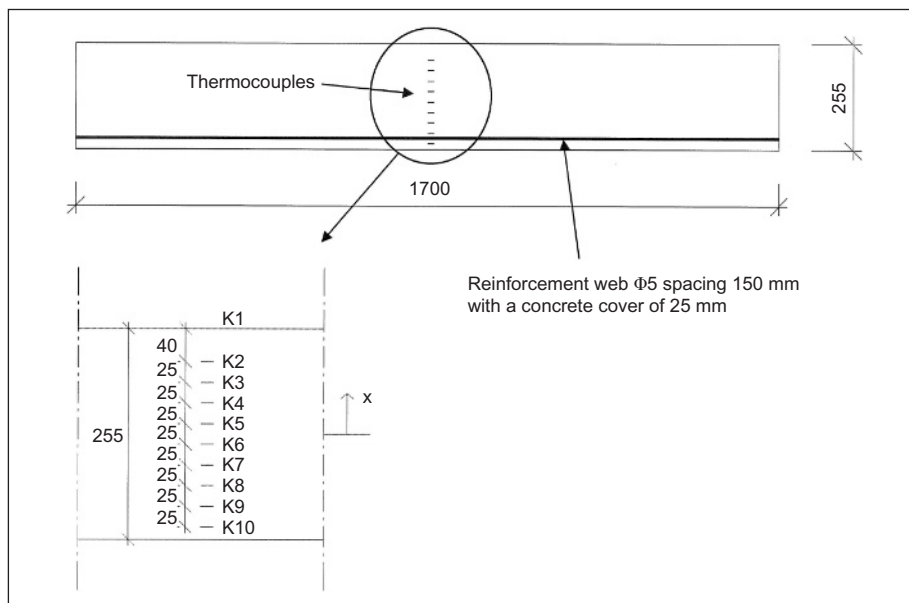
where ρ is the density (kg/m^3), c is the specific heat capacity ($\text{J/kg } ^{\circ}\text{C}$) and k is the thermal conductivity ($\text{W/m } ^{\circ}\text{C}$) of concrete. The heat generated in the concrete due to hydration, q_v , can be neglected here when the temperature is calculated for already hardened concrete. The boundary condition for the heat transfer problem is

$$k \frac{dT}{dx} n_x - q = 0 \quad (2)$$

where q is the rate of heat transferred from the environment to the concrete surface per unit area (W/m^2) and n_x is the direction cosine of the unit outward vector normal to the boundary surface. The heat transferred between the concrete surface and the



△ Figure 2 Governing thermal factors affecting a bridge cross-section



△ Figure 3 Dimensions (mm) of the slab and the positions of the thermocouples at various heights. K1–K10 are labels for the thermocouples. The origin is located mid-height in the slab

environment consists of different parts: solar radiation q_s , long-wave radiation q_r and convection q_c added together

$$q = q_s + q_r + q_c \quad \text{W/m}^2 \quad (3)$$

Solar radiation has a great impact on the temperature in concrete. It will cause the temperature to increase rapidly at the exposed surface and then successively increase further into the concrete at a slower rate. This causes a large increase in the positive linear temperature gradient, as well as an increase of average temperature in the structure. The gradient is positive if the temperature is higher in the top part than in the bottom part and if it is higher in the bottom part the gradient is negative. To model the effect of solar radiation on a horizontal concrete surface the incident global radiation must be known. This has been measured with a BF3-pyranometer, which measures both global and diffuse radiation. The solar radiation can be modelled using a heat flux load, with the measured values as input data. As some radiation is reflected, the amount of global radiation G must be multiplied with an absorption coefficient a to obtain the correct heat flux, see Equation 4. The absorption coefficient is mainly dependent on the colour and texture

of the surface.¹³ Normally, a bridge deck is covered with a layer of asphalt with darker surface and higher absorption coefficient. The concrete used in this investigation has a bright colour and the absorption coefficient is

therefore chosen to be 0.5

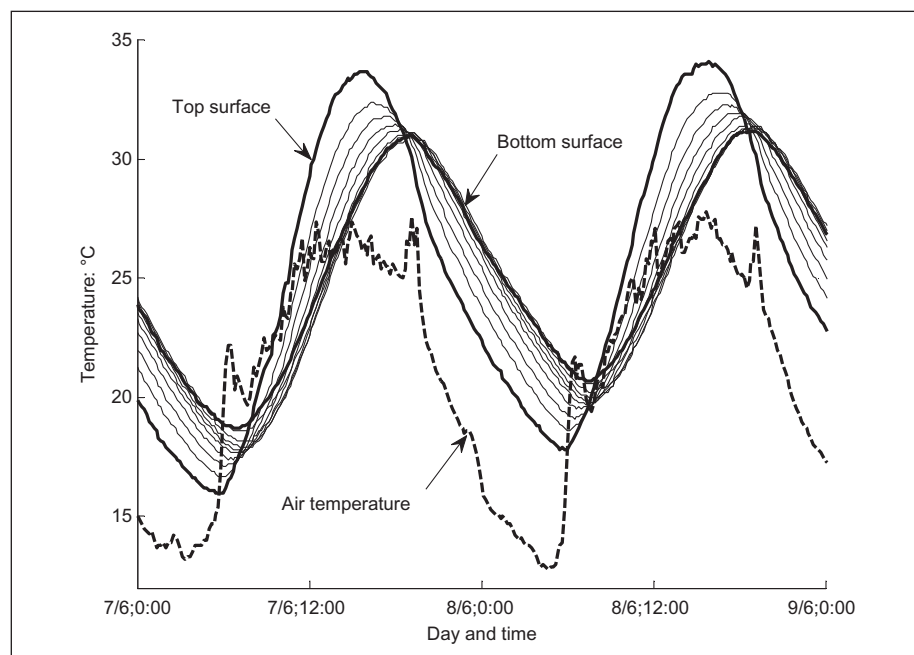
$$q_s = a G \quad \text{W/m}^2 \quad (4)$$

At night the temperature in concrete will be most affected by the air temperature and the outgoing long-wave heat radiation. The effects of outgoing radiation are the reverse of the effects of solar radiation; it will get colder at the surface, which is most exposed to the sky, and the temperature will successively decrease further into the concrete. Outgoing long-wave radiation causes a negative linear temperature profile in the concrete.

The outgoing long-wave radiation q_r depends on how much of the surface is exposed to the sky, the cloudiness and the equivalent sky temperature. This temperature is a fictitious value that describes what temperature the sky would have if it was a plane surface. The outgoing long-wave radiation is modelled using the Stefan–Boltzmann law¹²

$$q_r = q_s - q_{sky} = \sigma \epsilon_c (T_s^4 - T_{sky}^4) \quad \text{W/m}^2 \quad (5)$$

where q_s is the long-wave radiation from the concrete surface, q_{sky} is the long-wave radiation from the sky, σ is the Stefan–Boltzmann



△ Figure 4 Measured temperatures at various heights in the slab mainly affected by solar radiation. See Figure 3 for positions of the thermocouples

constant, ε_c is the emissivity of the concrete surface, T_s is the surface temperature and T_{sky} is the equivalent sky temperature. In the FE model, the emissivity and the equivalent sky temperature must be specified. The emissivity for concrete is 0.9 according to Branco and Mendes,² while the equivalent sky temperature is measured indirectly using a pyrgeometer, which measures the long-wave radiation coming from the sky q_{sky} . From this the equivalent sky temperature T_{sky} can be derived using the Stefan–Boltzmann law

$$T_{sky} = \sqrt[4]{\frac{q_{sky}}{\sigma \varepsilon_c}} \quad ^\circ\text{C} \quad (6)$$

Another climatic factor that affects concrete is heat convection between the concrete surfaces and the surrounding air. Convection consists of two processes, natural convection and forced convection. Natural convection is created when the surface is heated and warm air is rising from the vicinity of the surface to the surrounding air. Forced convection will appear when the wind is blowing across the surface and heat is then transferred between the air and the surface. Convection is modelled using Newton's law of cooling¹²

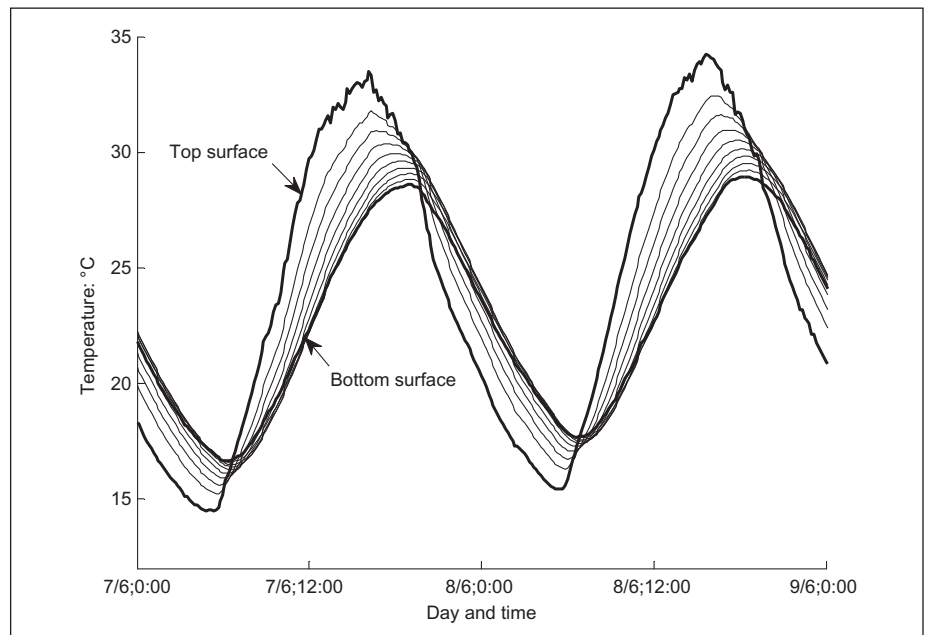
$$q_c = h_c (T_s - T_{air}) \quad \text{W/m}^2 \quad (7)$$

where T_s is the surface temperature, T_{air} is the temperature in the surrounding air and h_c is the convection coefficient. The surrounding air temperature is the climatic factor which affects the concrete the most; but as the temperature changes relatively slowly all around the slab, it will contribute less to extreme values for the linear temperature variations. Changes in air temperature will mostly affect the average temperature in the concrete.

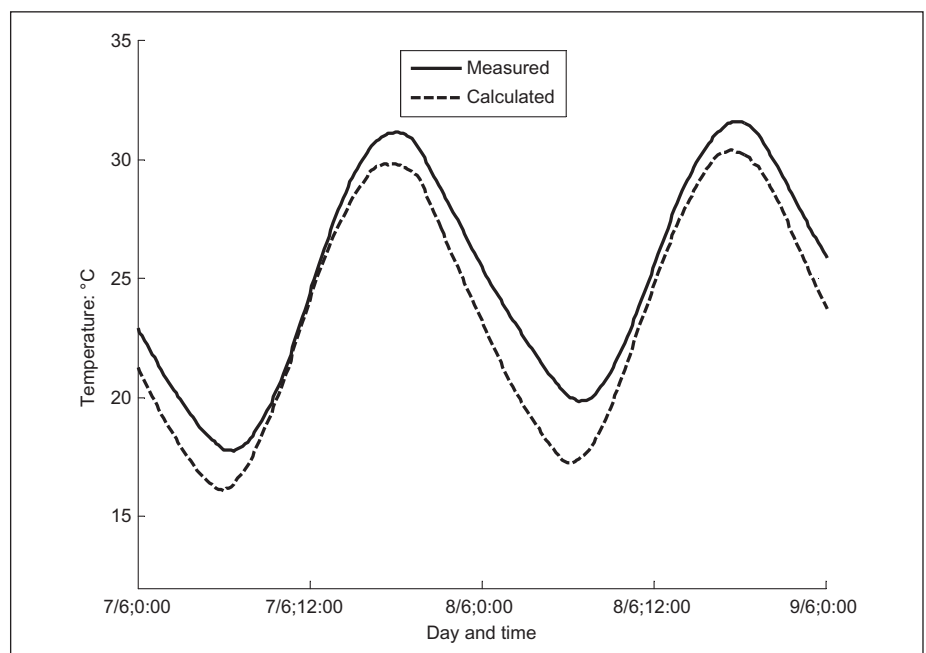
The convection coefficient can be expressed in different ways, for example as in Duffie and Beckman¹³

$$h_c = 5.7 + 3.8V \quad \text{W/m}^2 \text{ } ^\circ\text{C} \quad (8)$$

where V is the wind speed (m/s). The expression states that the natural convection is affecting the concrete at lower wind velocities, but at higher velocities the convection is dominated by forced convection. This equation is specially designed for a 0.5 m² large slab. For a larger slab, which is more useful for the slab in this investigation, the



△ Figure 5 Temperature at various heights in the slab from FE analysis mainly affected by solar radiation



△ Figure 6 Average temperature in the cross-section of the slab from measurements and FE analysis mainly affected by solar radiation

following expression from Nevander and Elmarsson¹⁴ can be used:

$$h_c = 6 + 4V \quad \text{W/m}^2 \text{ } ^\circ\text{C} \quad \text{if } V \leq 5 \text{ m/s} \quad (9a)$$

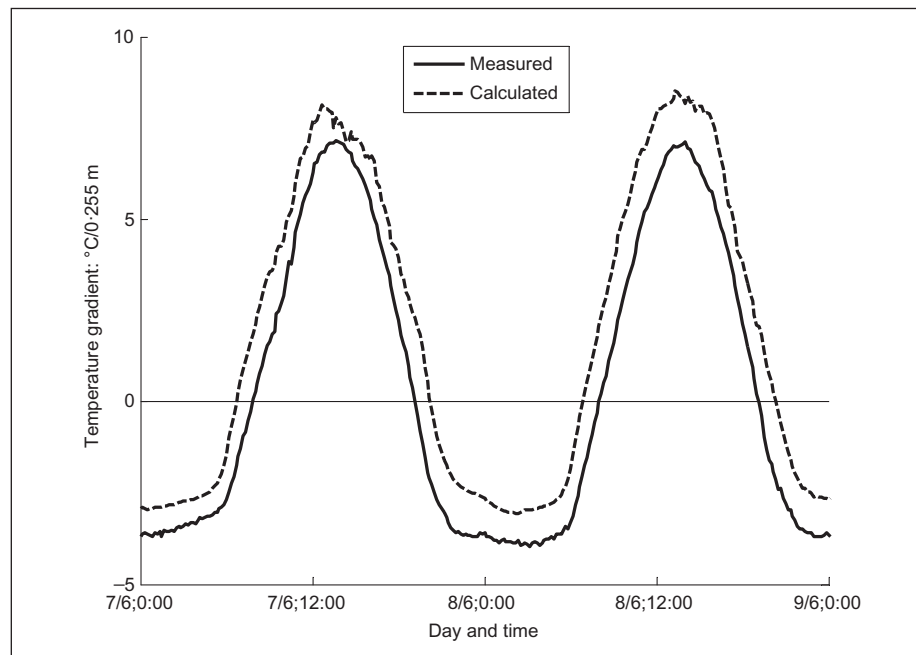
$$h_c = 7.4V^{0.78} \quad \text{W/m}^2 \text{ } ^\circ\text{C} \quad \text{if } V > 5 \text{ m/s} \quad (9b)$$

The first of these expressions is similar to the expression from Duffie and Beckman, which indicates that the difference between different surface sizes is not very large. Equations 9a and 9b are used in the present analysis. Another factor that can affect the

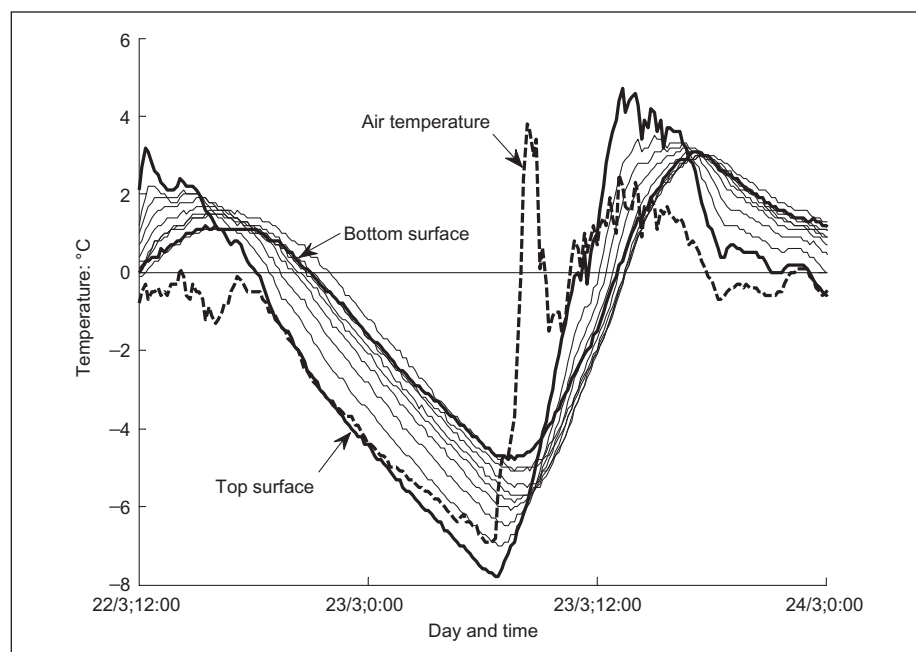
temperature is rain; if the concrete is wet some of the heat from solar radiation is consumed to make it dry again. This will cause the temperature to rise more slowly than it would if the concrete were dry from the start. The effect of rain is countering the extreme temperature variations that can occur, so it is not considered in the calculations.

The material parameters that affect the temperature variation in concrete are density, specific heat capacity and heat conductivity. In the model the material parameters used have been taken from the literature and have not been measured for this particular case study. This is because the model will in the future be used for general concrete structures where the material parameters are undefined. The density of concrete typically varies between 2100 and 2500 kg/m³ according to *Betonghandbok, Material*,¹⁵ in the present paper the value used is 2400 kg/m³. Similar intervals are found in Neville¹⁶ for the specific heat capacity, which varies between 840 and 1170 J/kg °C; the value used in the present paper is 900 J/kg °C. The variation in specific heat capacity is mainly due to the moisture content, temperature and water–cement ratio of the concrete. As the temperature range in the present case is small, the effect of temperature change on the specific heat capacity will also be small. The heat conductivity of concrete is mainly dependent on the heat conductivity of the cement paste and aggregate; it can vary from 1.4 to 3.6 W/kg °C;¹⁶ and the value used in the simulations is 2.5 W/kg °C.

As the heat transfer in the slab is considered to be one-dimensional, two-node heat transfer bar elements are used in the model. To obtain correct values, different element subdivisions have been tested. The element size is also governed by the positions of the thermocouples in the slab; the size is adapted to obtain the corresponding values from the calculations. In the model an element size of 5 mm is used, which leads to a division into 50 layers. For the calculations the commercial FE program Brigade/Plus is used, which is based on an Abacus/CAE preprocessor and an Abacus/standard solver.



△ Figure 7 Linear temperature gradient in the cross-section of the slab from measurements and FE analysis, mainly affected by solar radiation



△ Figure 8 Temperature at various heights in the slab from measurements, mainly affected by outgoing long-wave radiation

Temperature components

The average temperature, as well as the linear temperature gradient, is calculated over the cross-section both from the measurements and the FE analysis. The average temperature

T_{avg} is calculated as a sum over the entire slab thickness as

$$T_{\text{avg}} = \frac{1}{h} \sum T_i h_i \quad (10)$$

where T_i is the temperature in layer i , h_i is the

height of the layer and h is the thickness of the slab. The linear temperature gradient ΔT is calculated using

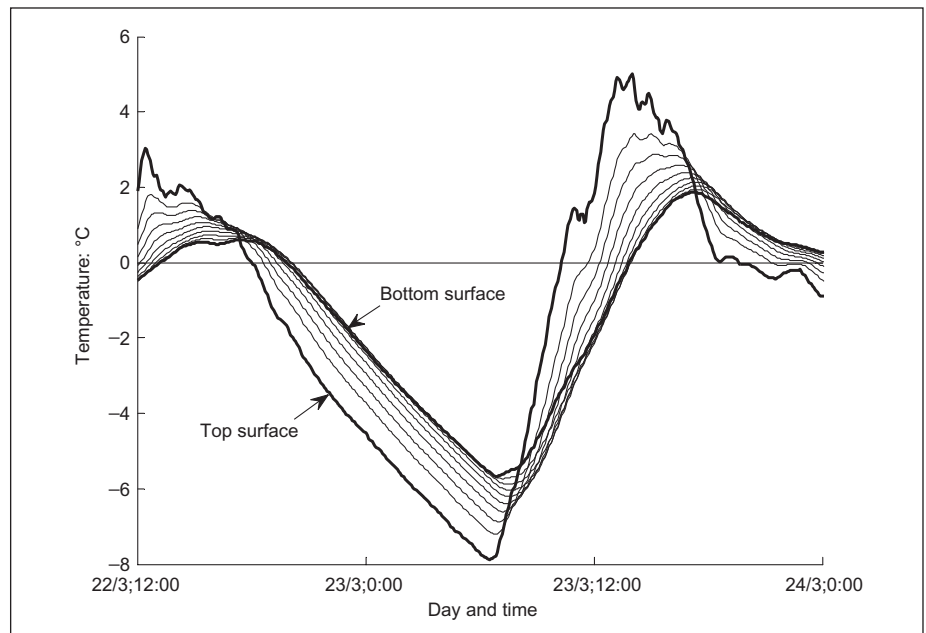
$$\Delta T = \frac{12}{h^2} \sum (T_i x_i h_i) \quad (11)$$

where x_i is the coordinate of the centre of layer i with the x coordinate defined in Figure 3. When processing the test data, the thickness of the layers is defined as the distance from the centre between two thermocouples to the centre in the next space between thermocouples. When processing the results from FE simulations the layer thickness equals the element size.

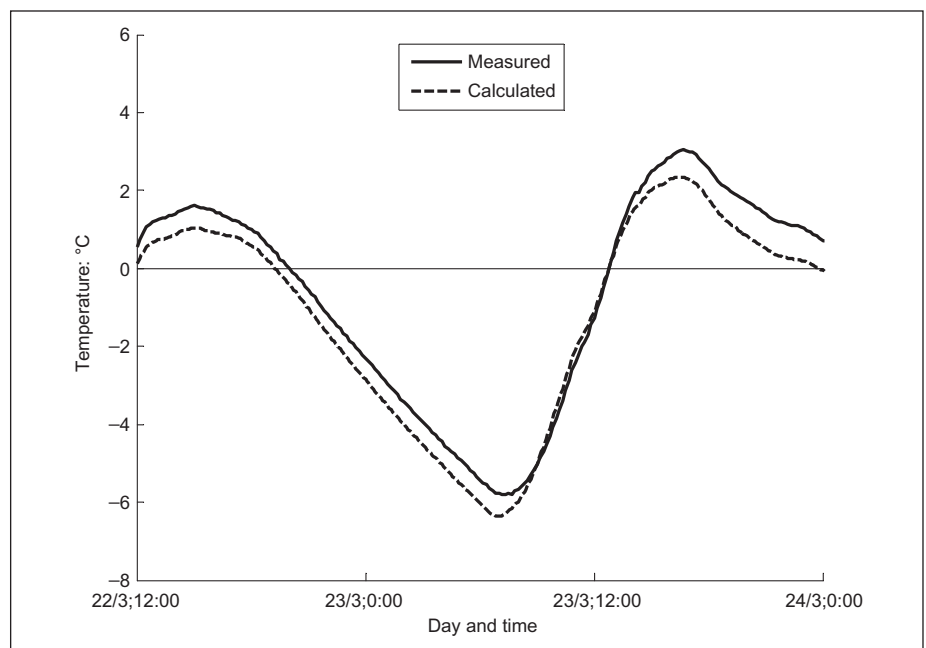
Results and discussion

As expected the temperature in the concrete normally varies in cycles over 24 h. The amplitude mainly depends on the outside temperature. On hot sunny days the temperature in the slab is several degrees higher than the outside air temperature and on cold days the opposite occurs. Measured temperature cycles for two hot summer days are shown in Figure 4. The temperature at the top surface varies more than the temperature in the lower parts of the slab. This indicates that solar radiation has a significant effect on the linear temperature gradient. For the same time period a FE analysis has been executed and temperature values extracted for the positions in the FE model that correspond to the positions of the thermocouples in the slab. These results are presented in Figure 5. The temperature for the FE model is similar to the measured values, but some differences can be observed. The FE model underestimates the temperature in the lower parts of the slab. (Note: in Figures 4 and 5, 8 and 9, and 12 and 13, the term 'bottom surface' is used for the values from the lowest thermocouple, located 1 cm from the bottom surface of the slab.)

For bridge design purposes it is more interesting to look at the average temperature and the linear temperature gradient in the concrete. The average temperatures from both measurements and calculations are presented in Figure 6. This shows that the model underestimates the average temperature slightly on a warm day and the following



△ Figure 9 Temperature at various heights in the slab from FE analysis, mainly affected by outgoing long-wave radiation



△ Figure 10 Average temperature in the cross-section of the slab from measurements and FE analysis, mainly affected by outgoing long-wave radiation

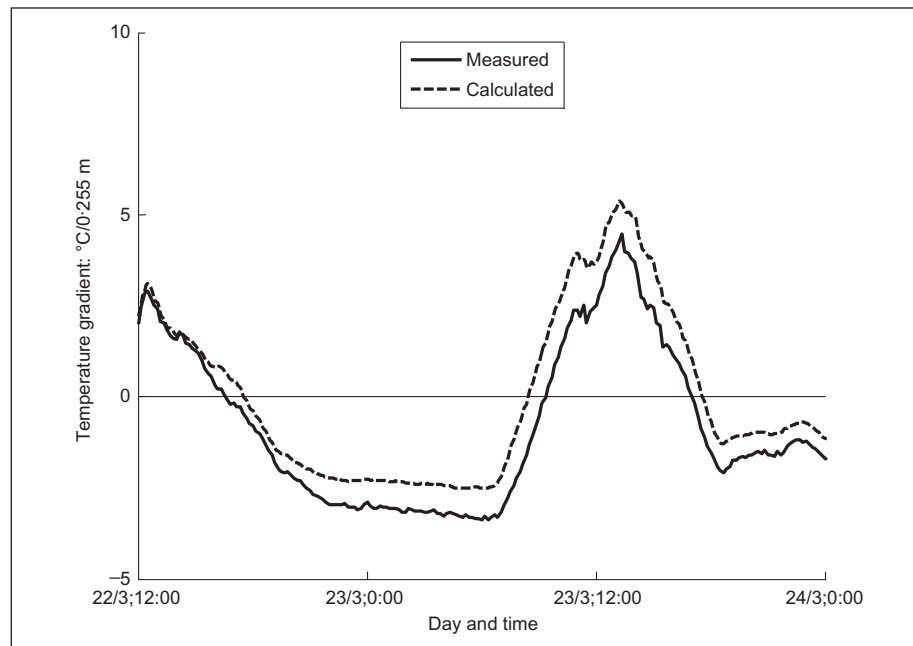
night. The difference is most likely owing to the fact that the material parameters used in the analysis are not measured values, but values taken from the literature. If the material parameters had been measured, the prediction could have been improved, but in

that case the model would be valid for this specific concrete and not for concrete with general material properties. The difference between maximum and minimum temperature, however, shows better agreement with the measurements, which is more important

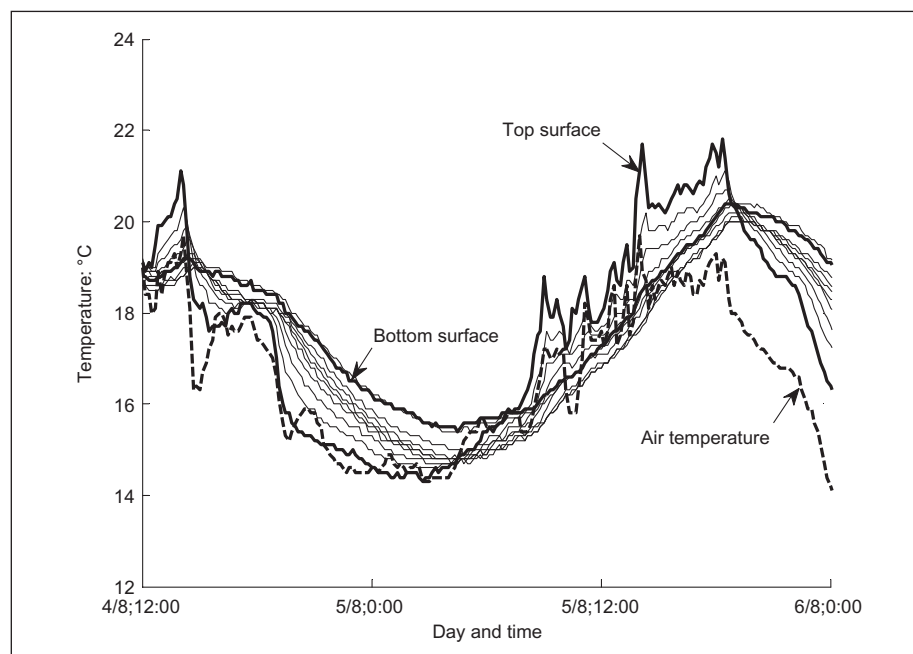
from a design point of view. The linear temperature gradient is presented in Figure 7 for the measured and calculated temperatures. Here the calculated values are constantly one degree higher than the measured ones. This can probably also be explained by the uncertainty of the material parameters for the concrete. In Figures 4–7, however, the calculated temperatures are close to the actual measurements, which indicates that the model is consistent with reality. The extreme value for maximum positive linear gradient for a slab without a surface layer is 12°C according to the Swedish standard based on the Eurocode.¹¹ The maximum linear temperature gradient from the measurements is 8°C and this is only an annual value for the maximum linear gradient. The comparison between these values shows that the value in the Swedish standard could be somewhat underestimated, because it should be an extreme value that will only occur with a certain probability, whereas the measured value is from a one-year cycle and probably more representative for an average year.

For a cold and clear winter day and night the temperature in the slab is much lower. Figure 8 shows the measured temperature variation in the slab for a night with large outgoing long-wave radiation and Figure 9 shows the temperatures from the FE analysis for the same time period. The spatial temperature variations are here not as large as the differences caused by solar radiation. From the figure it can be seen that the FE model captures the temperature variation and the change of temperature when the sunrise occurs. The model underestimates the temperature at the bottom of the slab, which it also does for a hot day with solar radiation effects. This indicates, as discussed before, that the underestimation is caused by lack of exact material parameters for this particular concrete.

In Figure 10 the average temperature and in Figure 11 the linear temperature gradient for the cold night, calculated in the same way as for the hot day scenario, are presented. Here the same tendencies as in the previous scenario can be spotted. The average temperature is slightly underestimated in the analysis and the linear temperature gradient is of the order of one degree lower. The



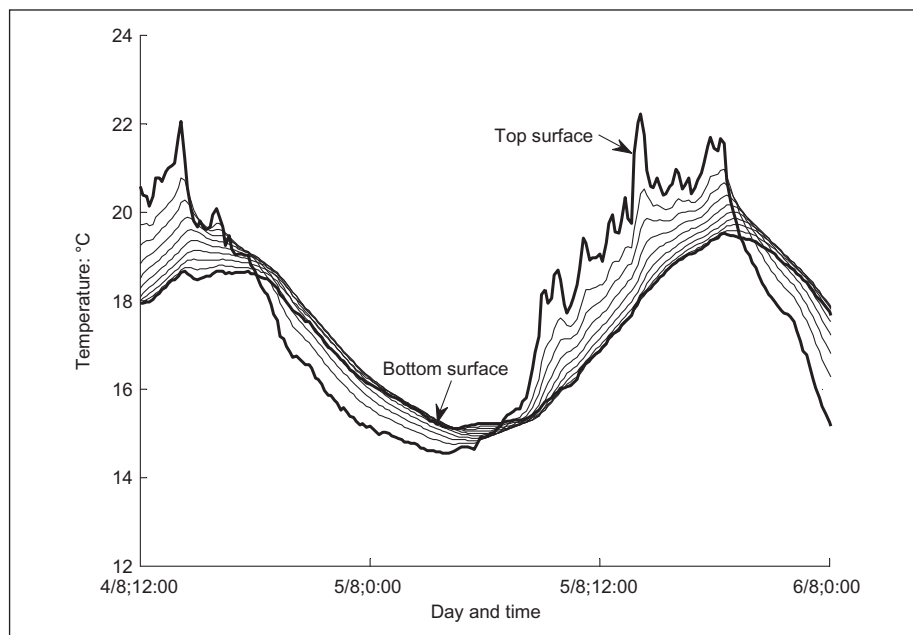
△ Figure 11 Linear temperature gradient in the cross-section of the slab from measurements and FE analysis, mainly affected by outgoing long-wave radiation



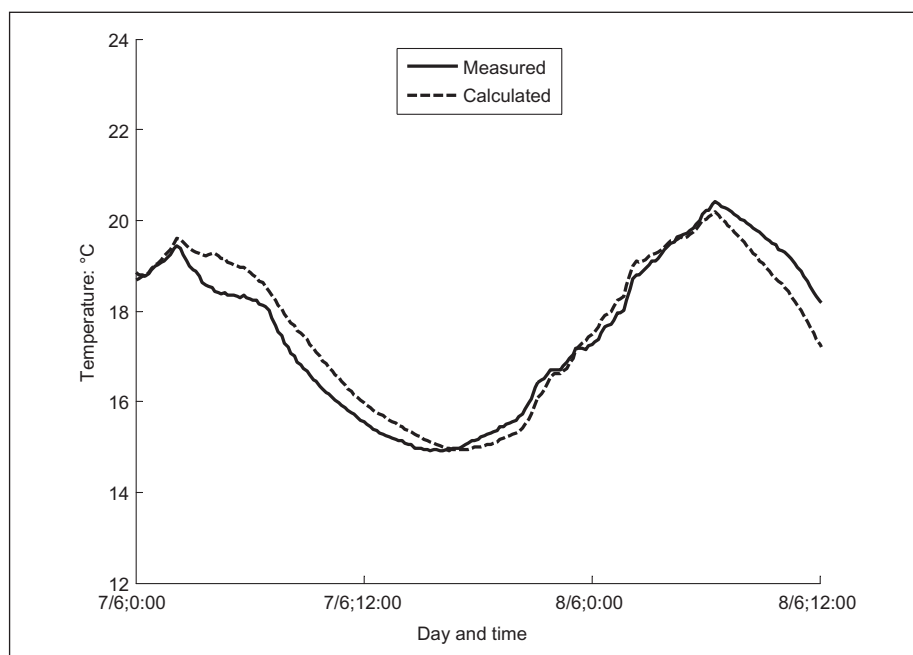
△ Figure 12 Temperature at various heights in the slab from measurements, mainly affected by convection

largest negative linear temperature gradient in this investigation is about -4°C while the specified design value in the Swedish standard is -8°C .¹¹ When compared with the previous scenario, Figure 6, it is clear that the negative linear temperature gradient is not larger for

the cold night scenario, which suggests that large absolute values of negative linear temperature gradients can occur during the entire year and not only in winter time. In the previous research for Swedish conditions it was assumed that the largest negative linear



△ Figure 13 Temperature at various heights in the slab from FE analysis, mainly affected by convection



△ Figure 14 Average temperature in the cross-section of the slab from measurements and FE analysis, mainly affected by convection

temperature gradient only occurs during winter time,¹⁰ but other researchers have taken care of this phenomenon in a more suitable way. The results in this investigation show that it is important to use climatic data for an entire year and not only winter

conditions when predicting the maximum negative temperature gradient in concrete structures.

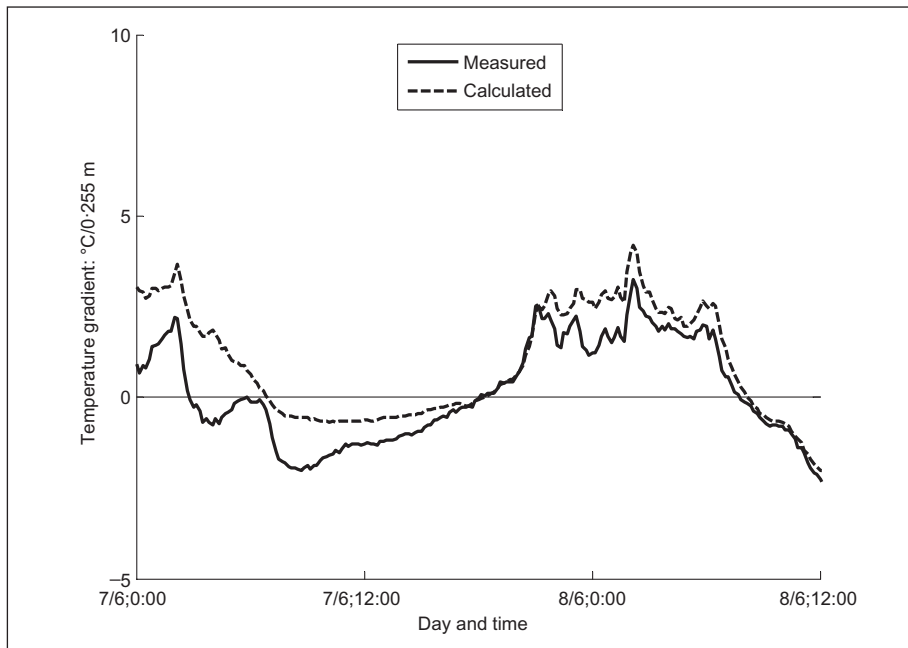
Changes in heat transfer due to increased convection are, as discussed before, mainly dependent on wind speed. In Figure 12 the

measured temperatures in the slab for 36 h are presented and in Figure 13 the same scenario is presented for the FE analysis. The weather conditions in this time period are windy with clouds covering the sky, which implies that the magnitude of solar radiation and outgoing long-wave radiation is low. This leads to a temperature change in the concrete which only follows the outside air temperature and the linear temperature variations are not as large as in the previous scenarios. Figures 12 and 13 show that the ability of the FE model to handle effects of convection is very good. They also show that increased heat transfer from convection owing to higher wind speed does not affect the temperature in the concrete to the same extent as solar radiation and long-wave radiation. Increased convection can, however, reduce the temperature at the surface on a hot day with large intensity of solar radiation and therefore reduce both the average temperature and linear temperature gradients. This is not of any great importance in concrete bridge design, however, as it is more important to consider extreme values and therefore scenarios without wind effects are more interesting. At night, convection can either reduce the temperature at the surfaces or increase it, depending on whether the air temperature is higher or lower than the temperature of the concrete. When the night is clear with a high level of outgoing long-wave radiation, the wind speed is low and will not affect the temperature variation in a significant way.

The comparison made between measurements and analysis for average temperature for these climate conditions is presented in Figure 14 and confirms that the ability of the model to capture effects of increased heat transfer due to convection is very good. In Figure 15 the linear temperature gradient is presented, showing that a climatic scenario with increased heat convection as the main factor does not give any extreme situations compared to the previous ones.

Conclusion

The most important climatic factors that affect the temperature profile in concrete structures are



△ Figure 15 Linear temperature gradient in the cross-section of the slab from measurements and FE analysis, mainly affected by convection

- (a) air temperature
- (b) solar radiation
- (c) outgoing long-wave radiation.

Ambient air temperature is the governing factor for the spatial average temperature in the structure. Extreme temporal variations occur mainly as a result of annual climate changes. For the linear temperature gradients the most important factors are solar radiation and outgoing long-wave radiation. The linear gradients vary owing to daily variations of these factors. Large levels of solar radiation striking the surface give large positive gradients and a clear night with large outgoing long-wave radiation gives large negative gradients. Negative gradients can occur during clear nights any time of the year. High wind speed is not a main factor when considering extreme cases of temperature distribution in concrete structures. The FE

model developed is able to capture these effects with high accuracy and is well suited for use in future studies of other concrete structures with other sets of climatic data.

References

1. European Committee for Standardization. *Basis of Design and Actions on Structures Part 1–5 – Thermal Actions*. European Committee for Standardization, Brussels, Belgium, 2002, ENV 1991-1-5.
2. Branco, F. A. and Mendes, P. A. Thermal actions for concrete bridge design. *Journal of Structural Engineering*, 1993, **119**, No. 8, 2313–2331.
3. Comité Euro-International du Béton. *Bulletin 167 Thermal Effects in the Design of Concrete Structures*. CEB, Lausanne, 1985.
4. Mirambell, E., Aguado, A., Mendes, P. and Branco, F. Design temperature differences for concrete bridges. *Structural Engineering International*, 1991, **1**, No. 3, 36–40.
5. Dwivedi, A. K., Bhargava, P. and Bhandari, N. M. Temperature effects in the design of concrete bridges. *Proceedings of National Conference on Advances in Bridge Engineering, Roorkee, 24–25 March, 2006*, 555–568.
6. Soukhov, D. Representative values of thermal actions for concrete bridges. *Progress in Structural Engineering and Material*, 2000, **2**, No. 4, 495–501.
7. Elbadry, M. M. and Ghali, A. Nonlinear temperature distribution and its effects on bridges. *IABSE Proceedings*, 1983, No. 3, 169–191.
8. Comité Européen de Normalisation. *Background Document of ENV 1991-2-5 Thermal Actions*. CEN, Brussels, Belgium, 1996, ENV 1991-2-5.
9. Alavizadeh-Farhang, A. *Applicability of the Effective Bridge Temperatures Derived from ENV 1991-2-5:1997 for Bridge Design Purposes in Sweden*. Structural Design and Bridges, KTH, Stockholm, 1999.
10. Alavizadeh-Farhang, A. *Applicability of the Positive and Negative Linear Temperature Differences from ENV 1991-2-5:1997 for Bridge Design Purposes in Sweden*. Structural Design and Bridges, KTH, Stockholm, 1999.
11. European Committee for Standardization. *Eurocode 1: Actions on Structures – Part 1–5: General Actions – Thermal Actions*. European Committee for Standardization, Brussels, Belgium, 2003, Svensk standard SS EN 1991-1-5.
12. Incropera, F. P., Dewitt, D. P., Bergman, T. L. and Lavine, A. S. *Fundamentals of Heat and Mass Transfer*, 6th edn. Wiley, Hoboken, 2007.
13. Duffie, J. A. and Beckman, W. A. *Solar Engineering of Thermal Processes*, 3rd edn. Wiley, Hoboken, 2006.
14. Nevander, L. E. and Elmarsson, B. *Fukthandbok*. Svensk Byggtjänst, Stockholm, 2001.
15. Ljungkrantz, C., Möller, G. and Petersons, N. *Betonghandbok, Material*. Svensk Byggtjänst, Stockholm, 1994.
16. Neville, A. M. *Properties of Concrete*, 4th edn. Longman, Harlow, 1995.

II

Estimating extreme values of thermal gradients in concrete structures

Oskar Larsson · Sven Thelandersson

Received: 30 October 2009 / Accepted: 23 February 2011 / Published online: 18 March 2011
© RILEM 2011

Abstract Temperature variations due to climate changes are a major cause of movements in a concrete structure, both in the longitudinal and transversal directions and between different parts of the structure. If these movements are restrained, stresses will be induced which may contribute to cracking. The movements are caused by complex interactions of several factors such as solar radiation, air temperature, long-wave heat radiation and wind speed. To predict the varying thermal conditions in a concrete structure a finite element model has been used. A validation of the model has been performed using field measurements in a concrete slab together with climate data from the Swedish Meteorological and Hydrological Institute to be able to use the model for simulations over long time periods and for situations with no available local thermal data. The daily variations in the temperature distribution is captured by the model and it is well suited to be used for estimating extreme values for linear temperature differences based on climate data from meteorological stations. The analyses of extreme values for simulations with longer time periods show that the values for the positive linear temperature gradients in the Eurocode are underestimated for the investigated conditions. There is also a tendency towards

geographical differences which has not been included before. An asphalt paving layer increases positive linear temperature gradients while they decrease with a concrete paving.

Keywords Thermal actions · Concrete · Extreme values · Finite element model · Climate data

1 Introduction

Effects of the surrounding climate give temperature variations in both time and space for concrete bridges. The temperature variations will give induced strains varying over cross sections and between different parts of the structure. This can be a significant problem for modern large span bridges and affect the performance and durability of such structures. The temperature distribution in a concrete cross section is affected by temporal variations in climatic factors such as air temperature, solar radiation, wind speed and long-wave radiation, see Fig. 1. The temperature profile also depends on the material properties of the concrete; density, thermal conductivity, specific heat and surface color.

The temperature profile in a cross-section can be divided into four time dependent components, illustrated in Fig. 2:

- An average temperature change producing longitudinal movements.

O. Larsson (✉) · S. Thelandersson
Division of Structural Engineering, Lund University,
P.O. Box 118, 221 00 Lund, Sweden
e-mail: oskar.larsson@kstr.lth.se



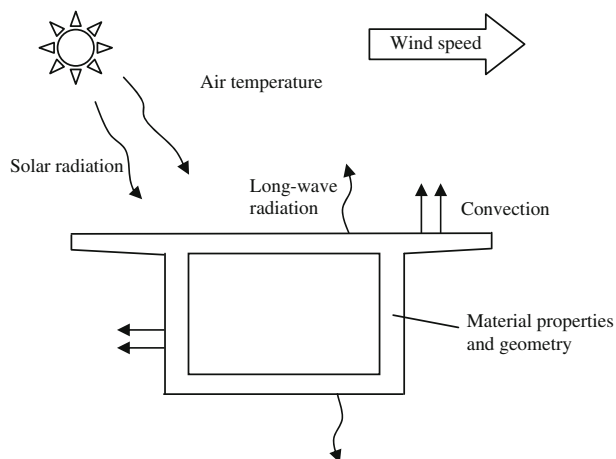


Fig. 1 Governing thermal factors affecting a bridge cross section

- A linear temperature distribution over the cross section in the vertical direction leading to curvature.
- A linear temperature distribution over the cross section in the horizontal direction leading to curvature.
- A non-linear temperature distribution producing eigenstresses due to differential thermal movements between sub elements in the cross section.

The linear parts of the temperature profiles will be referred to as linear temperature gradients in this paper.

Variations in average temperature in a concrete structure over time are mainly due to annual variations in air temperature while the linear and non-linear temperature gradients varies mainly due to variations in incoming solar radiation and daily climate changes. The temperature variations and gradients will cause movements in the structure. If the movements are restrained, stresses will be induced which may contribute to cracking. Inspections of concrete bridges have shown that cracks are sometimes more frequent on sides that are more

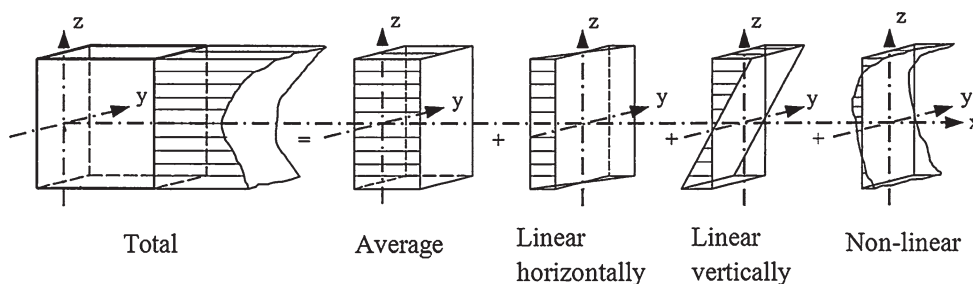
exposed to solar radiation. This indicates that the surrounding environment can have significant effects on concrete structures.

Many large span concrete bridges have been constructed during the latest 50 years. Due to durability concerns and the development of more advanced analysis methods, these bridges were designed with reduced number of joints and bearings. This led to additional problems with thermal effects and several accidents were reported [3]. A CEB task group was formed in 1985 to develop a guide concerning practical information and suggestions to engineers about thermal actions in concrete structures [5]. Analysis of temperature variations in concrete bridge cross sections have since then been made by several different authors for different climate areas in the world, e.g. [9, 11, 14, 18]. Earlier research used finite difference analysis to execute the calculations, but most recent researchers have used the finite element method to evaluate temperature variations.

In the background document of ENV 1991-2-5 [6], the different approaches concerning thermal effects in concrete structures for different European countries are discussed. The background document led to the development of ENV 1991-1-5 [7] where a method is presented for calculating the temperature variations with a statistical approach. This has been made for some areas in Europe. Research has also been made to verify the code regarding Swedish conditions, but only using temperatures from some areas and a general set of climate data [1, 2]. No previous investigation has been made using large sets of climate data from several years, which is necessary to estimate extreme situations with specified degree of probability.

In the previous research in this field the solar radiation has been treated by using the daily total radiation as input parameter, for example in [18]. Since the solar radiation is a main factor for positive linear gradients [12], it is treated by using hourly

Fig. 2 The four components of a temperature profile in a concrete cross section [7]



The meteorological data were obtained for two different locations; solar radiation from Lund where the test site was located and air temperature and wind speed from Malmö, 20 km from Lund. This was due to poor resolution of the temperature and wind speed data from Lund. Due to lack of data from SMHI for long-wave heat radiation for 2008 at the specified locations, the measured data for this factor is used in both of the FE-simulations.

To model a slab with one-dimensional transient heat transfer in the center, 2-node heat transfer bar elements are used. Different element mesh sizes were tested for convergence check. The element size is also governed by the positions of the thermo-couples in the slab; the locations of the nodes in the FE-model are adapted to get the corresponding temperatures. For the calculations the commercial FE-program BRIGADE/Plus [4] is used, which is based on an ABAQUS/cae preprocessor and an ABAQUS/Standard solver.

The temperature distribution in a structure is also affected by several different material properties such as conductivity, specific heat capacity, density, solar radiation absorptivity, emissivity and convective heat transfer coefficient. The first three are properties of the structural material while the latter ones affect the amount of heat that is transferred between the surface and the surrounding environment. For a slab which has a large length and width in relation to the thickness the heat flow can be modeled as one-dimensional as

$$\rho c \frac{dT}{dt} = \frac{d}{dx} \left(k \frac{dT}{dx} \right) + q_v \quad (1)$$

where ρ is the density (kg/m^3), c is the specific heat capacity ($\text{J/(kg } ^\circ\text{C)}$) and k is the thermal conductivity ($\text{W/(m } ^\circ\text{C)}$) of concrete. The heat generated in the concrete due to hydration, q_v , can be neglected in this case if the simulations are limited to already hardened concrete. The boundary condition for the one-dimensional heat transfer problem is

$$k \frac{dT}{dx} n_x - q = 0 \quad (2)$$

where q is the rate of heat transferred from the environment to the concrete surface per unit area (W/m^2) and n_x is the direction cosine of the unit outward vector normal to the boundary surface. The heat transferred between the concrete surface and the

environment consists of three different parts; solar radiation q_s , long-wave radiation q_r and convection q_c added together: [10]

$$q = q_s + q_r + q_c \quad \text{W/m}^2 \quad (3)$$

For a horizontal surface the amount of heat absorbed by the concrete is depending on the amount of incoming global solar radiation. The absorption is also affected by the color and texture of the surface, since some of the radiation will be reflected. Therefore the global radiation must be multiplied with an absorption coefficient:

$$q_s = a \cdot G \quad \text{W/m}^2 \quad (4)$$

where a is the absorption coefficient and G is the incoming global radiation on the surface (W/m^2). The absorption coefficient can vary between 0.5 and 0.7 for concrete [3, 11, 14], in this study the value used is 0.5. The heat transfer between the top surface and the air due to long-wave heat radiation is modeled by using the Stefan-Boltzmann law to get the following equation:

$$q_r = q_s - q_{\text{sky}} = \sigma \varepsilon_c (T_s^4 - T_{\text{sky}}^4) \quad (5)$$

where q_s is the long-wave radiation from the concrete surface, q_{sky} the long-wave radiation from the sky, σ is the Stefan-Boltzmann constant, ε_c the emissivity of the concrete surface, T_s the surface temperature and T_{sky} the equivalent sky temperature. The equivalent sky temperature is a fictitious temperature which represents what temperature the sky would have if it was a surface. It is calculated by using a rewritten form of the Stefan-Boltzmann law, see Eq. 6.

$$T_{\text{sky}} = \sqrt[4]{\frac{q_{\text{sky}}}{\sigma \varepsilon_c}} \quad (6)$$

The emissivity for concrete is 0.9 according to [3] while the long-wave radiation from the sky q_{sky} can be measured by using a pyrgeometer. For the bottom surface the air temperature is used instead of the equivalent sky temperature. This is because the long-wave radiative heat transfer to or from the bottom surface is only affected by the ground, which is assumed to have the same temperature as the surrounding air. In the previous research in this field where this factor is discussed, [3, 9, 10, 14], a simplification is used regarding the long-wave heat radiation, where air temperature has been used for estimating the radiation. By using the approach

described here, the effect of cloud cover can be more accurately considered in the simulations. The heat transfer due to convection consists of two processes; natural and forced convection. Natural convection is created when the surface is heated and warm air is rising from the vicinity of the surface to the surrounding air. Forced convection will appear when the wind is blowing across the surface and heat is then transferred between the air and the surface. Convection is modeled using Newton's law of cooling

$$q_c = h_c(T_s - T_{\text{air}}) \quad \text{W/m}^2 \quad (7)$$

where T_s is the surface temperature, T_{air} is the temperature in the surrounding air and h_c is the convection coefficient. The convection coefficient can be expressed in different ways, for example: [8]

$$h_c = 5.7 + 3.8V \quad \text{W/(m}^2 \text{ } ^\circ\text{C)} \quad (8)$$

where V is the wind speed in m/s. This equation is valid for a slab with the size 0.5 m^2 . For a larger sized slab which is the case in this research the following expressions can be used: [15]

$$h_c = 6 + 4V \quad \text{W/(m}^2 \text{ } ^\circ\text{C)} \quad \text{if } V \leq 5 \text{ m/s} \quad (9a)$$

$$h_c = 7.4V^{0.78} \quad \text{W/(m}^2 \text{ } ^\circ\text{C)} \quad \text{if } V > 5 \text{ m/s} \quad (9b)$$

The first of these expressions is similar to the expression from Duffie and Beckman, which indicates that the difference between different surface sizes is not very large. Equations 9a and 9b are used in the present FE-analyses.

To be able to use the model for cases when the material parameters are unknown, all parameters are taken from literature. They have therefore not been measured for the concrete used in this study. The specific heat capacity of concrete is typically varying between 840 and 1170 J/(kg °C) [16]. The variation in specific heat capacity is mainly due to moisture content, temperature and water–cement ratio of the concrete. Since the temperature range in our case is small, the effect of temperature change on the specific heat capacity will also be small. The value used in the calculations is 900 J/(kg °C). The heat conductivity of concrete is mainly dependent on the heat conductivity of the cement paste and aggregate. It can vary from 1.4 to 3.6 W/(kg °C) [13], the value used in the simulations is 2.5 W/(kg °C). A similar interval is found for the density which varies between 2100 and

2500 kg/m³ [13], in this paper the value used is 2400 kg/m³.

For the case with a pavement layer there are some differences in the material properties for asphalt compared to concrete. The largest difference is the solar radiation absorption coefficient which is increased to 0.9 due to the darker color of asphalt [11]. There are also differences in the internal material properties; the density is set to 2200 kg/m³, the conductivity to 0.7 W/(kg °C) and the specific heat capacity to 880 J/(kg °C) [3].

To analyze the results the average temperature as well as the linear temperature gradient is calculated over the cross section both from the measurements and the FE-analysis. The average temperature T_{avg} is calculated as a sum over the entire slab thickness as:

$$T_{\text{avg}} = \frac{1}{h} \sum T_i h_i \quad (10)$$

where T_i is the temperature in layer i , h_i is the height of the layer and h is the thickness of the slab. The linear temperature gradient ΔT is calculated with the equation below:

$$\Delta T = \frac{12}{h^2} \sum (T_i x_i h_i) \quad (11)$$

where x_i is the coordinate of the centre of layer i with x -coordinate defined in Fig. 3. When processing the test data the thickness of the layers is defined as the distance from the center between two thermo-couples to the center in the next space between thermocouples. When processing the results from FE-analysis the layer thickness equals the element size. For the FE-analysis with a paving layer the average temperature and linear temperature gradient are calculated for the concrete slab alone.

3 Validation results

In Fig. 4 the temperature in the slab at the various positions is shown for two hot days in June 2008. The figure shows large temperature variations between the top and bottom surfaces of the slab. When the top is warmer than the bottom the slab has a positive linear temperature gradient and if the bottom is warmer than the top the gradient is negative. Large positive gradients occur during days with a large range of temperature and a lot of incoming solar radiation. It is



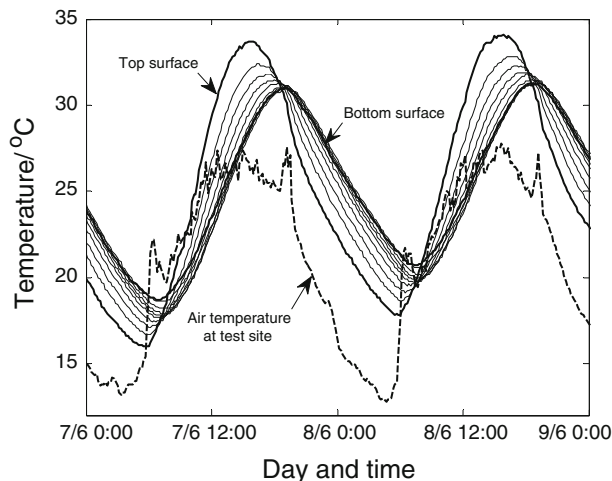


Fig. 4 Temperature from measurements at the various positions in the slab, air temperature at the test site

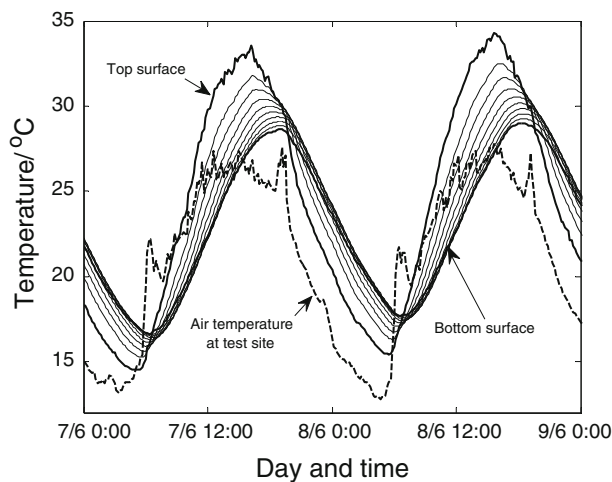


Fig. 5 Temperature from FE simulation at the various positions in the slab using locally measured climate data, air temperature at the test site

therefore important that the FE-model can capture these effects. Figure 5 shows the temperature for the corresponding positions in the FE-model from the calculations with the measured input data. The FE-model gives a good agreement with the measurements and captures the temperature variations in the slab.

When comparing the measurements with the temperatures calculated from the FE-simulation using meteorological data the agreement is not as good, see Fig. 6. The temperature from this calculation is much lower, but there is still a significant variation between night and day. The reason for the lower temperature

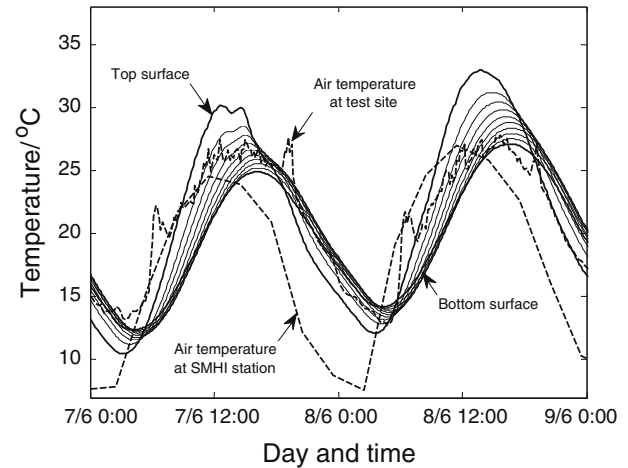


Fig. 6 Temperature from FE simulation at the various positions in the slab using meteorological climate data, air temperature at the test site and at the meteorological station

in this simulation is that the air temperature at the meteorological station was lower than the air temperature at the test site during the investigated time period. This indicates that the air temperature has a significant impact on the temperature level in a structure.

To get a more precise comparison for the further use of the FE-model the average temperature and linear temperature gradient for the slab is calculated. The results are presented in Figs. 7 and 8. The average temperature for the FE-simulation with meteorological climate data is much lower, which was expected from the comparison between Figs. 4, 5 and 6. In Fig. 8 the linear temperature gradients are presented, where the difference between the measurements and the two FE-simulations are much smaller. This indicates that the most important factor for the positive linear temperature gradient is solar radiation. Another thing that can be deduced from Fig. 8 is that the lower air temperature used from the station in Malmö does not affect the linear temperature gradient, the variation in temperature between the day and night is more important than the actual level of temperature.

The results show that the model is well suited for calculating positive linear temperature gradients caused by solar radiation and can be used for studies with climate data from longer time periods. Since the linear temperature gradients can be both positive and negative it is important to investigate the ability of the model to estimate the negative gradients as well.

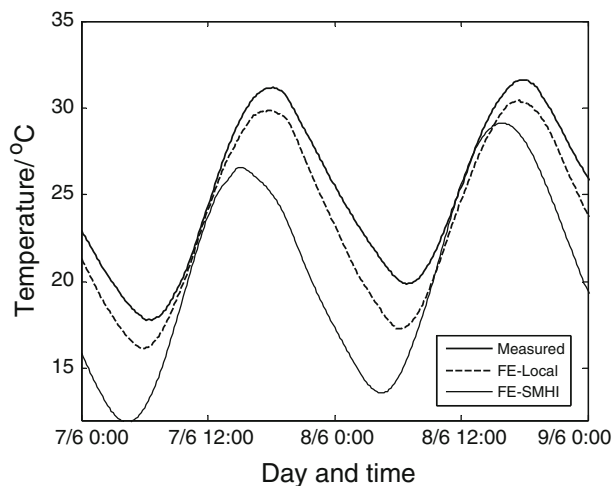


Fig. 7 Average temperature in the slab from measurements, FE analyses with local climate data and FE analyses with meteorological climate data (SMHI)

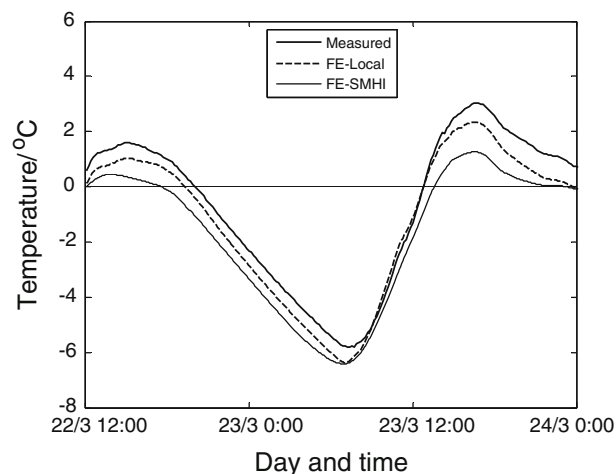


Fig. 9 Average temperature in the slab from measurements, FE simulation with local climate data and FE simulation with meteorological climate data (SMHI)

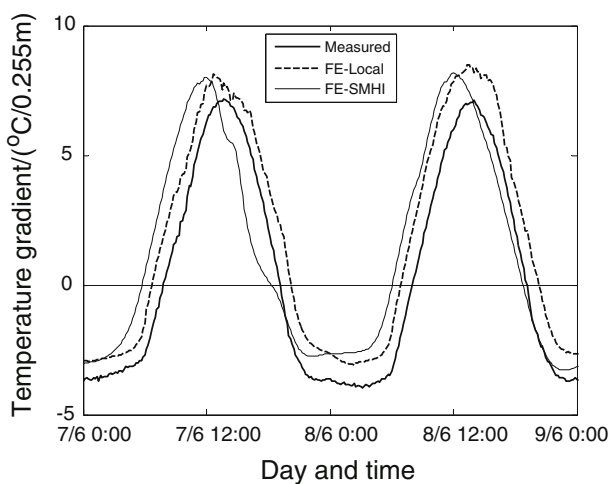


Fig. 8 Linear temperature gradients in the slab from measurements, FE simulation with local climate data and FE simulation with meteorological climate data (SMHI)

Large negative gradients occur during clear nights with a large range of outgoing long-wave heat radiation. This can happen during the entire year. In Fig. 8 it can be seen that the two models give a bit lower value for the negative gradient than the measurements. Figure 10 shows the linear temperature gradients for measurements and calculations during a night and day in March 2008 when there was a clear sky. The absolute values for the negative gradients from the FE-simulations are a bit weaker than for the measurements for this case as well. The two FE-simulations have almost the same values, which is probably due to the usage of the same type

of data for the long-wave heat radiation since this is the governing factor for the negative temperature gradient. In Fig. 9 the average temperature is presented for the three different cases. The differences between the FE-simulations and the measurements are small, which confirms the validity of the model.

When comparing the two figures showing linear temperature gradients, Fig. 8 and Fig. 10, it can be deduced that a large linear temperature gradient can occur at any night during the year. It is therefore important to simulate the temperature for entire years when extreme values are of interest. Several previous researchers [2, 18] have only made extreme value calculations for certain cases of climatic factors and not for actual situations.

4 Determining extreme linear temperature gradients

To be able to perform long-term simulations of the temperature distribution and to analyze the extreme thermal actions, climate data have been obtained for four different locations in Sweden. Since the FE-model used in this investigation needs input values for solar radiation, air temperature, wind speed and long-wave radiation, the extent of measurements for these factors governs the time period for the calculations. The factor that has been least measured is the long-wave radiation; it has only been measured at four different locations and only between the years

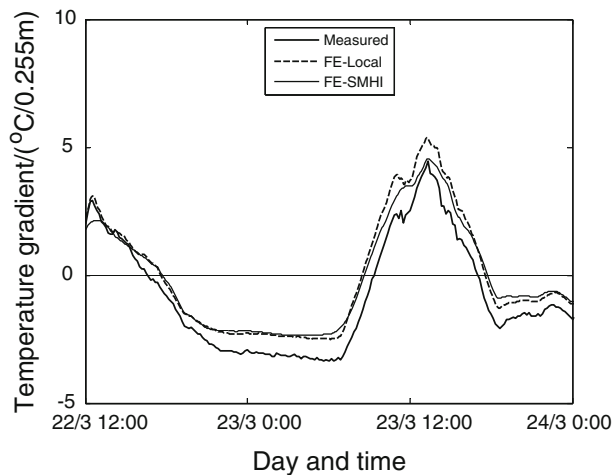


Fig. 10 Linear temperature gradients in the slab from measurements, FE simulation with local climate data and FE simulation with meteorological climate data (SMHI)

1983 and 2000. The longest time period is for the measuring station in Lund, where the measurements were ongoing for 17 years. The time period for the other sites were 16 years for Luleå and Stockholm and 9 years for Borlänge. The calculations were made with three different slab thicknesses; 600 mm, 900 mm and 1200 mm and either without paving or with a 50 mm thick paving layer of asphalt on top.

In the Eurocode concerning the present region [17] the maximum positive linear temperature gradient with a return period of 50 years is 15°C for a concrete slab bridge. The specified basic values in the Eurocode are for a structure with 50 mm paving. For an unsurfaced structure the basic values must be multiplied with 0.8 when the top is warmer than the bottom and 1.1 if the reversed case is valid. This

gives a positive linear temperature gradient of 12°C when there is no paving layer. For the negative linear temperature gradient the value in the Eurocode is 8°C with a paving layer and 8.8°C with no paving layer.

In Table 1 the upper 20% fractile for the positive and negative linear temperature gradients for the four different locations are listed for the 600 mm slab. The upper 20% fractile means that the temperature gradient will occur with a return period of 5 years. The reason for this limit is to be able to compare the different locations despite the different time periods. When compared with the Eurocode the value from the simulations indicates that the positive linear gradient is underestimated in the Eurocode. For a slab with no paving layer the 5-year values from the simulations are higher than the 50-year design value from the Eurocode for two of the locations. The values from the Eurocode are only reasonable for the simulations for Luleå and maybe for Lund.

In Fig. 11 cumulative distributions for annual maximum positive linear temperature gradients is presented for the entire time period of the simulations for Lund. The maximum value during this period is above the design value in the code, which is also an indication of the underestimation. It was found that the data fit reasonably well with the extreme value distribution type 1 (Gumbel).

For the case with asphalt paving only the value from Borlänge is above the Eurocode value, but the values for Lund and Stockholm are not far below the 50-year value. This confirms the underestimation in the code. It is also an indication of geographical differences since Lund is located in the south, Stockholm and Borlänge in the central and Luleå in

Table 1 Upper 20% fractile (5-year values) for the positive and negative linear temperature gradients for a slab thickness of 600 mm

	5-year values				50-year values
	Lund	Stockholm	Borlänge	Luleå	Design value Eurocode
Positive gradients					
No paving	11.0	13.7	13.1	10.1	12
50 mm asphalt	13.5	13.8	16.8	10.3	15
50 mm concrete	10.7	12.4	12.3	8.7	15
Negative gradients					
No paving	−4.7	−5.5	−4.5	−5.4	−8.8
50 mm asphalt	−2.8	−2.8	−3.5	−3.5	−8
50 mm concrete	−3.6	−4.1	−3.8	−3.1	−8

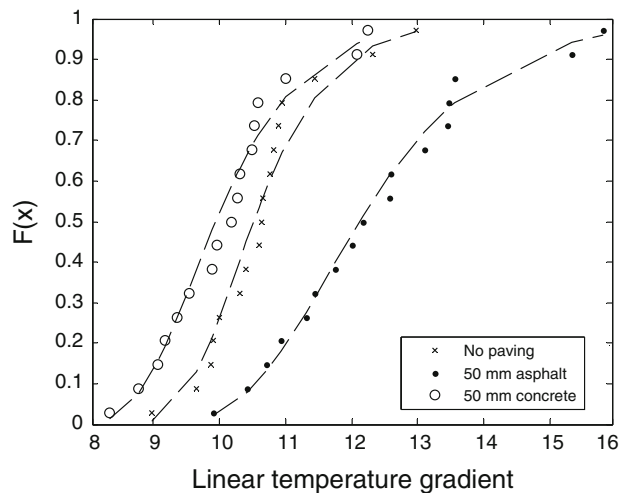


Fig. 11 Cumulative distributions for annual maximum positive linear temperature gradients from the simulations for a slab thickness of 600 mm located in Lund 1984–2000 with various paving conditions, fitted to extreme value distribution type 1 (Gumbel)

the north of Sweden. This is something that has not been considered before in the Eurocode. This geographical difference is not as clear for the negative linear gradients as for the positive.

The results in Table 1 show that there is a difference for the positive linear gradient depending on the type of paving on top of the slab. The gradients are higher for the case with asphalt paving than for concrete paving. This indicates that the assumption in some previous research [18] that the paving layer can be modeled as an additional concrete layer is not correct. This is because the insulation benefit of the paving layer is eliminated due to the asphalt's higher absorptivity of heat from solar radiation.

An asphalt paving layer has a more beneficial effect on the negative linear gradient. Table 1 shows that the temperature gradient is reduced by 1.5–2°C with a 50 mm asphalt layer on top of the slab. The reason for this decrease is that the outgoing heat in the night must first pass through the paving layer and therefore the effect on the concrete slab will not be as large.

In Table 2 the upper 20% fractile for different slab thicknesses are presented, using values from the simulations with input data from Lund. The results from the simulations show that the differences in linear gradients between different slab thicknesses are small. There is a slight decrease in gradients with increasing slab thickness, but it is not large enough to have an impact. This confirms the approach in the Eurocode where increasing thickness is not considered as an important factor.

5 Conclusions

Extreme values of linear temperature gradients are mainly affected by two different climatic factors. Large positive gradients appear due to large amounts of incoming solar radiation and will therefore only occur during the period from April to September each year. The negative gradient is mainly affected by the amount of clouds in the sky. A clear night will give large negative gradient during the entire year. The finite element model does not capture the absolute temperature values from the simulations with meteorological data, due to differing air temperature between the test site and the meteorological station.

Table 2 Upper 20% fractile (5-year values) for the positive and negative linear temperature gradients for Lund with different slab thicknesses

	5-year values			50-year values
	600 mm	900 mm	1200 mm	Design value Eurocode
Positive gradients				
No paving	11.0	10.2	9.6	12
50 mm asphalt	13.5	13.1	12.7	15
50 mm concrete	10.7	9.9	9.5	15
Negative gradients				
No paving	−4.7	−4.4	−4.4	−8.8
50 mm asphalt	−2.8	−2.7	−2.6	−8
50 mm concrete	−3.6	−3.4	−3.3	−8

The variations in temperature and the linear temperature gradients are captured, which makes the model suitable for simulating the linear gradients for longer time periods and situations when local thermal data is unavailable.

The design values for the positive gradient in the Eurocode may be underestimated for the investigated conditions, especially if a paving layer of asphalt is used. The extreme values with a five year return period are higher than the design values for certain conditions. There is also a tendency towards geographical differences not previously considered in the code. The insulating effect of asphalt is counteracted by the higher amount of absorbed solar radiation. If instead a layer of concrete is used as paving the linear temperature gradients are lower in the main concrete slab. For the negative gradients the values in the Eurocode are reasonable for all of the studied cases. The negative gradients are lower if a paving layer of asphalt or concrete is used.

References

1. Alavizadeh-Farhang A (1999) Applicability of the effective bridge temperatures derived from ENV 1991-2-5:1997 for bridge design purposes in Sweden. Structural design and bridges. KTH, Stockholm
2. Alavizadeh-Farhang A (1999) Applicability of the positive and negative linear temperature differences from ENV 1991-2-5:1997 for bridge design purposes in Sweden. Structural design and bridges. KTH, Stockholm
3. Branco FA, Mendes PA (1993) Thermal actions for concrete bridge design. *J Struct Eng* 119(8):2313–2331
4. BRIGADE/Plus version 3.1-1 (2010) Scanscot Technology, Lund
5. CEB (1985) Bulletin 167: Thermal effects in the design of concrete structures. Lausanne
6. CEN, European Committee for Standardization (1996) ENV 1991-2-5: background document of ENV 1991-2-5 thermal actions
7. CEN, European Committee for Standardization (2002) ENV 1991-1-5: basis of design and actions on structures part 1–5. Thermal Actions
8. Duffie JA, Beckman WA (2006) Solar engineering of thermal processes, 3rd edn. Wiley, Hoboken, NJ
9. Dwivedi AK, Bhargava P, Bhandari NM (2006) Temperature effects in the design of concrete bridges. Proceedings of National Conference on Advances in Bridge Engineering, Roorkee, pp 555–568
10. Elbadry MM, Ghali A (1983) Nonlinear temperature distribution and its effects on bridges. *IABSE Proc* 3:169–191
11. Emerson M. (1973) The Calculation of the Distribution of Temperature in Bridges, TRRL Report LR 561. Crowthorne
12. Larsson O (2009) Modeling of temperature profiles in a concrete slab under climatic exposure. *Struct Concrete* 10:193–201
13. Ljungkrantz C, Möller G, Petersons N (1994) Betonghandbok, material. Svensk Byggtjänst, Stockholm
14. Mirambell E, Aguado A, Mendes P, Branco F (1991) Design temperature differences for concrete bridges. *Struct Eng Int* 3:36–40
15. Nevander LE, Elmarsson B (2001) Fukthandbok. Svensk Byggtjänst, Stockholm
16. Neville AM (1995) Properties of concrete, 4th edn. Longman, Harlow
17. SIS, Swedish Standards Institute (2005) SS EN 1991-1-5, Eurocode 1: actions on structures—part 1–5: general actions—thermal actions
18. Soukhov D (2000) Representative values of thermal actions for concrete bridges. *Prog Struct Eng Mater* 2(4): 495–501

III

Modelling of Climatic Thermal Actions in Hollow Concrete Box Cross-Sections

Oskar Larsson, PhD Student, Lund University - Division of Structural Engineering, Lund, Sweden and Raid Karoumi, Prof., Royal Institute of Technology (KTH) - Division of Structural Design and Bridges, Stockholm, Sweden. Contact: oskar.larsson@kstr.lth.se

DOI: 10.2749/101686611X12910257102550

Abstract

The temperature distribution in concrete structures varies as a result of fluctuations in solar radiation, air temperature, wind speed and long-wave radiation. Variations in temperature may cause longitudinal and transverse movements. If these movements are restrained, stresses and strains can be induced, which may contribute to cracking in the structure. To predict such thermal actions in a hollow concrete section, a finite element (FE) model was developed. Hourly resolution of climatic input data was used in the FE model to capture the daily temperature variations in the structure. The FE model was validated against temperature measurements performed in the hollow concrete arch of the New Svinesund Bridge located at the border between Sweden and Norway. To be able to use the developed model for future studies of other structures, an iterative method to consider the inside cavity air was also developed. The results of the simulations show that the model can capture the daily temperature variations. In addition, the proposed model shows acceptable agreement with the measurements from the bridge, and the calculated linear temperature differences for the bridge show good agreement with the design values in the Eurocode. The model is well suited for predicting temperature distributions and can be used for further studies of bridges, including those with box cross-sections, as well as for other concrete structures.

Keywords: New Svinesund Bridge; concrete arch; FE-model; temperature distribution; solar radiation.

Introduction

Temperature variations due to varying climate are a major cause of movements in concrete structures, both in the longitudinal and the transverse directions and between different parts of the structure (see Fig. 1). If such movements are restrained, stresses can be induced, which may contribute to cracking in the structure.

Movements are caused by complex interactions of several factors. Longitudinal movements depend on variations in average bridge temperature, which is mainly affected by annual variations in air temperature. Transverse movements, such as vertical or horizontal curvatures, depend mainly on linear and non-linear temperature differences in the structure which are caused by incident solar radiation and outgoing long-wave heat radiation. The temperature profile of

the concrete also depends on material parameters such as density, conductivity, heat capacity, solar radiation absorptivity and the convective heat transfer coefficient, a factor which is mainly affected by wind speed. Given the complexity of these effects and the possible severity of the problems they cause, it is important to develop methods that are able to capture the relevant temperature variations and the induced stresses. Such methods are needed both for assessments of existing bridges, where thermal effects have a large impact, and for development

of new bridges with special design conditions.

Several studies of thermal effects have been performed during the last 40 years.¹⁻⁸ The main reason for these studies is that problems due to these effects have been reported in a large number of concrete bridges constructed during this period. The problems have mainly occurred because of a reduced use of bearings and movement joints, which in turn is due to the use of more advanced analysis methods and on account of durability concerns. The previous studies of thermal effects for different situations and geographical areas show that it is possible to simulate the temperature variations accurately, both for solid structures and for bridges with hollow box cross-sections.

Unfortunately, existing models use climate data with low resolution. In most cases, only daily values of climatic factors are used as input data, for example the daily total radiation.³⁻⁷ If instead hourly values for solar radiation and long-wave radiation were used, the model could potentially capture temperature variations with higher resolution. This improvement would also increase the ability to consider temperature variations in all the directions of a bridge, as the difference in incident solar radiation between different directions can be included in the simulations. This improvement is also possible because of the development of more advanced computers,

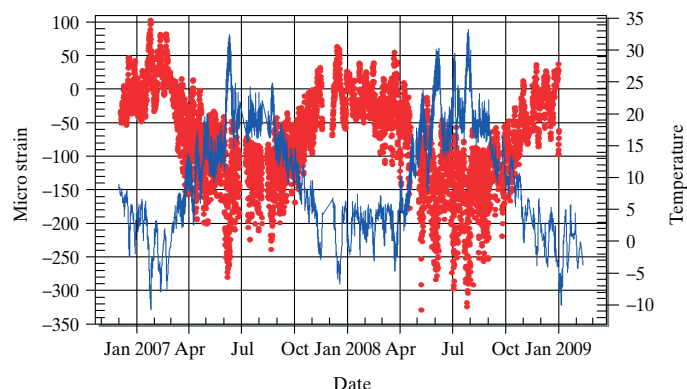


Fig. 1: Temperature effect (solid line) on the strain (dotted) at top flange of arch base on the Swedish side

Peer-reviewed by international experts and accepted for publication by SEI Editorial Board

Paper received: April 13, 2010
Paper accepted: July 30, 2010

which shortens the computing time and makes it possible to create more detailed models.

Many different methods have been applied to a common problem while modelling a hollow box cross-section: the thermal effect of the air inside the cavity. Some authors have used complex ways of calculating the inside air temperature,² whereas others have not discussed this factor at all.⁶ In order to allow simulations in design and assessment of bridges, a way of modelling this heat exchange is needed for this study.

In this study, a finite element (FE) model has been developed to simulate the temperature in a hollow box concrete bridge section. The model is able to consider the effects from the surrounding climate with hourly input values. An investigation of a suitable modelling technique for the heat exchange between the inner air and the concrete has also been performed. An extensive validation of the model has been carried out against measurements from the arch of the New Svinesund Bridge between Sweden and Norway.

FE Model and Measurements

The FE model was developed using a FE program⁹ which is based on an Abaqus/CAE pre-processor and an Abaqus/Standard solver. The model has been validated previously for situations with one-dimensional heat flow in a concrete slab.¹⁰ The results show that it can capture the temperature variations with good accuracy in such a structure.

In this study, the FE model was validated against measurements performed on the New Svinesund Bridge¹¹ located at the border between Sweden and Norway. The bridge has a total length of 704 m and was opened for traffic in 2005. The main span of the bridge consists of a single hollow concrete arch. The arch has a span of 247 m and



Fig. 2: The New Svinesund Bridge joining Sweden and Norway

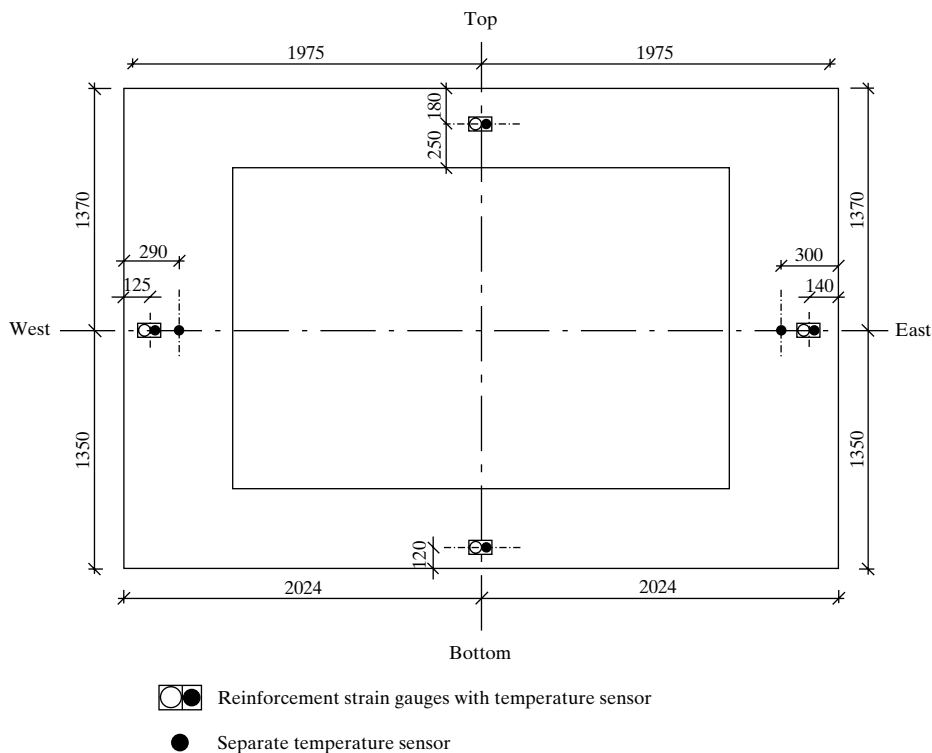


Fig. 3: Placement of temperature sensors in the top section of the arch (Units: mm)

carries a steel box bridge deck on each side (see Fig. 2).

Due to the importance of the bridge, an extensive monitoring program was initiated. The installed monitoring system continuously logs data from 72 sensors (strain gauges, temperature gauges, accelerometers, load cells, displacement sensors and a wind sensor) and has gathered data since the casting of the first arch segment in the spring of 2003. The monitoring project was coordinated^{12,13} at The Royal Institute of Technology (KTH), where maintenance and operation of the system as well as for data analysis, verification and reporting was taken care of. Figure 3 shows the location of the temperature sensors in the top section of the arch.

On the top of the arch, additional equipment was installed in 2009 for measuring solar radiation and incoming long-wave radiation (see Fig. 4). Data from April 2009 to February 2010 obtained from the sensors were used together with measurements of ambient air temperature and wind speed as input in the model. The air temperature at the centre of the box cavity was also measured and used in some of the simulations. As a bridge is a large structure, shading from clouds can cause some variation in temperature between different parts of the structure. This detail is not considered in this study, as it is unlikely that extreme

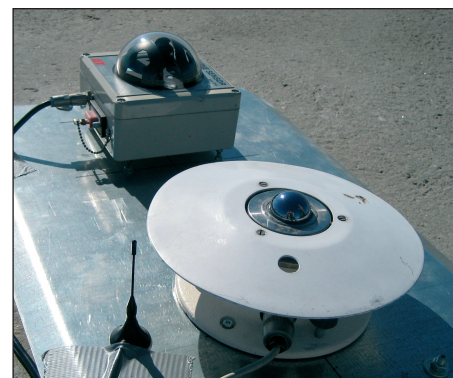


Fig. 4: Measuring equipment for solar radiation (upper) and incoming long-wave radiation (lower)

temperature situations will occur during days with a cloudy sky.

As the top part of the bridge is almost horizontal and the length of this part is large in relation to the width and height, the heat flow can be considered to be two dimensional. Therefore, 4-node linear heat transfer elements are used to model the cross-section. A sensitivity study was conducted using different mesh sizes, and 50 mm elements were selected.

Heat Transfer Theory

A two-dimensional heat flow can be described as:

$$\rho c \frac{\partial T}{\partial t} = k \left(\frac{\partial^2 T}{\partial x^2} + \frac{\partial^2 T}{\partial y^2} \right) + q_v \quad (1)$$

where p is the density (kg/m³), c is the specific heat capacity (J/(kg·°C)), $\partial T/\partial t$ is the change in temperature over time (°C/s), k is the thermal conductivity (W/(m·°C)) of concrete and $\partial^2 T/\partial x^2$, $\partial^2 T/\partial y^2$ are the second spatial derivatives (thermal conductions) of temperature in the x and y directions, respectively. The heat generated in the concrete due to hydration, q_v , can be considered negligible as the simulations are limited to already hardened concrete. The boundary conditions for the two-dimensional heat transfer problem are described by:

$$k \left(\frac{\partial T}{\partial x} n_x + \frac{\partial T}{\partial y} n_y \right) - q = 0 \quad (2)$$

where q is the rate of heat transferred from the environment to the concrete surface per unit area (W/m²), n_x , n_y are the direction cosines of the unit outward vector normal to the boundary surface and $\partial T/\partial x$, $\partial T/\partial y$ are the temperature change in the x and y directions. The rate of heat transferred from the surrounding environment to the concrete consists of three different parts:

$$q = q_s + q_c + q_r \text{ (W/m}^2\text{)} \quad (3)$$

where q_s is the solar radiation, q_c is the convection heat transfer and q_r is the long-wave radiation.

The amount of heat absorbed by the concrete from the sun depends on the intensity of the incident solar radiation and the colour and texture of the surface. As some of the solar radiation is reflected, the total amount of solar radiation absorbed by a surface is calculated according to Duffie and Beckman¹⁴ as:

$$q_s = a \left(I_{b,n} \cos \theta + I_{d,h} \times \left(\frac{1 + \cos \beta}{2} \right) + I_h \left(\frac{1 - \cos \beta}{2} \right) \rho_g \right) \text{ (W/m}^2\text{)} \quad (4)$$

where a is the absorption coefficient, $I_{b,n}$ is the direct radiation on a surface perpendicular to the sun, θ is the incidence angle, $I_{d,h}$ is the diffuse radiation on a horizontal surface, β is the slope of the surface relative to the horizontal plane, I_h is the horizontal global radiation and ρ_g is the ground reflection factor. The absorption coefficient can vary between 0,5 and 0,7 for concrete.^{2,4,5} In Larsson's work,¹⁰ it was

stated that 0,5 is reasonable to use in this kind of study.

The long-wave radiative heat transfer between the top surface and the air can be described using the Stefan-Boltzmann law¹⁵:

$$q_r = q_s - q_{inc} = \sigma \epsilon_c (T_s^4 - T_{eq}^4) \text{ (W/m}^2\text{)} \quad (5)$$

where q_s is the long-wave radiation from the concrete surface, q_{inc} is the incoming long-wave radiation from the surrounding environment, σ is the Stefan-Boltzmann constant, ϵ_c is the emissivity of the concrete surface, T_s is the surface temperature and T_{eq} is the equivalent temperature for the surrounding environment. The emissivity for concrete is 0,9 according to Branco and Mendes.² The equivalent temperature was described for a horizontal surface as a fictitious temperature the sky would have if it were a surface and could thus be calculated by using a rewritten form of the Stefan-Boltzmann law. This is called the sky temperature, T_{sky} , in this paper and is derived by using the following equation:

$$T_{sky} = 4 \sqrt{\frac{q_{sky}}{\sigma \epsilon_c}} \text{ (}^\circ\text{C)} \quad (6)$$

where q_{sky} is the long-wave radiation from the sky which is obtained from measurements taken by a pyrgeometer. For a vertical surface, the equivalent temperature is a fictitious value combining the sky temperature and the temperature of the ground, which can be assumed to be equal to the air temperature, T_{air} . The equivalent temperature for a vertical surface is calculated by using Eq. (7):

$$T_{eq} = \frac{T_{sky} + T_{air}}{2} \text{ (}^\circ\text{C)} \quad (7)$$

For the bottom surface, the air temperature is used instead of the equivalent sky temperature in Eq. (5), as the long-wave radiative heat transfer to or from the bottom surface is only affected by the underlying ground, water and bridge deck.

The convective heat transfer part, q_c , consists of two processes: natural convection and forced convection. Natural convection occurs when the surface is heated and warm air rising from the vicinity of the surface is replaced by colder air. Forced convection will take place when wind is blowing across the surface, causing heat transfer between

the surface and the air. Convection can be described in the model by using Newton's law of cooling, see Eq. (8):

$$q_c = h_c (T_s - T_{air}) \text{ (W/m}^2\text{)} \quad (8)$$

where T_s is the surface temperature, T_{air} is the temperature in the surrounding air and h_c is the convection coefficient. The convection coefficient for a larger structure can be expressed as shown by Nevander and Elmarsson¹⁶:

$$h_c = 6 + 4V \text{ if } V \leq 5 \text{ m/s (W/(m}^2\cdot^\circ\text{C))} \quad (9a)$$

$$h_c = 7,4V^{0,78} \text{ if } V > 5 \text{ m/s (W/(m}^2\cdot^\circ\text{C))} \quad (9b)$$

where V is the wind velocity.

The inside cavity in the arch also influences the temperature distribution in the concrete. A heat exchange occurs between the internal air and the inside surfaces as a result of both radiative and convective heat transfer. To simplify the complex interactions, the internal air temperature is used as input for both the radiative and the convective parts:

$$q_{in} = q_{c,in} + q_{r,in} = h_c (T_s - T_{in}) + \sigma \epsilon_c (T_s^4 - T_{in}^4) \text{ (W/m}^2\text{)} \quad (10)$$

where $q_{c,in}$ is the convective heat transfer, $q_{r,in}$ is the radiative heat transfer, T_{in} is the internal air temperature and the other parameters are as defined earlier. The convection coefficient can be set to 2 W/(m²·°C) for the internal interactions according to Emerson.⁵ As the FE model can be used for studies of similar structures in other climate conditions than in the present location, another approach had to be tested for the effects of the inside cavity. This is due to the lack of measurements of the inside air temperature at other locations or for yet to be constructed bridges. According to Bohn and Anderson,¹⁷ the average core temperature for a fluid in an enclosed space depends on the average temperature of the inside walls. The inside air temperature, T_{in} , is therefore calculated from the temperatures of the inside walls using iteration. The start value for T_{in} can be set to the ambient air temperature; the simulation is then repeated with a new T_{in} calculated from the previous results.

The additional material properties needed in the FE model are density, specific heat capacity and heat conductivity. These are discussed thoroughly by Larsson.¹⁰ It is stated that,

for a concrete with unknown material properties, it is reasonable to set the density to 2400 kg/m³, the specific heat capacity to 900 J/(kg·°C) and the conductivity to 2,5 W/(kg·°C). As measured material properties for the concrete used in the Svinesund Bridge are unavailable, the listed general values were used in the model.

Temperature Components

To analyse the results and get a relevant comparison, the average temperatures as well as the linear temperature differences were calculated over the cross-section from the results of the different FE simulations. The average temperature T_{avg} is calculated as an integral over the entire cross-section:

$$T_{avg} = \frac{1}{A} \int_A T(x,y) dA \quad (^\circ\text{C}) \quad (11)$$

where $T(x,y)$ is the temperature in the elemental area dA and A is the cross-section area. The linear temperature difference ΔT is calculated either vertically or horizontally as follows:

$$\Delta T_x = \frac{12}{Ab} \int_A T(x,y) x dA \quad (^\circ\text{C}) \quad (12a)$$

$$\Delta T_y = \frac{12}{Ah} \int_A T(x,y) y dA \quad (^\circ\text{C}) \quad (12b)$$

where ΔT_x is the linear temperature difference in the horizontal direction, ΔT_y is the linear temperature difference in the vertical direction, b is the width of the cross-section, h is the height, x and y are the distances from elements dx and dy to the centre of gravity in the horizontal and vertical directions, respectively.

Results

The FE model developed was used to simulate the temperature distribution

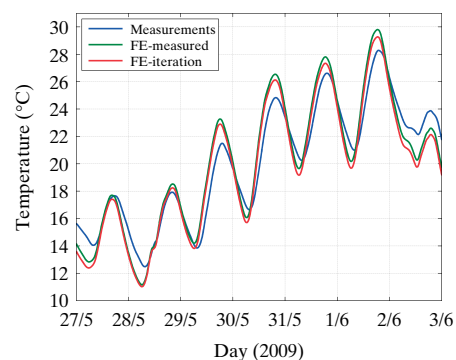


Fig. 5: Temperatures for the top sensor from measurements and FE-simulations

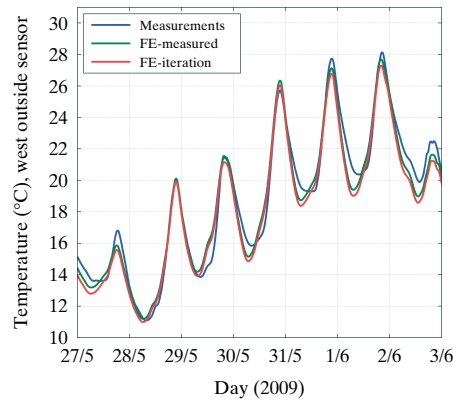
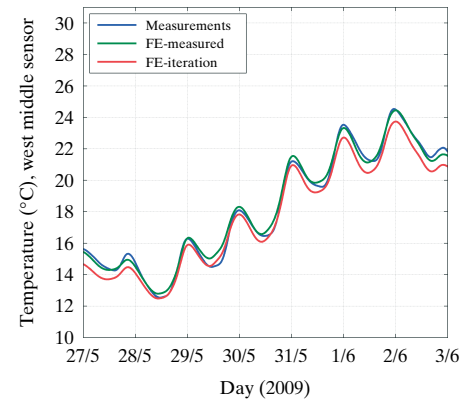


Fig. 6: Temperatures for the west sensors, see Fig. 3, from measurements and FE-simulations



in a hollow concrete box cross-section. A validation of the model was performed against temperature measurements from the arch of the Svinesund Bridge.

In Fig. 5, the temperature during a warm week in May/June 2009 for the sensor in the top flange of the arch is presented, together with the corresponding temperatures from the simulations using either measured inside air temperature (FE-measured) or inside air temperature calculated by iteration (FE-iteration). During this period, there were large amounts of incident solar radiation and fairly high variation in ambient air temperature between night and day. As the figure shows, the model could capture the daily temperature variations in the arch. The highest temperatures from the simulations are, however, about 1,5°C more than the highest temperatures from the measurements. This could indicate that the general set of material parameters used in the model is not the same as the real material parameters, which unfortunately were not available.

In addition, Fig. 5 shows that the difference between the simulations using either measured inside air temperature (FE-measured) or calculated from iteration (FE-iteration) is small. This indicates that the modelling technique using iteration to estimate the inside air temperature is capable of predicting the temperature distribution in a structure. But because the temperature sensor is located closer to the outside surface, where the temperature is mostly affected by the outside input factors, the technique has to be evaluated further.

The temperature variations are also captured by the model for the west wall, as shown in Fig. 6, where temperatures from the simulations are presented together with the corresponding values

from the temperature sensors. The sensor positions are as shown in Fig. 3; the left diagram is for the sensor position closest to the outside boundary. Here the agreement between the measurements and the simulated values is even better than for the top flange. The comparison shows that the model is capable of accurately simulating the horizontal temperature variations in this wall.

The differences between the two FE simulations are small for the west wall as well. The temperature for the sensor position near the outside shows almost no difference, which is expected as the temperature here is mostly affected by the outside input factors. The difference for the innermost sensor position is slightly larger; the FE simulation using iteration for the inside temperature gives a lower value, which indicates that the inside air temperature calculated from iterations is somewhat lower than the measured one.

The temperature values for the east wall, presented in Fig. 7, confirm the model's suitability for capturing horizontal variations. The temperature values from the simulations are somewhat lower than the measured temperatures, which are different from the results for the top flange in Fig. 5, where the model overestimated the temperature levels. This may indicate that the model somewhat overestimates the effect of the incoming global horizontal solar radiation. But as the magnitude of the daily temperature variation is the same for both the measured and the simulated values, the model is still valid for simulating the temperature distribution. The reason for this is that, if a bridge is not restrained in the longitudinal direction, the temperature variations and gradients are more likely to induce strains and stresses in the structure rather than the actual temperature levels themselves. If a structure

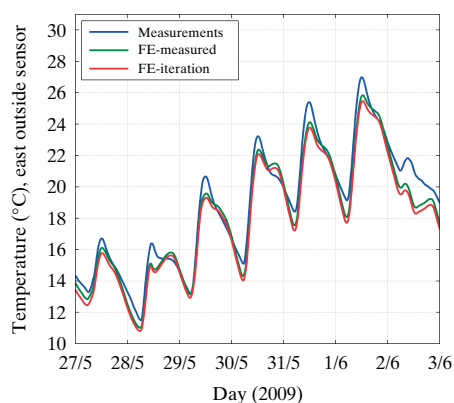


Fig. 7: Temperatures for the east sensors, see Fig. 3, from measurements and FE-simulations

is restrained, the actual temperature levels will also have an impact on the stress levels.

The two FE simulations show similar differences for the east wall as for the west. The simulation using inside air temperature from the iteration is slightly lower near the middle of the wall as compared with the outside.

The FE model can also capture the daily temperature variations of the sensor in the bottom flange (see Fig. 8). The temperature values are slightly lower for the FE simulations than for the measurements, which is the opposite of the temperatures in the top flange in Fig. 5. As the bottom flange is almost unaffected by solar radiation, this confirms the large impact it can have on the temperature. The difference observed between the FE simulations is only in the absolute temperature level and not in the temperature variations, which is a more important factor as stated before.

Simulations have also been performed for a colder period with a large range of outgoing long-wave radiation at night. Figure 9 shows the temperatures from measurements and simulation for the top flange sensor during a cold week in February 2010. The model accurately captures the temperature variations of the nightly drop in temperature. The same difference is found here as was discussed above between the measurements and the simulations. This difference indicates that the model consistently underestimates the temperature level in the concrete and overestimates the impact of the global horizontal solar radiation during warm periods. The differences in temperature between the measurements and the simulations are similar in all the cases studied.

As the developed FE model shows reasonable agreement with the measure-

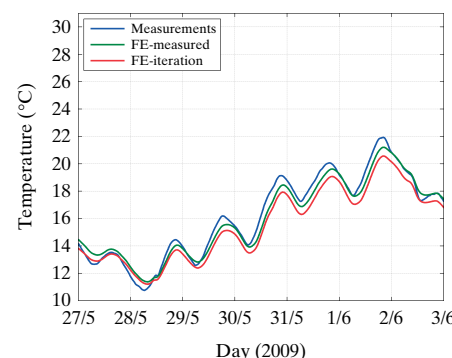
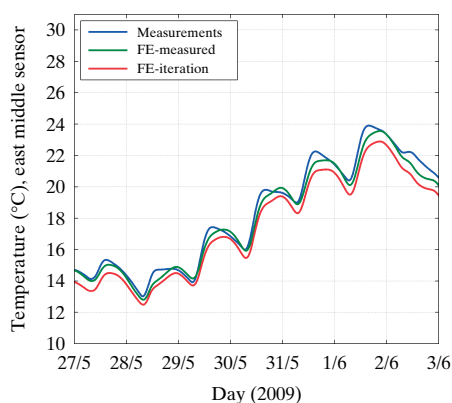


Fig. 8: Temperatures for the bottom sensor from measurements and FE-simulations

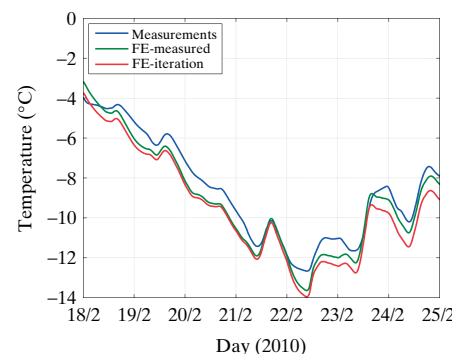


Fig. 9: Temperatures for the top sensor from measurements and FE-simulations

ments performed, it will be suitable for use in further studies of the bridge. The model can capture the temperature variations caused by solar radiation during day time and by outgoing long-wave heat radiation during night time. It can also capture variations in temperature in two directions, which is needed to predict stresses and strains in the arch. The model can be used for predicting temperatures and the resulting thermal strains and stresses in this bridge as well as in other bridges for which climate data is available. It will be especially useful for considering strains and stresses caused by temperature gradients and/or temperature differences between different parts of a bridge deck, which can be the cause of cracking.

For further analysis of the iteration modelling technique, the linear temperature differences were calculated for the horizontal and the vertical directions of the structure. In Fig. 10, the horizontal linear differences over the entire cross-section of the arch from the simulations with measured air temperature and the calculated air temperature are presented. As can be seen, the horizontal linear difference varies during the day; in the morning, the east part is warmer and in the afternoon the west part is warmer. The magnitude of the linear difference is almost equal for both of the simulations; the lines are plotted almost over each other. As the temperature measurements in the concrete were carried out using only one or two sensors in each wall, it is neither possible nor relevant to calculate the linear temperature differences based on the measurements.

The behaviour of the vertical linear temperature difference in this structure is different from that of solid structures. During a warm period with high air temperature, the top is warmer than the bottom for the entire day and night (see Fig. 11). This behaviour is different for a solid structure, where the bottom is warmer than the top during night time. This means that large negative vertical linear differences can only occur during the cold period of the year, whereas in a solid structure they can appear during the summer as well (see Larsson¹⁰). The results of the simulations here are also almost equal, the same as the case for the horizontal linear difference. The main reason for the equality is the use of the same set of outside boundary conditions in the two simulations. The effect of the inside cavity on the linear differences is therefore unnoticeable.

During the considered period in May/June 2009, large amounts of solar

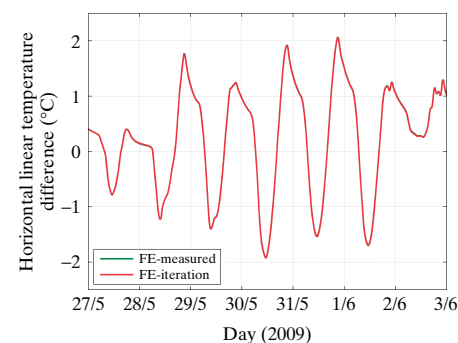


Fig. 10: Horizontal linear temperature difference over the whole cross-section from FE-simulations, west is warmer than east when positive

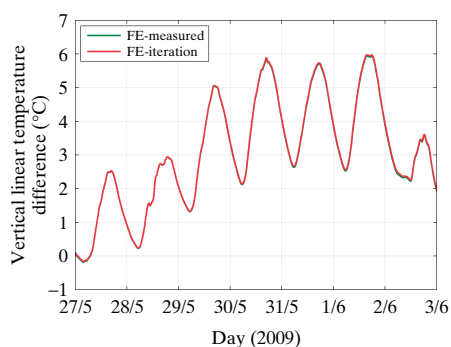


Fig. 11: Vertical linear temperature difference over the whole cross-section from FE-simulations, top is warmer than bottom when positive

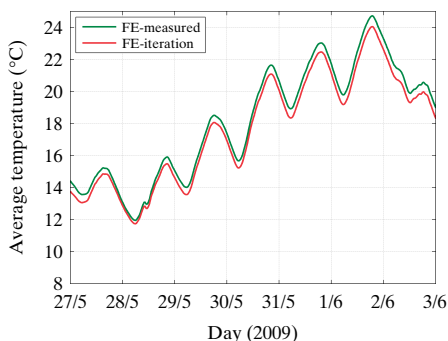


Fig. 12: Average cross-section temperature from FE-simulations

radiation and large ranges in ambient air temperature affected the bridge. The linear temperature differences can therefore be assumed to be large in comparison to other time periods. Both the horizontal and the vertical linear temperature differences are below the design values given in Eurocode ENV 1991-1-5.¹⁸ In the code, the values for the linear temperature differences with a return period of 50 years are 5°C in the horizontal direction and 10°C in the vertical.

As there is a difference between the FE simulations in the temperature levels at the measurement locations (Figs. 5 to 8) the average temperature in the cross-section is also analysed. In Fig. 12, it can be seen that the average temperature is higher for the simulation using the measured inside temperature. This confirms the previously discussed underestimation of the inside air temperature calculated from iteration but

as the linear temperature differences are more important concerning stresses and strains in bridge cross-sections, the small difference can be neglected.

Conclusion

The FE model captures the daily temperature variations in a hollow box cross-section caused by variations in incident solar radiation, long-wave radiation, air temperature and wind speed. The temperature variations are captured in both the vertical and the horizontal directions. The differences in absolute temperature values between the FE simulations and the measurements are smaller for the horizontal direction than for the vertical. As the model overestimates the temperature in the top and underestimates it in the bottom concrete flange, the differences in the vertical direction indicate that the global horizontal solar radiation affects the concrete less in reality than in the model.

The differences in concrete temperature between the simulation using the measured inside cavity air temperature and the one using iteratively calculated inside cavity air temperature are small. The differences are larger closer to the inside surfaces than the outside. The vertical and horizontal linear temperature differences are almost equal for both simulations, which confirms the validity of the iterative approach for the inside air temperature. Thus, the model is well suited for studies of unmonitored bridges and other future bridges, for which climate data can be obtained. The model will be useful for predicting temperatures and corresponding thermal strains and stresses, which may cause cracks to appear in a bridge deck.

References

- [1] CEB—Comite Euro—International du Beton. *CEB Bulletin No. 167: Thermal Effects in the Design of Concrete Structures*. CEB—Comite Euro—International du Beton, 1985.
- [2] Branco FA, Mendes PA. Thermal actions for concrete bridge design. *J. Struct. Eng.* 1993; **119**(8): 2313–2331.

- [3] Mirambell E, Aguado A, Mendes P, Branco F. Design temperature differences for concrete bridges. *Struct. Eng. Int.* 1991; **3**: 36–40.
- [4] Elbadry MM, Ghali A. Nonlinear temperature distribution and its effects on bridges *IABSE Proc.* 1983; **3**: 169–191.
- [5] Emerson M. *The Calculation of the Distribution of Temperature in Bridges*, TRRL Report LR 561, Crowthorne, 1973.
- [6] Soukhov D. Representative values of thermal actions for concrete bridges. *Prog. Struct. Eng. Mat.* 2000; **2**(4): 495–501.
- [7] Roberts-Wollman CL, Breen JE, Cawrse J. Measurements of thermal gradients and their effects on segmental concrete bridge. *J. Bridge Eng.* 2002; **7**(3): 166–174.
- [8] Suzuki J, Ohba Y, Uchikawa Y, Hoshikawa K, Kimura K. Monitoring temperatures on a real box-girder bridge end energy budget analysis for basic information on bridge cooling and surface freezing. *J. Bridge Eng.* 2007; **12**(1): 45–52.
- [9] BRIGADE/Plus version 3.1-1, *Scanscot Technology*, Lund, 2010.
- [10] Larsson O. Modelling of temperature profiles in a concrete slab under climatic exposure. *Struct. Conc.* 2009; **10**(4): 193–201.
- [11] Darholm T, Lundh L, Ronnebrant R, Karoumi R, Blaschko M. *Technical Book about the Svinesund Bridge*, Swedish Road Administration: Uddevalla, 2007.
- [12] Karoumi R, Andersson A. Load testing of the New Svinesund Bridge: presentation of results and theoretical verification of bridge behaviour. *TRITA-BKN. Rapport 96*, Royal Institute of Technology (KTH), Stockholm, 2007.
- [13] Karoumi R, Ronnebrant R, Harryson P, Darholm T. Understanding the real behaviour of The New Svinesund Bridge by monitoring. *The Fifth Symposium on Strait Crossings*, Trondheim, 2009.
- [14] Duffie JA, Beckman WA. *Solar Engineering of Thermal Processes*, 3rd edn. Wiley: Hoboken, NJ, 2006.
- [15] Incropera FP, Dewitt DP, Bergman TL, Lavine AS. *Fundamentals of Heat and Mass Transfer*, 6th edon. Wiley: Hoboken, NJ, 2007.
- [16] Nevander LE, Elmarsson B. *Fukthandbok, Svensk Byggtjänst, Stockholm*, 2001.
- [17] Bohn MS, Anderson R. Temperature and heat flux distribution in a natural convection enclosure flow. *J. Heat Transfer* 1986; **108**: 471–475.
- [18] European Committee for Standardization, *ENV 1991-1-5: Basis of Design and Actions on Structures Part 1–5–Thermal Actions*, CEN, Brussels, 2002.

IV

Transverse Thermal Stresses in Concrete Box Cross-sections from Climatic Exposure

Oskar Larsson, M. Sc., Corresponding Author
Division of Structural Engineering, Lund University
P.O. Box 118
SE-221 00, Lund, Sweden
e-mail: oskar.larsson@kstr.lth.se

Sven Thelandersson, Prof.
Division of Structural Engineering, Lund University
P.O. Box 118
SE-221 00, Lund, Sweden
e-mail: sven.thelandersson@kstr.lth.se

Abstract

Spatial and temporal temperature variations in a concrete structure due to variations in the surrounding climate will produce movements which, if restrained, may induce stresses in the structure. To get a better understanding of transverse thermal stresses due to climatic effects in concrete box cross-sections, FE simulations have in this study been performed using extensive climatic input data directly or by simplified methods to simulate the temperature and resulting stress fields in a section of the hollow concrete arch of the New Svinesund Bridge. Studies of other cross-sections with varying height, width and wall thicknesses have also been performed to investigate the geometrical influence. The results show an overestimation of the maximum thermal tensile stress when using a linear temperature differential approach compared to directly using climate data which includes the non-linear part of the temperature distribution. The effect of height, width and orientation is negligible compared to variations in thickness between the slabs and walls. For box-sections with slabs/walls having different thicknesses the transverse thermal stresses will be significantly larger in the thinner members, independent of the actual orientation and placement of the member.

Key Words, Concrete, Box- cross-section, Thermal stress, Finite element method, Thermal factors, Climate data

Introduction

The temperature in a concrete structure is affected by complex interactions of climatic factors such as solar radiation, air temperature, wind speed and long-wave heat radiation. A spatial temperature field can be divided into different components; average temperature, vertical and horizontal linear temperature differentials and a non-linear temperature variation. Annual variations in air temperature mainly affect the average temperature of a structure, while the linear and non-linear temperature differentials are mostly affected by solar radiation and long-wave heat radiation.

Varying temperature in both time and space in a concrete structure will give rise to thermal movements. A change in average temperature will mainly give longitudinal movements while

the linear as well as non-linear differences also produce transverse movements. In a rectangular hollow concrete box-section, most often used for bridge structures, the movements in a wall are restrained by the adjacent walls. When a difference in temperature exists between the inside and outside surface of a wall, the wall is curved. Due to the restraint from the adjacent walls, transverse stresses will appear in the section. If the outside is warmer than the inside, e.g. due to heating from solar radiation, tensile stresses appear on the inside surfaces while if the outside is cooler than the inside, e.g. due to outgoing long-wave radiation during night time, tensile stresses appear on the outside surfaces. These tensile stresses may, by themselves or in combination with stresses from other design loads, contribute to cracking in the structure.

Temperature differentials over the entire cross-section may also lead to a curvature of the entire structure. If, as an example, the wall facing south is warmer than the wall facing north, thermal tensile stresses can appear in the north part due to restraint from supports. Thermal stresses may also appear due to differences in temperature between different parts of a structure.

During the latest 30 years, several investigations have been performed concerning thermal actions and stresses in concrete structures [1-9]. This development was due to the construction of larger bridges using fewer bearings and joints, which was possible since more advanced analysis methods were available and used in the design process. Several of these investigations have been performed on thermal stresses in indeterminate concrete bridges [3,4,6,7]. The investigations have mainly been focused on longitudinal stresses, and transverse stresses have only been analysed and discussed briefly.

The previous research on thermal actions has mainly been focused on the temperature levels and differentials [1,5,9]. In most cases concerning long-term simulations general sets of data have been used; for example daily total solar radiation instead of using hourly data. The long-wave heat radiation, which is governed in a large way by the cloud cover, is also treated in a simplified way. In Larsson and Karoumi [10] a heat transfer FE-model was used with hourly climate input data to estimate the temperature distribution in the hollow concrete box cross-section of the new Svinesund Bridge and compared with measured temperatures in the concrete, see Fig. 1. The results showed that the model is well suited for predicting the temperature distribution in the concrete based on time series of meteorological data.



Fig. 1 The New Svinesund Bridge

For the research presented in this paper the same FE-model as in Larsson and Karoumi [10] is used to simulate temperature distributions and resulting thermal stresses in hollow concrete cross-sections with different geometries and orientations with respect to solar radiation. Extensive long-term climate data from two locations in Sweden are used for the temperature simulations. The temperature profiles are in turn used in a linear-elastic general static stress FE-model of the same cross-section to predict stresses induced from thermal expansion. The focus in the present research is less on absolute values of stress and more on relative effects, which are captured with a linear elastic model. Additional FE-simulations are performed using temperature components for the different walls extracted from the calculated temperature fields. The main objective of these simulations is to investigate if thermal stresses from using linear temperature differentials can be used in general situations for design purposes and if there are certain temperature situations that causes unfavourable stresses. Thermal stress fields from FE-simulations using cross-sections with differing geometry are also analysed to investigate the importance of variations in different geometry factors such as height, width and wall/slab thickness.

FE-model and Simulation Method

The FE-models used has been developed using the commercial FE-program BRIGADE/Plus [11], which is based on an Abaqus/CAE pre-processor and an Abaqus/Standard solver. The heat transfer model has previously been validated against measurements performed on the New Svinesund Bridge, see Fig. 1. The New Svinesund Bridge is a 92 m high, 704 m long concrete arch bridge carrying a steel deck with a largest span of 247 m [12]. The validation was presented in Larsson and Karoumi [10]. The model has also previously been validated for situations with a one-dimensional heat flow in a concrete slab [13].

In Larsson and Karoumi [10] the possibility to simulate the concrete temperature in a hollow box cross-section was investigated; see Fig. 2 for the dimensions of the cross-section used, which was the top section of the concrete arch. Measurements of solar radiation, long-wave radiation, wind speed and air temperature were used in an FE-model to simulate the temperature distribution. Measurements of these climate factors were performed at the bridge

site using a BF3 sunshine sensor for the solar radiation, a pyrgeometer for the incoming long-wave radiation, temperature sensors for the ambient and inside air temperatures and an anemometer for the wind speed. How these factors are used in the model is described in [10] and summarized here. The solar radiation is treated as surface heat fluxes for the global and diffuse radiation while the incoming long-wave radiation is used to calculate a fictitious temperature for the surrounding sky which is used for radiative heat transfer. The ambient air temperature and wind speed are used for convective heat transfer, with the wind speed governing the convection coefficient. Two-dimensional DC2D4 transient heat transfer elements with a size of approximately 50 mm were used for the temperature simulations.

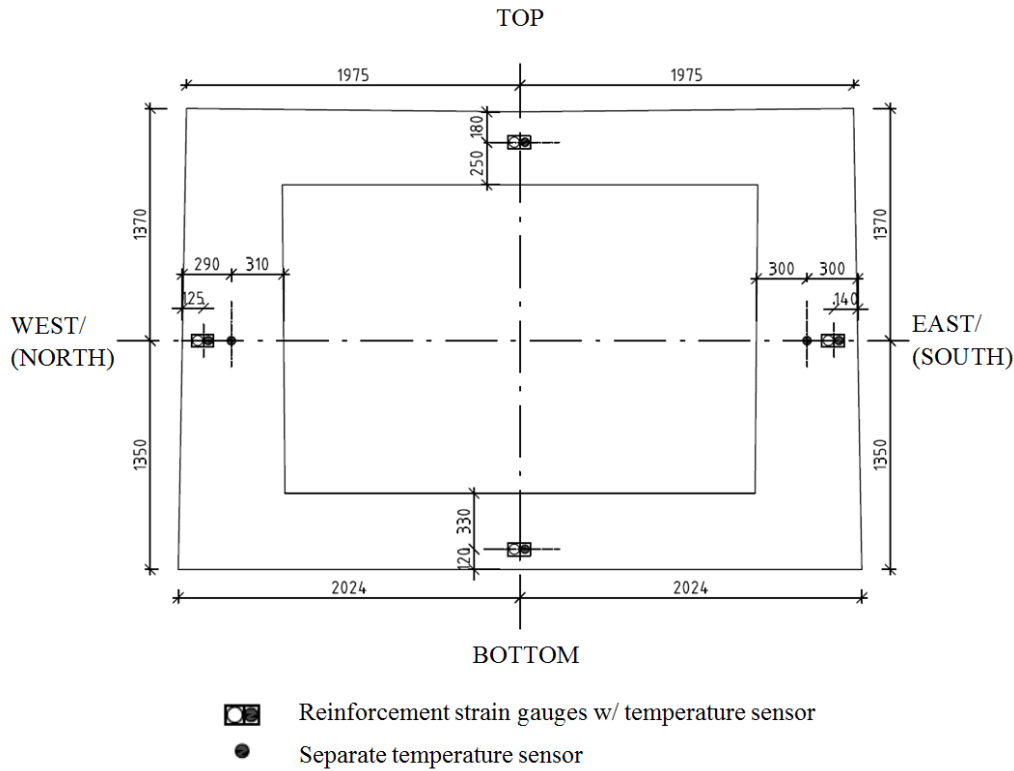


Fig. 2 Dimensions of the top section of the arch and placement of the temperature sensors

Two different approaches were tested in Larsson and Karoumi [10] for the consideration of the inside cavity; in the first case the inside air temperature was measured and the second case the inside air temperature was calculated from the temperature of the inside surfaces using iteration. According to Bohn and Andersson [14] the inside cavity temperature can be approximated as the average temperature of the surrounding surfaces. This relation was used in the iterations, with the start value set to the outside air temperature. The measured or calculated inside air temperature was used for radiative and convective heat transfer. The results from the two simulations were compared with measurements from several temperature sensors cast into the concrete section, see Fig. 2. The investigation showed that the FE-model can capture the temperature variations in an accurate way, see Fig. 3 for an example of the agreement between the measurements from the sensors in the west wall and the FE-simulations using either measured or calculated inside air temperature. Both cases for considering the effect of the inside cavity give reasonable results compared to the

measurements. The FE-model is therefore suitable to use in this investigation, where no data for the inside cavity exists.

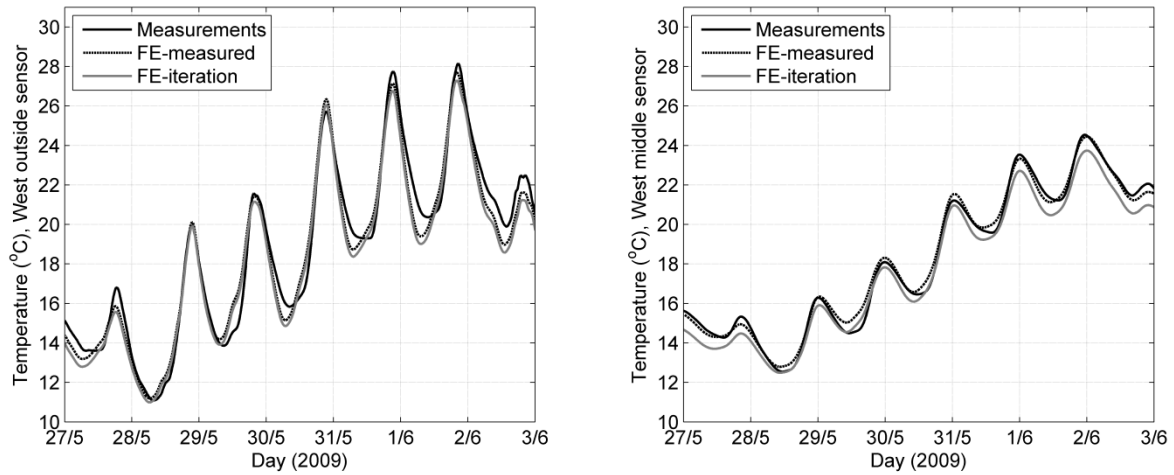


Fig. 3 Temperatures for the west sensor positions from measurements and FE-simulations

In this study the FE-model is used with climate data from two meteorological stations in Sweden, the station in Stockholm in the middle part and the station in Luleå to the north. The distance between the stations is approximately 900 km. The amount of years available for simulation is governed by the amount of long-wave radiation measured; 15 years for both stations. The bridge is assumed to be located either east-west, with walls to the south and north, or north-south, with walls to the east and west. The climate factors needed for the temperature simulations are as stated in the previous section solar radiation, ambient air temperature, incoming long-wave radiation and wind speed. The material parameters used in the model are density, 2400 (kg/m^3), conductivity, 2.5 ($\text{W/(m} \cdot ^\circ\text{C)}$), specific heat capacity, 900 ($\text{J/(kg} \cdot ^\circ\text{C)}$), emissivity, 0.9, and solar absorptivity, 0.5. The climate data and material properties are used in the transient heat transfer model to calculate the temperature distribution in the cross-section.

The temperature distributions achieved from the heat transfer simulations are used as input in a general static stress FE-model using two-dimensional CPE4R plane strain elements with the same mesh as for the temperature simulations. This leads to that the cross-section should be viewed as a part of a prism beam bridge instead of part of an arch bridge. This choice was made to get the possibility of analysing the results with a more general bridge in mind and not just an arch structure. Other box-girder bridges have in most cases an overhang which shades the upper parts of the vertical walls, this aspect is not included in this study.

The level of thermal strains in a structure depends on the temperature difference and a thermal expansion coefficient which, according to EN 1991-1-5 [15], can be set to $10 \cdot 10^{-6}$ ($1/^\circ\text{C}$). If the structure or parts of a cross-section as in our case is not free to expand, varying temperature will cause stresses. The magnitude of the thermal stresses also depends on the amount of restraint and the modulus of elasticity, which is set to 30 GPa. This corresponds roughly to a tensile strength of 2.7 MPa. The concrete material is assumed to be linear-elastic with a

Poisson's ratio of 0.2. The simplification of using a linear elastic material was made to be able to get comparable stress levels from different years and situations since the aim of this investigation is to identify extreme situations and stresses appearing during a large time span of 15 years. As stated earlier, the focus in the present research is less on absolute values of stress and more on relative effects. Creep effects or other effects which alters the concrete properties could be included, but this would only modify the absolute stress values and not affect the relative effects in the results.

From the resulting temperature distributions, $T(x,y)$ denoted *Climate*, the average temperature, T_{avg} , and linear temperature differential, ΔT , have been calculated over each slab and wall according to Eqs. 1 and 2 as

$$T_{avg} = \frac{1}{A} \int_A T(x, y) dA \quad [^{\circ}\text{C}] \quad (1)$$

$$\Delta T = \frac{12}{Ah} \int_A T(x, y) x dA \quad [^{\circ}\text{C}] \quad (2)$$

where $T(x,y)$ is the temperature in element dA , A is the wall area and dA is the element area; h is the thickness of the slab/wall; x is the distance from element dA to the centre of gravity in the direction of the linear gradient. New general static stress simulations using these extracted temperature components as input over each slab and wall have been performed, both separately and combined. The results are compared to the results from original simulations, where the average temperature, the linear temperature differential and the non-linear temperature differential are all present.

In EN 1991-1-5 section 6.1.4 [15] it is stated that temperature differentials in a box cross-section should be considered, and a difference of 15°C between the outside and inside surfaces is given as a recommendation. An additional general static stress FE-simulation has been performed using this value as input, as a comparison to the simulations where the previously calculated linear differentials were used.

EN 1991-1-5 section 6.1.4 [15] also states that “care should be taken when designing large bridges, since large temperature differences can appear between the inside and outside of the web walls”. Additional studies have been performed using various cross-sections with variations in geometry, to be able to analyse how the relations between geometrical attributes such as height, width and slab/wall thickness will affect a structure. Table 1 shows the different widths, heights and slab/wall thicknesses used in the FE-simulations. For the geometry labelled “*Rotated*” the vertical walls have the dimension of the horizontal slabs from the original cross-section and vice-versa. Six more cross-sections with equal slab/wall thickness over the four parts are studied. Four “*Squares*” with an identical outer width and height in each case but with varied absolute values, and two “*Rectangles*” with differing width and height. In all of these simulations climate data from 1 year only was chosen, since the

results are used as a comparison of the different geometries and not for calculating extreme values. The climate data chosen was for Stockholm in the year 1986. For the geometry studies only the full climate simulations which include all temperature components are analysed, and not the separate temperature components simulations.

Table 1. Width, height and thickness at centre of each slab and wall of the various cross-sections, based on Fig. 2. (mm)

Cross-section	Top slab		Bottom slab		South wall		North wall	
	Outside length	Thickness	Outside length	Thickness	Outside length	Thickness	Outside length	Thickness
Original	3950	430	4048	450	2720	600	2720	600
Rotated	2720	600	2720	600	3950	430	4048	450
Square 1	2800	450	2800	450	2800	450	2800	450
Square 2	2800	600	2800	600	2800	600	2800	600
Square 3	4000	450	4000	450	4000	450	4000	450
Square 4	4000	600	4000	600	4000	600	4000	600
Rectangle 1	4000	450	4000	450	2800	450	2800	450
Rectangle 2	2800	450	2800	450	4000	450	4000	450

Results and Discussion

An FE-model has been used with climatic input data to estimate temperature fields in a section of the hollow concrete arch of the New Svinesund Bridge. The temperature fields are used to directly estimate thermal stresses in the structure. In addition, average and linear temperature differential components have been extracted and used to estimate the corresponding thermal stresses. The annual maximum tensile stress level has been extracted from different parts of the structure for all of the simulations.

When the non-linear temperature component in the temperature distribution is excluded the maximum tensile stress in the cross-section, which appears on the inside top surface, is overestimated. In Fig. 4 the annual maximum tensile stress for the inside surface of the top slab using climate data from Stockholm is presented for the bridge located either east-west (a), or south-north (b). In the figure the results for the simulations including all temperature components (*Climate*) are compared to the results from the simulations using linear temperature differentials (ΔT) separately and in combination with average temperature ($\Delta T + avg$) as input. The difference in maximum stress level between *Climate* and ΔT is about 1 MPa for each year independent of the bridge direction. The combination $\Delta T + avg$ gives a slightly lower maximum stress level than that for ΔT only, but the difference towards the regular simulations is still large. When the bridge is located south-north the stress level is somewhat lower than the case when the bridge is located east-west. This indicates that the impact of the solar radiation is slightly larger when one of the vertical walls faces south, since this is the only climate factor that is affected by the direction of the bridge.

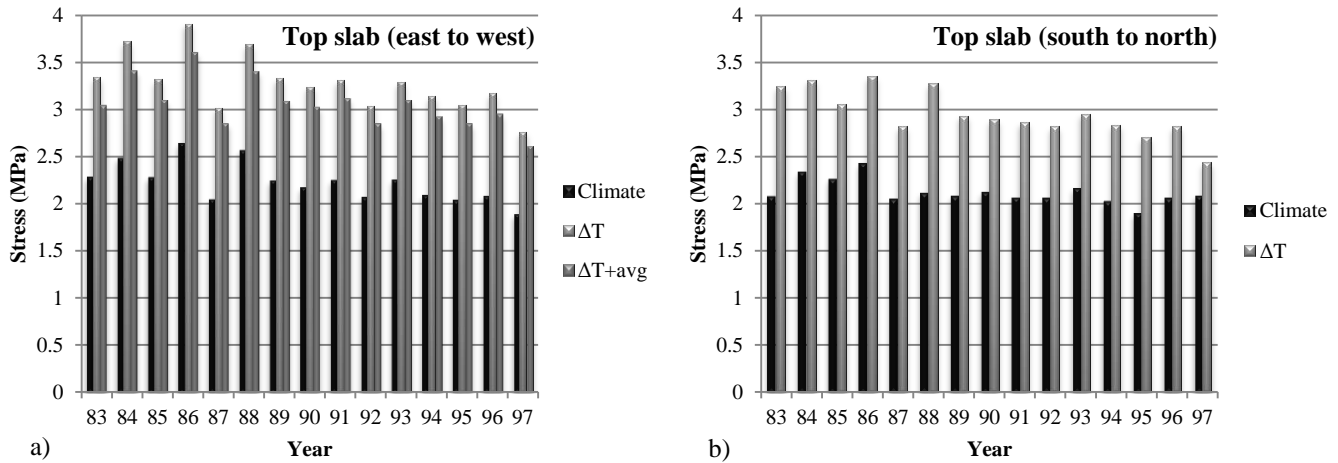


Fig. 4 Annual maximum tensile stress on the inside of the top slab for Stockholm, with the bridge located east to west (a) or south to north (b)

For the FE-simulations using climate data from Luleå the results for the tensile stress on the inside surface of the top slab are lower than the case of Stockholm. The results are presented in Table 2, which also includes stresses from the vertical walls for both Stockholm and Luleå with the bridge located either east to west or south to north. The maximum, the 80 % fractile (statistical value with a return period of 5-years) and the mean of the annual maxima for the stress levels are presented in the table. A similar difference in stress level was found between the simulations including all temperature components (*Climate*) and the simulations with only the linear temperature differentials (ΔT) for the top slab for both Luleå and Stockholm data. The tensile stresses in the top slab are somewhat larger when the bridge is located east-west for Luleå as well; this further indicates that the top slab is more affected by the solar radiation when located in that direction.

Table 2. Annual maxima of transverse thermal tensile stresses on the inside surface of the respective slabs or walls

	Bridge Location	Slab/Wall (inside surface)	Stress, <i>Climate</i> (MPa)			Stress, ΔT (MPa)		
			Max	80 percentile	Mean	Max	80 percentile	Mean
Stockholm	East-West	Top slab	2.65	2.39	2.23	3.91	3.52	3.29
	North-South	Top slab	2.43	2.22	2.13	3.35	3.26	2.96
	East-West	South wall	0.90	0.79	0.72	2.57	2.33	2.17
	East-West	North wall	0.64	0.60	0.55	1.69	1.63	1.50
	North-South	East wall	0.94	0.84	0.77	2.17	2.12	1.89
	North-South	West wall	0.72	0.67	0.62	2.15	1.97	1.88
Luleå	East-West	Top slab	2.69	2.29	2.15	3.58	3.23	3.01
	North-South	Top slab	2.69	2.12	2.05	3.58	2.87	2.77
	East-West	South wall	0.89	0.73	0.70	2.39	2.20	2.03
	East-West	North wall	0.92	0.75	0.67	2.31	1.77	1.64
	North-South	East wall	0.89	0.75	0.71	2.39	1.92	1.81
	North-South	West wall	0.92	0.75	0.68	2.32	1.86	1.78
Stress, ΔT 15°C (recommended code value)								
EN 1991-1-5 [13]	Independent of bridge direction	Top slab	3.51					
		Vertical walls	2.35					

To further analyse the difference between the full *Climate* simulations and the separate temperature components simulations the stress distributions over the top slab have been extracted when the annual maximum inside tensile stress occurs for Stockholm 1986, and the result is presented in Fig. 5. The stress distribution is extracted 100 mm from the upper right corner of the inside cavity, since this is in most cases close to where the maximum inside tensile stress appears. The *Climate* stress distribution is close to being linear; but the impact of the non-linear temperature component causes the difference in maximum stress level. The figure also gives further indication that the difference in average temperature between the walls only has a small impact on the tensile stresses.

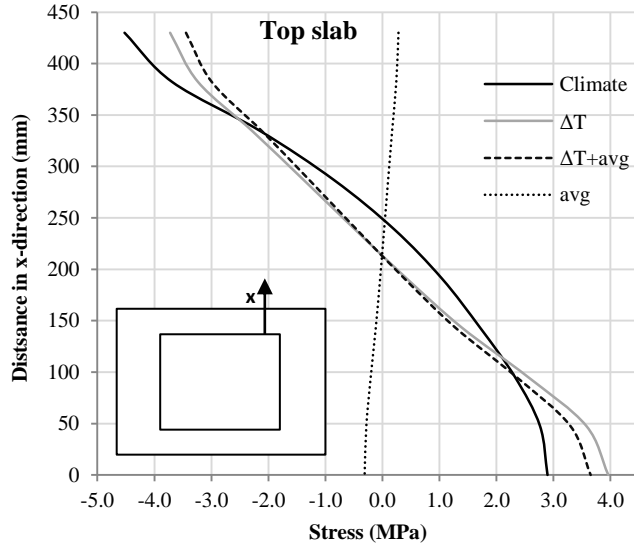


Fig. 5 Stress distribution in the top slab when annual maximum tensile stress occurs on the inside of the top slab for Stockholm 1986, positive in tension

Considering the vertical walls for Stockholm and Luleå in Table 2, it is clear that the linear approach overestimates the inside tensile stress in these parts of this cross-section. The stress level is 3-4 times as large when ΔT is used as input compared to when all components are included. This is due to the difference in thickness between the horizontal slabs and the vertical walls in this cross-section, which amplifies the non-linearity of the thermal stress distribution caused by the non-linear temperature component. This is further analysed in a later section in the article. When the bridge is located east-west, the largest tensile stress on the inside walls appears near the south corners for Stockholm, while for Luleå the largest tensile stresses on the vertical walls appear on the north side. When the bridge is located north to south the largest tensile stresses on the inside surfaces of the vertical walls for Stockholm appear on the east wall, while the west have larger stress for Luleå. This indicates that the different climate situations due to the geographical distance between Luleå and Stockholm have an impact on the thermal stresses.

The stress distributions over the south wall when the annual maximum inside surface tensile stress occurs in 1986 for Stockholm are presented in Fig. 6 for the *Climate* and separate temperature component simulations. The distribution is extracted 100 mm from the upper right corner; the position is chosen for comparison uses, it is not certain that this is where the maximum tensile stress appears on the inside surface. But since the stress field is similar along the entire wall, the chosen distribution can be seen as representative. The figure confirms the thermal stress distribution from the *Climate* simulation as more non-linear for the side wall than for the top slab. The linear differential approach is not suitable to use as an estimation of the stress distribution in this part of the cross-section.

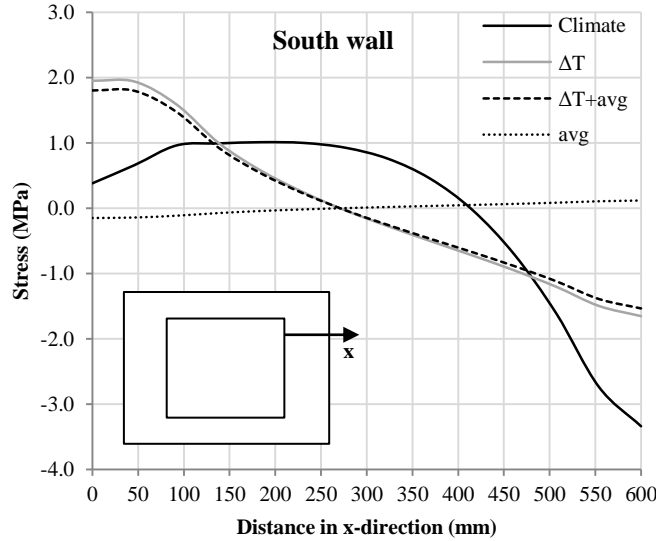


Fig. 6 Stress distribution in the south wall when annual maximum tensile stress on the inside of the wall for Stockholm 1986 occurs, positive in tension

For the outside surface of the top slab the maximum tensile stress is significantly lower than for the inside, see Fig. 7. But here, the linear approach gives a lower stress level for the outside surface by about 0.5 MPa. The annual maximum tensile stress on the outside surface of the south wall is larger than the inside maximum from Table 2. For the south wall the linear approach also gives a lower stress level; about half of the *Climate* case. Here the tensile stresses are larger than on the inside if compared with the values from Table 2. The overestimation of tensile stresses on the inside and the underestimation on the outside when using a linear temperature differential approach is caused by the removal of the non-linear temperature component.

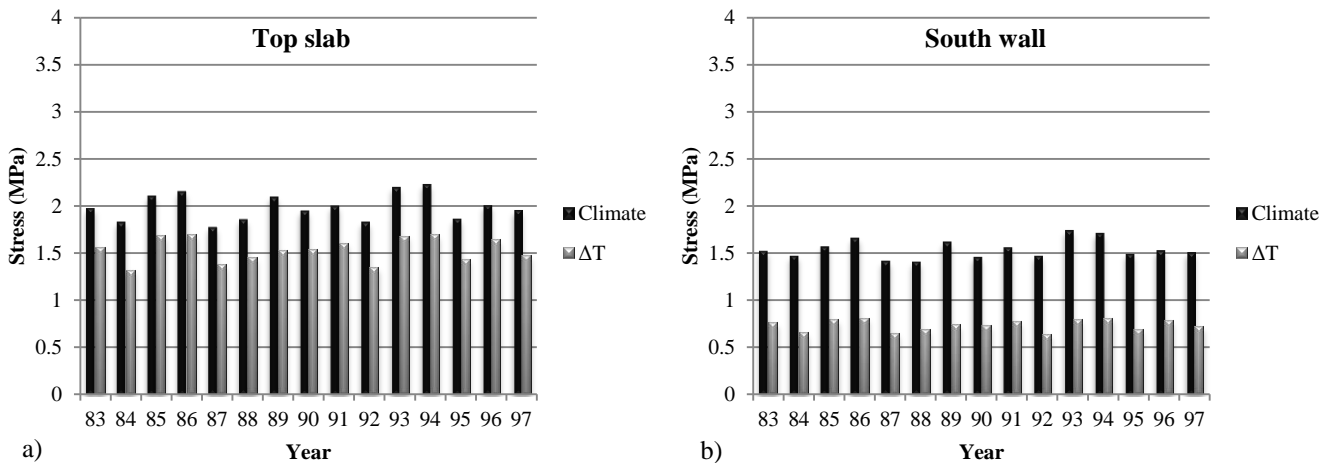


Fig. 7 Annual maximum tensile stress on the outside of the top slab (a) and south wall (b) for Stockholm

The results from the simulations using calculated linear temperature differentials as input are similar to the results from the simulation using the linear temperature difference given in the Eurocode EN 1991-1-5 [15], see Table 2. For Stockholm the 5-year values are almost equal to

the Eurocode results. A large difference compared to the *Climate* simulations can be observed for both the calculated linear differentials and the Eurocode differential cases. This indicates that when the recommended approach in the Eurocode is used, the thermal tensile stresses due to climatic exposure are overestimated for the investigated region and that the non-linear part of the temperature distribution may be beneficial if included in the thermal stress calculations.

To investigate the geometrical effects, several cross-sections with similar size but different relations between height and width and with variations in slab/wall thickness were used with climate data from Stockholm 1986. All following stress distributions are extracted 100 mm from the upper right inside corner. In Fig. 8(a), the stress distribution over the top slab for the cross-section with the “*Rotated*” geometry is presented, see Table 1 for dimensions. The distribution is similar to the stress distribution over the south wall from the original case in Fig. 6. In Fig. 8(b) it can be seen that the stress distribution over the south wall for the “*Rotated*” case is similar to the distribution over the top slab from the original case in Fig. 5. This shows that the orientation of the cross-section is not influencing the thermal tensile stresses; it is instead the thickness of the members which is the most important factor. The largest tensile stress occurs in the thinner member, top slab in the original case and south wall in the “*Rotated*” case. The actual placement of the thinner member has a limited influence. This leads to the conclusion the geometry have a large influence concerning thermal stresses compared to the orientation, and that varying geometry in a cross-section may give unfavourable stress levels.

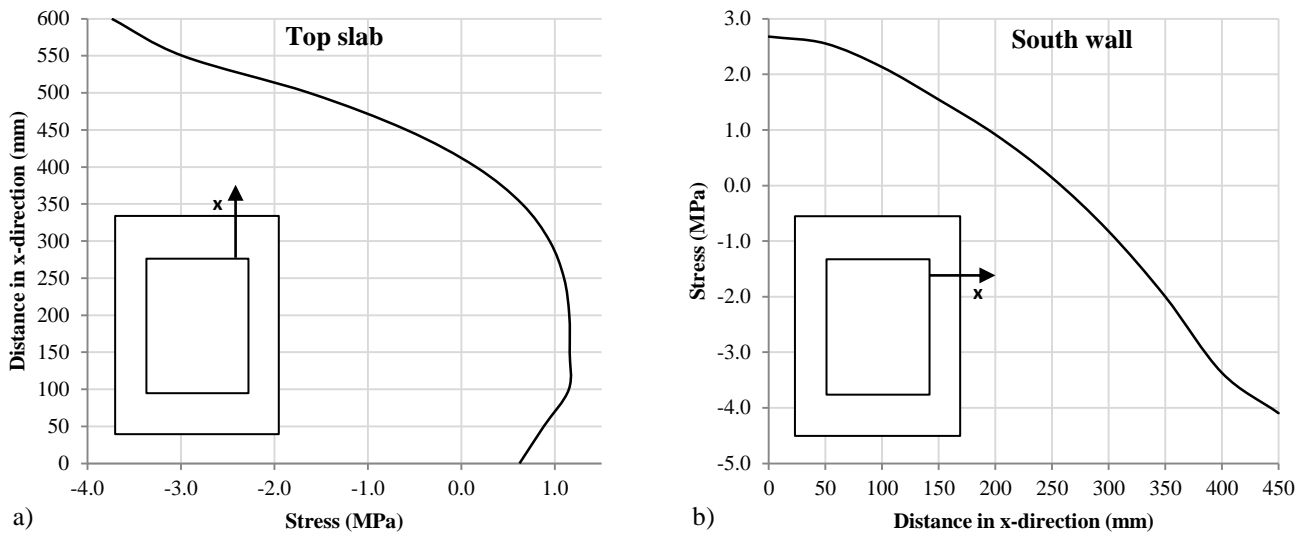


Fig. 8 Stress distribution in the top slab (a) and south wall (b) when annual maximum tensile stress on the inside occurs for Stockholm 1986.

To further analyse how the geometry affects the thermal stresses six more simulations were performed. The slab/wall thickness ratio was 1:1 in all cases, but the absolute value varied from case to case; either 450 or 600 mm. All geometries are presented in Table 1. The outer dimensions were also varied; four “*Squares*” with identical height and width but with varied absolute values and two “*Rectangles*” with differing height and width were used. In Fig. 9 the

stress distributions over the top slab and south wall from the performed simulations are presented. Here it can be seen that the annual maximum thermal tensile stress is almost the same for all six cases for both the top slab and the south wall. There is no longer any difference in stress level between the top slab and the south wall, which confirms the previous statement that the orientation has a limited effect on the thermal stresses. The maximum tensile stress levels are lower than for the thinner members in the original case, Figs. 5 and 6, and the “*Rotated*” case, Fig 8, which confirms the influence of the thickness ratio between the members on the thermal stresses. If the thickness varies between the slabs and walls, large tensile stresses may appear on the inside surfaces of the thinner member, independent of whether the member is horizontal or vertical. However, a study of more cross-sections could be needed to confirm these results, including box-sections with the walls partially shaded from over-hangs.

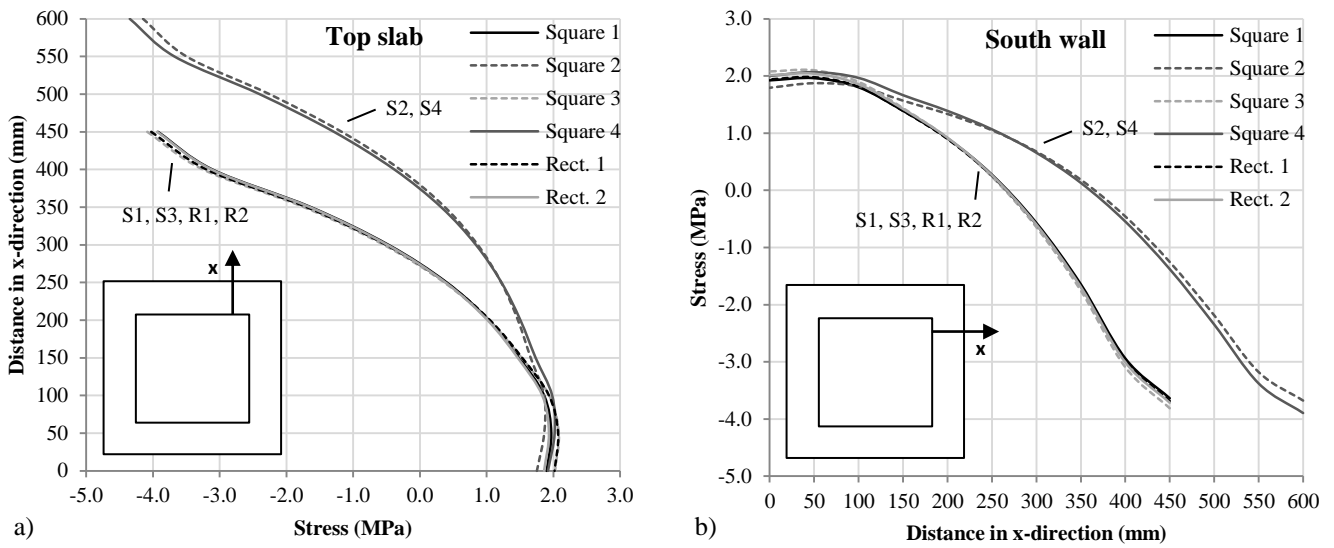


Fig. 9 Stress distribution in the top slab (a) and south wall (b) when annual maximum tensile stress on the inside surface occurs for Stockholm 1986, see Table 1 for dimensions

To investigate whether large tensile stresses appear at the inside of the slabs and walls when certain temperature distributions occur, the input data for the simulations are examined. In Table 3 the annual maximum tensile stress for the inside surface of the top slab from the *Climate* simulations and the linear temperature differential over the top slab at the same time are presented. The results are taken from the simulations using data for Stockholm with the bridge located east-west. When the maximum tensile stress occurs, the linear temperature differential is large; the yearly maxima coincide for 13 of the 15 years. This shows that the linear temperature differentials over the individual walls and slabs have a large impact on the transverse stresses.

Table 3 also shows the annual maximum tensile stress at the inside surface of the south wall from the *Climate* simulations and the corresponding linear temperature differential over the south wall. Here the connection is not as clear as for the top; the yearly maximum only coincides for 5 of the 15 years. However the linear temperature differential when the

maximum tensile stress occurs is still large. This confirms that transverse tensile stresses are mainly dependent on the individual linear temperature differentials affecting the cross-section. But, as the previous results from Fig. 6 and Fig. 7 show, the linear temperature differential approach may not be suitable to use to estimate the stress level due to the effect of the non-linear temperature differential, it can however be useful for identifying when and where high thermal stresses occur.

Table 3. Relation between maximum inside surface tensile stress from the “*Climate*” case and the individual linear temperature differential over the top slab or south wall

Year	Top slab			South wall		
	Max inside surface tensile stress (MPa)	ΔT_{top} when max stress (°C)	Max ΔT_{top} if other time (°C)	Max inside surface tensile stress (MPa)	ΔT_{south} when max stress (°C)	Max ΔT_{south} if other time (°C)
1983	2.29	14.0		0.75	10.4	12.1
1984	2.49	14.7		0.85	13.1	
1985	2.29	13.5	14.3	0.78	11.7	13.1
1986	2.65	15.8		0.90	12.2	
1987	2.05	12.2		0.66	9.6	13.7
1988	2.57	13.9		0.80	13.6	13.7
1989	2.25	13.2		0.74	11.3	
1990	2.18	13.1		0.68	12.4	
1991	2.26	13.1		0.68	11.4	
1992	2.08	12.3	12.8	0.63	11.0	11.1
1993	2.26	13.4		0.66	11.7	12.7
1994	2.10	13.2		0.68	9.7	12.3
1995	2.04	12.7		0.69	10.1	10.6
1996	2.09	12.6		0.69	10.4	11.5
1997	1.89	12.4		0.61	8.8	12.3

Conclusions

Extreme values of transverse thermal stresses generated in concrete box sections due to climatic influences have been investigated in the present paper. The effects of various parameters related to cross section geometry, bridge orientation and geographical location were studied in simulations based on meteorological time series over 15 years. Some conclusions valid for this type of cross section at least under Northern European climate conditions can be drawn. Generalisation to common bridge box sections with cantilever slabs protruding from the box should however be made with care, since cantilevering slabs will affect e.g. the incoming solar radiation and thereby partly shade the vertical walls. The conclusions in this study are:

- For box cross-sections such as the top section of the arch of the New Svinesund Bridge the largest tensile stresses appear on the inside of the thinner horizontal top slab.
- For this cross-section the maximum transverse tensile stress on the inside surface of the top slab may be overestimated if it is predicted on the basis of linear temperature differences over the slabs and walls only. The maximum tensile stress on the inside of the thicker vertical walls can be even more overestimated if a linear approach is used, due to geometrical and size effects.
- The results indicate that the given value of a linear temperature differential of 15 °C in the Eurocode may give an overestimation of the maximum thermal stresses if used in the design of box-girder bridges.
- With a varying thickness between the slabs and walls, large tensile stresses may appear on the inside surfaces of the thinner member independent of the orientation and placement of the member.
- If the thickness is uniform between the slabs and walls, the maximum tensile stress is similar for the top slab and south wall and reduced compared to the stress level in the thinner member for a cross-section with varying thickness. The outer dimensions have a limited effect on the thermal stress distributions for these cases.
- A direct relation between the occurrence of the annual maximum tensile stresses and large positive linear temperature differentials over the slabs and walls is observed. This indicates that a linear approach can be used to identify where and when large thermal stresses may occur, although it is not always suitable to use for estimating the stress level.

References

- [1] Branco FA, Mendes PA. Thermal actions for concrete bridge design. J Struct Eng 1993;119(8):2313–31.
- [2] CEB Bulletin No. 167: Thermal Effects in the Design of Concrete Structures. CEB - Comité Euro International du Béton 1985.
- [3] Cooke N, Priestley MJN, Thurston SJ. Analysis and Design of Partially Prestressed Concrete Bridges Under Thermal Loading. PCI Journal 1984;29(3):94–114.
- [4] Elbadry M, Ghali A. Thermal Stresses and Cracking of Concrete Bridges. ACI Journal 1986;Title No. 83-90:1001-9.
- [5] Emerson M. The Calculation of the Distribution of Temperature in Bridges. TRRL Report LR 561. Crowthorne; 1973.
- [6] Mirambell E, Aguado A. Temperature and Stress Distributions in Concrete Box Girder Bridges. J Struct Eng 1990;116(9):2388-409.

- [7]Prakash Rao DS. Temperature Distributions and Stresses in Concrete Bridges. ACI Journal 1986;Title No. 83-52:588-96.
- [8]Roberts-Wollman CL, Breen JE, Cawrse J. Measurements of thermal gradients and their effects on segmental concrete bridge. J Bridge Eng 2002;7(3):166–74.
- [9]Soukhov D. Representative Values of Thermal Actions for Concrete Bridges. Prog in Struct Eng and Mat 2000;2(4):495-501.
- [10]Larsson O, Karoumi R. Modelling of Climatic Thermal Actions in Hollow Concrete Box Cross-Sections. Struct Eng Int 2011;21(1):74-9.
- [11]BRIGADE / Plus version 3.1-1. Scanscot Technology. Lund; 2010
- [12]Darholm T, Lundh L, Ronnebrant R, Karoumi R, Blaschko M. Technical Book about the Svinesund Bridge. Swedish Road Administration. Uddevalla; 2007.
- [13]Larsson O. Modelling of temperature profiles in a concrete slab under climatic exposure. Struct Conc 2009;10(4):193–201.
- [14]Bohn MS, Anderson R. Temperature and Heat Flux Distribution in a Natural Convection Enclosure Flow. J of Heat Transfer 1986;180:471-5.
- [15]European Committee for Standardization, CEN. ENV 1991-1-5: Basis of Design and Actions on Structures Part 1-5 - Thermal Actions. CEN, Brussels; 2003

V

Climatic thermal stresses in the Vätösund box-girder concrete bridge

Oskar Larsson, M. Sc.
Division of Structural Engineering, Lund University
P.O. Box 118
SE-221 00, Lund, Sweden
e-mail: oskar.larsson@kstr.lth.se

Summary

Severe cracks have been found in several box-girder bridges in Sweden, with the cracks being more frequent on the south side than the north. This indicates that solar radiation has a large impact on the stress field of these bridges, since this is the only factor that is significantly different between the walls. In this study the Vätösund Bridge has been modelled in a 3D FE-model to analyse the thermal stresses that occur due to climatic exposure. Meteorological data have been used to simulate the time variation of the temperature field, which is in turn used to simulate the resulting thermal stresses. The results show that the largest tensile stresses appear on the inside of the south wall, with a clear difference compared to the north. Large stresses appear both in the top and in the bottom parts of the south wall; this indicates that the cracks, which mainly appeared in the lower parts, at least partly originates from thermal effects. The boundary conditions at mid span have a large impact on the location and magnitude of the thermal tensile stresses. The results show that it is possible to predict where thermal stresses appear in a box-girder bridge using 3D FE-analysis.

Key Words: 3D FE-analysis, solar radiation, cracking, temperature distribution, thermal actions, concrete bridge

Introduction

Temperature effects and thermal actions from the surrounding environment have previously been discussed in a number of studies during the latest 40 years¹⁻⁶. The need for such investigations increased due to the construction of larger bridges with fewer bearings and joints. More advanced analysis methods such as the finite element method have contributed to this development together with higher demands of capacity and durability. Most previous research use general sets or approximations of climate data to estimate the temperature fields in a structure, where the data sets are assumed to give the worst temperature situations.

Several previous investigations have also been performed concerning stresses in concrete bridges under thermal loading.⁷⁻¹⁰ The studies were mainly focused on the behaviour and stresses in the longitudinal direction of indeterminate bridges. Transverse effects were only discussed briefly. Two-dimensional models and approaches have been used for these studies. Investigations of cracking due to thermal effects by using three-dimensional models have also been performed, e.g. by Peng-Hei et al.¹¹ Here temperature distributions from the Chinese standards were used to estimate the thermal stresses in a linear FE-model. No previous investigation has been found which includes longitudinal and transverse stresses from real climate situations in a three-dimensional model.

Inspections of several box-girder concrete bridges have been performed by the Swedish Road Administration, where severe cracks were discovered. The bridges are all of the same type, a prestressed balanced cantilever bridge with a concrete box girder including asphalt paving on top. In Fig. 1 the results from one of the visual inspections are presented for parts of the inside of the south and north walls of the box. No information concerning the characteristics of the cracks was available but an interesting find was that the cracks are visible on both sides, but the degree of cracking is much larger on the south wall. This indicates that solar radiation has a large impact on the cracks in this type of structure, since this is the only factor that is significantly different between the walls. Solar radiation is the main factor governing the temperature gradient in a concrete structure.

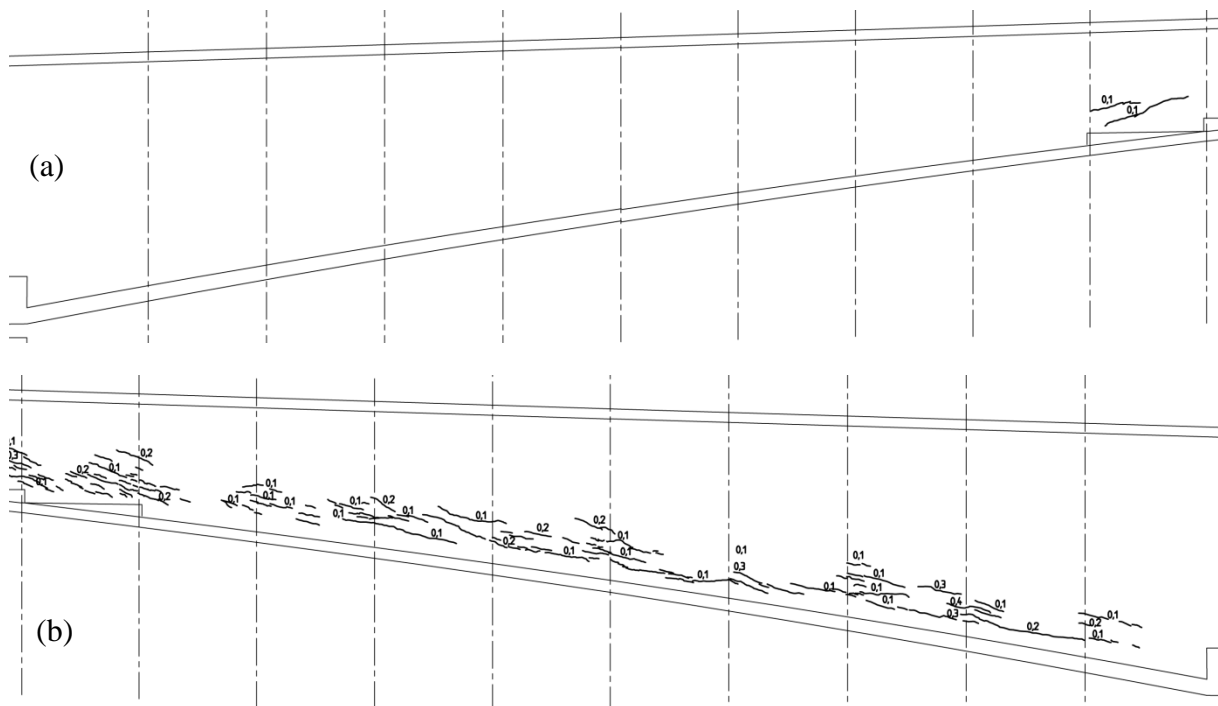


Fig 1 Cracks on the inside surface of the north (a) and south (b) vertical walls

The temperature field in a structure can be divided into different parts; an average temperature, vertical and horizontal temperature differences, and a non-linear temperature difference. Changes in the temperature field give rise to various movements. In a box-girder bridge longitudinal movements are mainly caused by annual changes in the average temperature of the structure. In indeterminate structures, e.g. a three span bridge, the restraint of the supports and/or lack of expansion joints can lead to severe stresses from the longitudinal movements.

Transverse movements are mainly caused by non-uniform temperature distribution over the bridge cross-section. Incident solar radiation during the day and outgoing long-wave heat radiation during the night are the main causes of the temperature differences. For a common box cross-section the restraint from the adjacent parts causes stresses to appear from the transverse movements. When, as an example, the outside surface of a wall is warmer than the

inside due to solar radiation effects, the restraint from the horizontal slabs causes tensile stresses to appear on the inside surface. If the opposite occurs and the outside is colder than the inside, e.g. due to outgoing heat radiation during night-time, tensile stresses appear on the outside. The longitudinal and transverse thermal stresses may, together with other design loads contribute to cracking in a concrete bridge.

In this study the Vätösund Bridge in Sweden have been modelled and analysed concerning thermal stresses. The basis for the model is a previously developed FE-model of top section of the concrete arch of the New Svinesund Bridge.¹² The simulations are performed on a full scale FE-model of one girder of the Vätösund Bridge with the aim to investigate where large thermal tensile stresses may appear in the structure, and compare this with the results from the crack inspections.

The temperature fields are estimated using hourly climate data from the closest meteorological station to the bridge site. The reasons for using hourly data have previously been discussed in both Larsson¹³ and Larsson and Karoumi¹². The temperature field can be modelled more realistically when using real data with a higher resolution, and not just general sets of data.

Model and Method

An FE-model was developed using the commercial program BRIGADE/Plus¹⁴, which is based on Abacus. Heat transfer FE-analysis was used to simulate the temperature in the bridge with climate data as input. The temperature fields achieved from the heat transfer simulations were used in a static stress FE-analysis to simulate the resulting stress fields.

The heat transfer FE-model used in the simulations have previously been validated and used together with measurements performed on the New Svinesund Bridge between Sweden and Norway. The validation was presented in Larsson and Karoumi¹². Global and diffuse solar radiation, incoming long-wave heat radiation, wind speed and outside and inside air temperature were measured at the Svinesund Bridge site. These climatic factors were used as input in the FE-model as a heat flux (solar radiation), ambient radiation heat transfer (long-wave heat radiation), inside cavity radiation heat transfer (inside air temperature), ambient convective heat transfer (outside air temperature and wind speed) and inside convective heat transfer (inside air temperature).

Two different approaches for considering the effect of the inside cavity were investigated, one using the measured inside air temperature and one where the inside air temperature was iteratively calculated from the temperature on the inside surfaces of the surrounding walls. The start value for the inside air temperature in the iteration case was set to the start value of the ambient air temperature. This was done to be able to use the model for cases where the inside air temperature is unknown, which is the situation when using climate data from meteorological stations as input.

The results from Larsson and Karoumi¹² showed that the FE-model can capture the temperature variations in a concrete box cross-section in an accurate way, when using either measured or iteratively calculated inside air temperature. The model is well suited to use with climate input data to simulate the temperature in such a structure. This was done in Larsson and Thelandersson¹⁵, where extensive climate data from 15 years for two locations in Sweden were used to simulate the temperature and resulting stresses due to thermal expansion of the concrete. It was shown that the geometry of the cross-section has a large impact on the thermal stresses in the cross-section. If the thicknesses of the horizontal slabs and the vertical walls are differing, severe tensile stresses may appear on the inside of the thinner walls.

For this study the Vätösund Bridge have been used, which is a box girder concrete bridge with a main span of approximately 160 meters; see Fig. 2 for a side view of the bridge. The bridge was constructed using the balanced cantilever method, where the girders are constructed in sections which simultaneously protrude from the columns. The main prestressed reinforcement is located in the top half of the girder as is shown in Fig. 3. The prestressing is applied in an arch pattern, which gives most prestress in the horizontal direction but also some prestress in the vertical direction. The orientation of the bridge is 30 degrees from an east to west direction, which means that the vertical walls are facing south and north. In the FE-model one girder is used for the geometry due to symmetry. The height of the cross-section, presented in Fig. 4, varies from 10 m at the supports to 2,8 m at the mid-span joint casting. The paving layer consists of 90 mm asphalt.

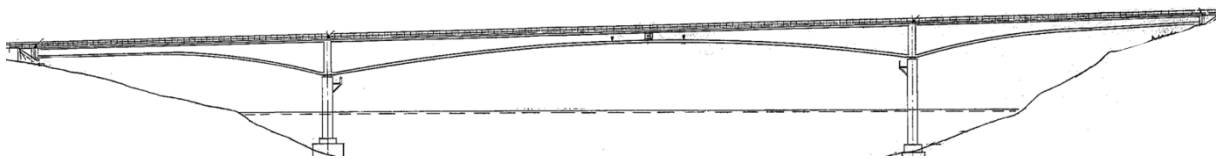


Fig. 2 The Vätösund Bridge

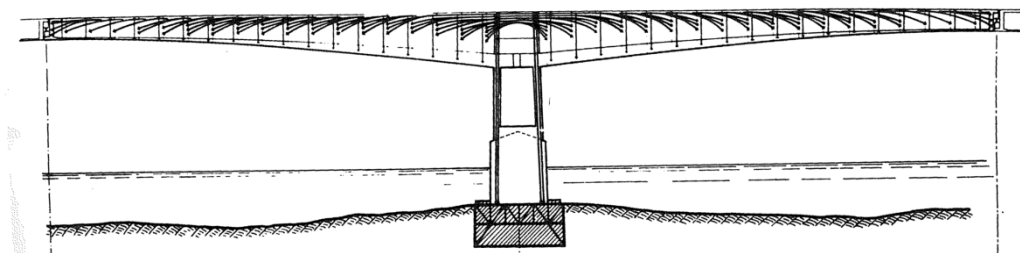


Fig. 3 Principle for placement of the prestressed reinforcement in a balanced cantilever bridge¹⁶

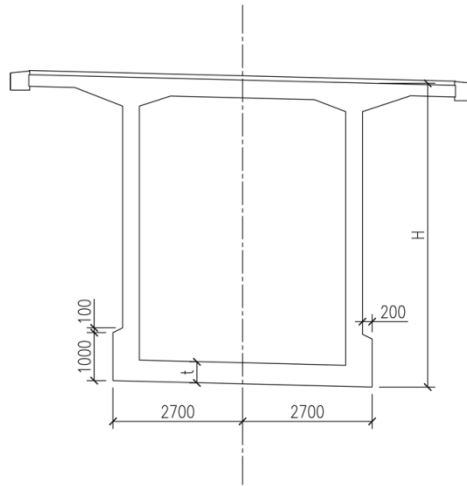


Fig. 4 Geometry of the cross-section (mm), H varies between 10.0 m and 2.8 m and t between 0.6 m and 0.37 m

For the heat transfer simulations 8-node DC3D8 elements are used with a mesh size of 50 mm in the transverse direction and 200 mm in the longitudinal direction. The material data used in the heat transfer model are obtained from the first investigation using the same model¹³. For the concrete the density, 2400 kg/m^3 , specific heat capacity, $900 \text{ J/(kg} \cdot ^\circ\text{C)}$, conductivity, $2.5 \text{ W/(m} \cdot ^\circ\text{C)}$, emissivity, 0.9, and solar absorptivity, 0.5 are used. These material properties have been proven to give good agreement between FE-simulations and measured temperature for both a concrete slab¹³ and the New Svinesund Bridge.¹² The asphalt paving has slightly different material properties²; density 2200 kg/m^3 , specific heat capacity $880 \text{ J/(kg} \cdot ^\circ\text{C)}$, conductivity $0.7 \text{ W/(m} \cdot ^\circ\text{C)}$, emissivity 0.9 and solar absorptivity 0.9³.

The temperature field in the heat transfer model are governed not only by the material properties, but also by the climatic input factors. The climatic input data was obtained from the meteorological station located in Stockholm, about 70 km from the bridge. The factors needed in the model are, as described earlier, global, diffuse and direct solar radiation, incoming long-wave heat radiation from the sky, ambient air temperature and wind speed. Due to the complexity and size of the model, climate data from only one week is used for the temperature simulations. This week is from June 1986, and chosen based on results from the previous investigation of the top section of the New Svinesund Bridge when exposed to climate data recorded in Stockholm¹⁵. The maximum tensile stresses in the concrete section in that investigation occurred during the selected week, and it is therefore seen as an extreme event which may give unfavourable stresses.

Due to the overhangs of the bridge, parts of the vertical walls are shaded. This influence on the temperature is treated by dividing the walls into 0.75-1 m high sections, with different input data depending on the shading. The maximum solar altitude at the location of the bridge is 51,5 degrees, which means that no surface below 3,8 meters from the top surface of the bridge is shaded. The sections of the south web wall surface which are above this angle will at some times during the day be shaded by the overhangs, and the incident solar radiation for the shaded sections will only consist of the diffuse part of the global radiation. The incidence

angle for the direct radiation is calculated using geometrical relations which are described by Duffie and Beckman¹⁷. When shaded by the overhangs, the incidence angle for the shaded section is set to zero which eliminates the direct part of the solar radiation. The un-shaded lower parts of the web wall will then be subjected to a larger temperature differential than the shaded upper parts.

The simulated temperature fields are used in a static stress model to simulate the stress field. C3D8R 3D-stress elements are used with the same mesh as for the heat transfer model. The resulting stress depends on the degree of restraint and the expansion coefficient of concrete. The concrete material is assumed to be linear elastic; this simplification is made since the model would be overly complex regarding the aim of the investigation to identify where the largest tensile stresses may appear if a non-linear material was used. The elastic modulus is set to 30 GPa, which corresponds to a tensile strength of roughly 2,7 MPa, and the Poisson ratio set to 0,2. The thermal expansion coefficient is set to $10 \cdot 10^{-6}$ ($^{\circ}\text{C}$) which is a given number from EN 1991-1-5¹⁸. No self-weight was included in the thermal stress model.

The asphalt paving is not connected mechanically to the concrete structure on the bridge. However, due to limitations in the FE-program, the asphalt and the concrete were connected in the model. This was solved by giving the asphalt a much lower elastic modulus of 3 MPa, and thus stiffness, than the concrete. The same thermal expansion coefficient was used for the asphalt as for the concrete.

The Vätösund Bridge consists of two main columns, with cantilevers protruding towards mid span and land. At mid span the cantilevers are cast together, and thus connected mechanically. In the model the cantilever is assumed to be prevented to move in the longitudinal direction at mid span due to this casting. At the column the cantilever is fixed in all directions. Another case with no connection at mid span is also investigated as a comparison. This was made to check how the thermal stress field would be altered by a change in the boundary conditions, and whether the balanced cantilever bridge is more efficient concerning thermal stresses with or without the mid span casting. A calculation was also performed concerning the stress field occurring due to self-weight in the bridge. This was made in a separate model and not combined with the thermal analysis, to be able to see the effects from each load more clearly. In this case the mid span casting was included in the model.

Results and Analysis

An FE-model has been used to estimate the temperature fields in the Vätösund Bridge in Sweden. The temperature fields are used in turn to estimate the resulting stresses from thermal expansion in the bridge.

The largest thermal tensile stresses in the structure are located on the inside surface of the vertical south wall. An image of the maximum principal stress distribution on this wall is presented in Fig. 5. The magnitude of the maximum tensile stress is about 1,5 MPa. The location of the maximum principal stress is in the top part of the wall, where the prestressed reinforcement is located as presented in Fig. 3. The tensile stresses may relieve some of the

vertical and horizontal prestress, but may be too small to cause any cracks. However, significant tensile stresses also appear in the lower parts of the wall where there is less reinforcement; the largest tensile stress in the lower half of the wall is about 1,3 MPa. These tensile stresses coincide with the most of the cracks visible in the bridge during the inspection, see Fig. 1. This indicates that the cracks on the south wall are at least partly caused by thermal effects. Cracking also occurred further out on the more narrow parts of the wall, where the thermal tensile stresses in the model are lower. These cracks may be caused by the placement of the prestressed reinforcement, shrinkage or other design loads, and are more or less unaffected by thermal stresses.

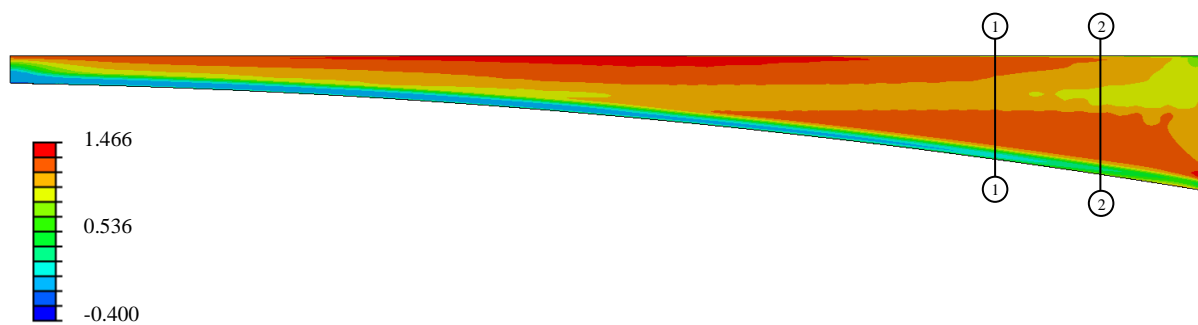


Fig. 5 Maximum principal stress on the inside surface of the south wall (MPa)

The direction of the principal stresses in Fig. 5 is almost perpendicular to the bottom surface of the wall. This further indicates that the cracks formed in the wall presented in Fig. 1 are affected by the thermal actions. The cracks have a direction almost parallel to the bottom surface of the wall which is a crack pattern would appear if caused by the principal thermal stresses.

On the inside surface of the north wall the tensile stresses are somewhat lower. In Fig. 6 an image of the maximum principal stress distribution is presented for the north wall. Here it can be seen that the largest tensile stresses occur in the upper parts of the wall where they are cancelled out by the vertical and horizontal components of the prestressing. The maximum tensile stress is about 1,3 MPa, which is almost similar to the south wall. In the lower parts of the wall however, the largest tensile stress is about 0,8 MPa, which is lower than for the south wall. This confirms the large effect of solar radiation on the thermal tensile stresses, since this is the only differing input factor between the walls in the model. This is also in agreement with the crack inspections, since the degree of cracking in the north wall close to the supports is low.

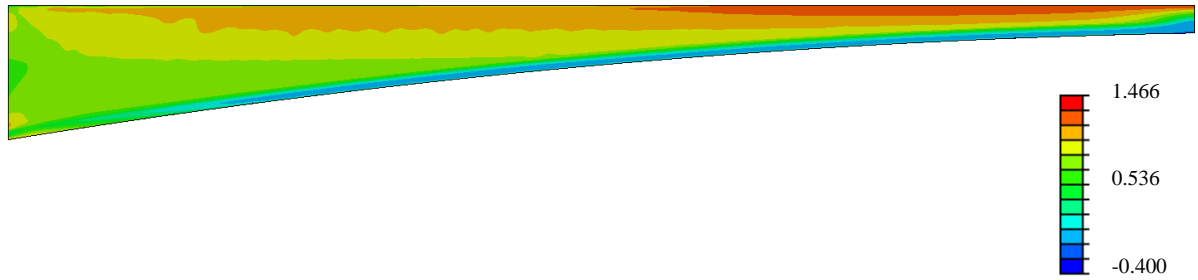


Fig. 6 Maximum principal stress on the inside surface of the north wall (MPa)

The effect of longitudinal restraint is the governing factor concerning the location of the largest tensile stresses in the bridge. The bridge is originally assumed to be prevented to move in the longitudinal direction at both the support, due to symmetry, and at mid span, due to the concrete casting connecting the cantilevers. These boundary conditions give the stress field described in the previous section. When the bridge instead is assumed to be unconnected at mid span, the largest tensile stresses appear in the top half of the inside surface of the south wall, see Fig. 7 for an image of the maximum principal stress distribution. The stress level in the top have increased; 1.9 MPa compared to 1.5 MPa for the previous case. But, as mentioned before, since this is where most of the prestressing is applied, the thermal tensile stresses will not give rise to cracking.

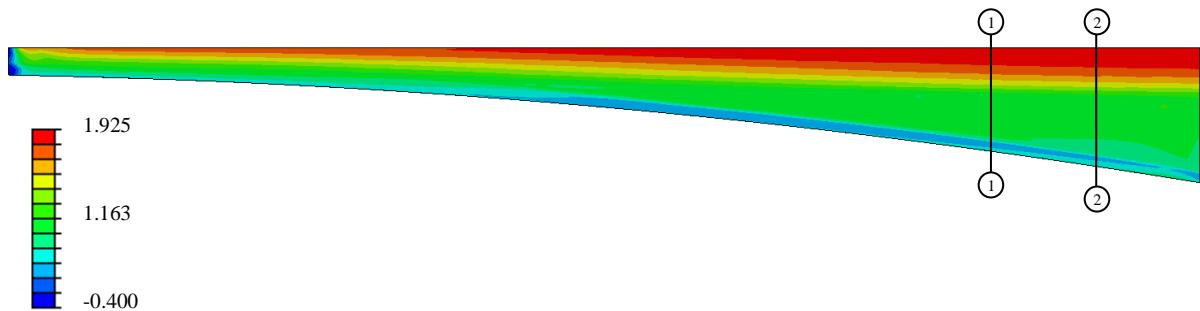


Fig. 7 Maximum principal stress on the inside surface of the south wall, no mid span casting (MPa)

In the bottom part of the wall, however, the tensile stresses are lower compared to the first case. This was expected since the greater thermal expansion in the top parts of the bridge combined with the assumption that the girder has a free end should give larger tensile stresses in the top parts. The stress level is now around 0.8 MPa compared to 1.3 MPa from the first case. The difference increases closer to the support as can be seen in Fig. 8, where the maximum principal stress distributions in section 1-1 and 2-2 are presented for the two cases. Section 1-1 is located 13.5 m from the support and section 2-2 6.4 m from the support. Fig. 9 shows the stress distribution of the vertical stress component in section 1-1. It can also be seen in the figures that the maximum principal stress distribution in the case without casting is more or less constant along the length of the bridge, while the tensile stress in the original case increases in the lower part closer to the support. For the case with mid span casting the maximum principal stress distribution is similar to the distribution of the vertical component.

From these results it can be concluded that the boundary conditions are, as expected, a very important factor concerning the location and magnitude of thermal stresses. The Figures also confirm that the maximum principal stresses in the case with mid span casting are almost perpendicular to the bottom surface and therefore contributing to cracking as was stated earlier.

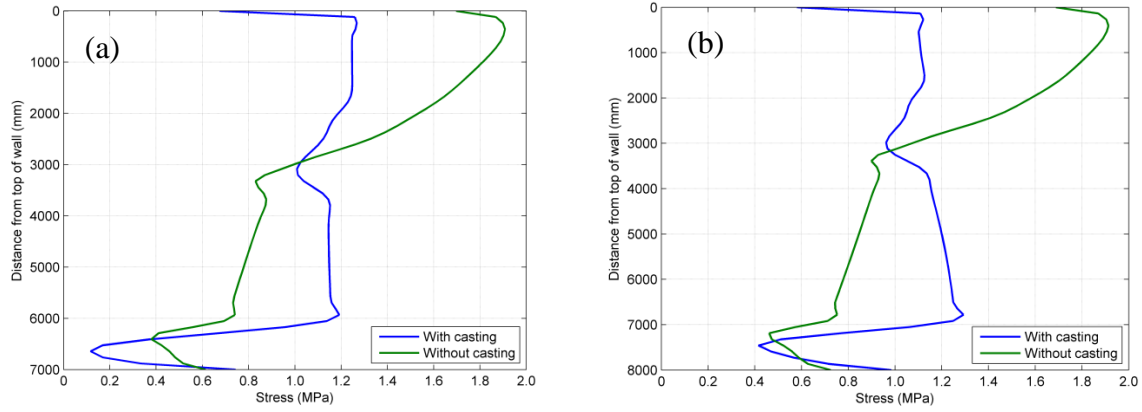


Fig. 8 Maximum principal stress distribution at section 1-1 (a) and 2-2 (b) in Figs. 5 and 7

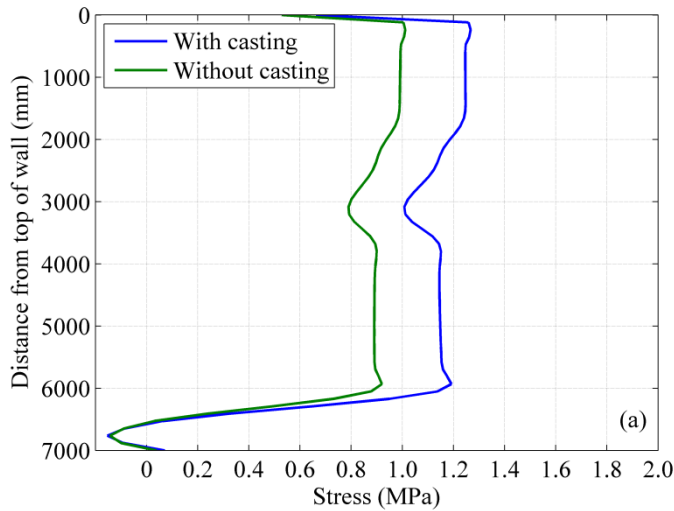


Fig. 9 Distribution of the vertical stress component at section 1-1 in Figs. 5 and 7

When the results from the simulation with only self-weight applied to the model are compared to the thermal simulation, it can be seen that the tensile stresses in the bottom part of the walls are much more affected by thermal actions than by self-weight. An image on the maximum principal stresses from self-weight on the inside surface of the south wall is presented in Fig. 10, and the maximum principal stress distributions in sections 1-1 and 2-2 are presented in Fig. 11. The tensile stresses from self-weight in the upper part of the wall are much larger than the stresses from thermal effects; 6-9 MPa compared to 1.4 MPa. In the lower parts however, the tensile stresses from self-weight are close to zero, while the thermal tensile

stresses were 1.2-1.3 MPa. This further indicates the effect of thermal actions on the cracks in the wall.

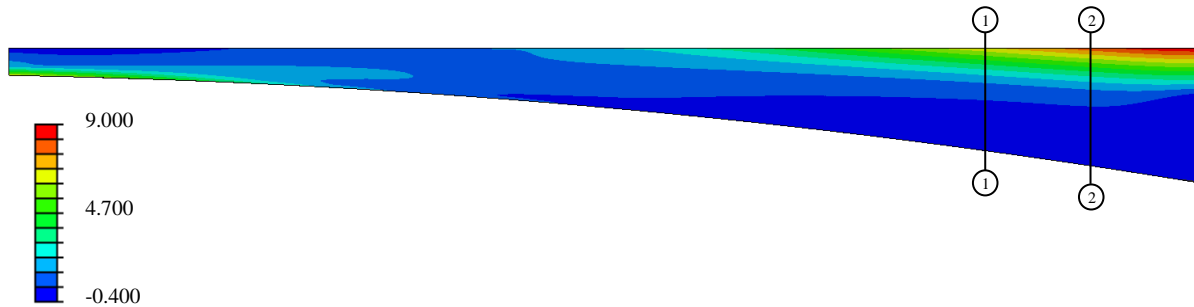


Fig. 10 Maximum principal stress from self-weight on the inside surface of the south wall (MPa)

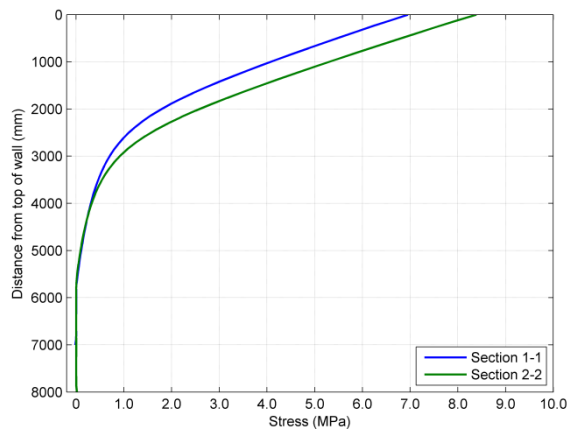


Fig. 11 Maximum principal stress distribution from self-weight at section 1-1 and 2-2 in Fig. 10

Conclusions

Large thermal stresses may appear in a concrete bridge due to effects from the surrounding climate. An investigation has been performed using the climate data from a warm week in June 1986, which was defined in a previous study as an extreme event. For a prestressed cantilever bridge with a box cross-section such as the Vätösund Bridge the largest thermal tensile stresses appear on the inside of the south wall. Large tensile stresses appear both in the top of the wall, where they are cancelled out by the prestressed reinforcement, and in the bottom. The thermal tensile stresses in the bottom part may have a large impact on the cracks found during visual crack inspections of the bridge, where the largest number of cracks was found on the inside of the south wall.

In the north wall the stress field is different. Large tensile stresses still appear in the top, but the tensile stresses in the bottom parts are lower than for the south wall. This is also in agreement with the crack inspections, since few cracks were found in the bottom part of the north wall. It also confirms the impact of solar radiation on the climatic thermal stresses in a

concrete box girder bridge. When the stress field in the vertical walls for the load case using self-weight is analysed, it is shown that the tensile stresses from self-weight is about 4-6 times as large as the thermal stresses in the top parts of the walls. In the bottom parts however, the thermal actions have a much larger impact since the tensile stress from self-weight is close to zero.

The boundary conditions at mid span are very important concerning the location of the large tensile stresses. If the cantilevers are cast together, as in the Vätösund Bridge, large tensile stresses appear both in the top and in the bottom half of the south wall. If there were no connection between the cantilevers but instead an expansion joint, the largest tensile stresses would appear close to the top of the south wall. The tensile stress level in the bottom parts of the wall would be lower than for the case with the mid span casting.

The investigation performed on the Vätösund Bridge shows that it is possible to predict where large thermal stresses may appear using three-dimensional FE-analysis. The insecurities concerning boundary conditions, geometry and reinforcement modelling does however contribute to the uncertainties of using this kind of extensive model.

References

- [1] CEB-Comite Euro-International du Beton. *CEB Bulletin No. 167: Thermal Effects in the Design of Concrete Structures*, CEB-Comite Euro-International du Beton, 1985.
- [2] Branco FA, Mendes PA Thermal Actions for Concrete Bridge Design, *J. of Struct. Eng.* 1993; **119**(8): 2313-2331.
- [3] Emerson M. *The Calculation of the Distribution of Temperature in Bridges*, TRRL Report LR 561, Crowthorne, 1973.
- [4] Soukhov D. Representative Values of Thermal Actions for Concrete Bridges, *Prog. Struct. Eng. Mat.* 2000; **2**(4): 495-501.
- [5] Roberts-Wollman CL, Breen JE, Cawrse J. Measurements of Thermal Gradients and their Effects on Segmental Concrete Bridge, *J. of Bridge Eng.* 2002; **7**(3): 166-174.
- [6] Suzuki J, Ohba Y, Uchikawa Y, Hoshikawa K, Kimura K. Monitoring Temperatures on a Real Box-Girder Bridge end Energy Budget Analysis for Basic Information on Bridge Cooling and Surface Freezing, *J. of Bridge Eng.* 2007; **12**(1): 45-52.
- [7] Mirambell E, Aguado A. Temperature and Stress Distributions in Concrete Box Girder Bridges, *J. Struct. Eng.* 1990; **116**(9): 2388-2409.
- [8] Prakash Rao DS. Temperature Distributions and Stresses in Concrete Bridges, *ACI Journal*, Title No. 83-52, 1986; 588-596.

- [9] Elbadry E, Ghali A. Thermal Stresses and Cracking of Concrete Bridges, *ACI Journal*, Title No. 83-90, 1986; 1001-1009.
- [10] Cooke N, Priestley MJN, Thurston SJ. Analysis and Design of Partially Prestressed Concrete Bridges Under Thermal Loading, *PCI J.* 1984; **29**(3): 94–114.
- [11] Pei-Heng L, Mao-Hua Z, Wei-Zhen C. Analysis of Temperature Stress for Concrete Box Girders Cracking, *2010 Int. Conf. on Mechanical Automation and Control Engineering*, Wuhan, China, 2010; 1590 - 1594
- [12] Larsson O, Karoumi R. Modelling of Climatic Thermal Actions in Hollow Concrete Box Cross-Sections, *Struct. Eng. Int.* 2011; **21**(1), 74-79.
- [13] Larsson O. Modelling of Temperature Profiles in a Concrete Slab under Climatic Exposure, *Struct. Conc.* 2009; **10**(4): 193-201
- [14] BRIGADE/Plus version 3.1-1, *Scanscot Technology*, Lund, 2010
- [15] Larsson O, Thelandersson S. Transverse Thermal Actions in Concrete Box Cross-sections from Climatic Exposure, *Eng. Struc.*, 2011, submitted
- [16] Mondorf PE. *Betonbroer, plade- og bjælkebroer*, J.J. Trykteknik A/S; 1981
- [17] Duffie JA, Beckman WA. *Solar Engineering of Thermal Processes*, 3rd Edn. Wiley; Hoboken, New Jersey, 2006
- [18] European Committee for Standardization, *ENV 1991-1-5: Basis of Design and Actions on Structures Part 1-5 – Thermal Actions*, CEN, Brussels, 2002